INVESTIGATION OF THE EFFECTS OF HEATER CHARACTERISTICS ON CHF AND POST-CHF PERFORMANCE OF A LONG VERTICAL ANNULUS IN HIGH PRESSURE WATER

By

ARTHUR KAM KI LEUNG, B.ENG., P.ENG.

A Thesis

Submitted to the School of Graduate Studies

in Partial Fulfilment of the Requirements

for the Degree

Master of Engineering

McMaster University

MASTER OF ENGINEERING (1982) McMASTER UNIVERSITY
(Engineering Physics Department) Hamilton, Ontario

TITLE: Investigation of the Effects of Heater Characteristics on CHF and Post-CHF Performance of a Long Vertical Annulus in High Pressure Water

AUTHOR: Arthur Kam Ki Leung, B.Eng. (McMaster University)

SUPERVISOR: Professor S. Banerjee

NUMBER OF PAGES: xii, 161

TABLE OF CONTENTS

TABLE OF CONTENTS (Cont'd)

ABSTRACT

CHF and Post-CHF tests were performed in water at 9.7 MPa using two vertical test assemblies having identical, internally heated annular flow channels, one heated directly, the other indirectly. Experiments were conducted to determine the effect of these methods of heating on CHF and Post-CHF heat transfer.

For the range of the test conditions investigated, the results show that the direct and indirect heaters have similar CHF performance. At heat fluxes above CHF and mass fluxes of 2.0 and 3.5 $Mg.s^{-1}.m^{-2}$, the indicated maximum wall temperatures of the heaters were similar, but at the highest mass flux for the tests, 5.0 $Mg.s^{-1}.m^{-2}$, the indirect heater had lower indicated maximum wall temperatures than the direct heater for a given heat flux above CHF.

A multi-fluid model, of the type used previously in the prediction of CHF, was derived and tested against the experimental data. The model, which considers droplet entrainment, deposition and evaporation in the annular flow regime, assumes dryout to occur when the liquid film flow on the inner rod approaches zero. The CHF predictions were in fairly good agreement with the experimental results. In general, the model under-predicted CHF at low inlet subcoolings and over-predicted CHF at high inlet subcooling. The error trend is consistent with that of the CHF prediction models of other researchers.

In addition to the CHF prediction model, a Post-CHF model to predict the vapour temperatures, and hence, the heated wall temperature is also presented in the report. The theory is based on a physical model of heat transfer in the liquid deficient regime. In the model, heat in the dry region is assumed to transfer from the heated wall to superheat the steam and some of this heat, in turn, is used to evaporate the droplets which are entrained in the vapour core. Droplet entrainment and deposition at the shroud (outer tube) film-vapour interface are modelled. Heat transfer enhancement due to increased turbulence downstream of the rod centering spacers is incorporated through an empirical correlation. The predicted results were compared to the direct heater experiments. In general, the predicted wall temperatures were in agreement with those in the experiments.

ACKNOWLEDGEMENTS

This research project was performed at the Atomic Power Division of Westinghouse Canada Inc. (WECAN) in Hamilton under contract to Atomic Energy of Canada Limited, Research Company (AECL-RC). I would like to express my gratitude to AECL for the permission to publish the material as a Master thesis.

Also I would like to express my deepest appreciation to Dr. S. Banerjee for his acceptance of me as one of his graduate students. Dr. Banerjee, being my thesis supervisor, provided me with expert advice during the course of the research work. I would like to acknowledge that it has been a great pleasure and gainful to work under his supervision.

My personal thanks go to Dr. D.C. Groeneveld of AECL-RC for the initiation of this project idea. Dr. Groeneveld, who coordinated this contract work, also acted as my off-campus supervisor, gave me encouragement and provided me with valuable technical advice. I am grateful to Dr. Groeneveld.

I am also grateful to Dr. S.Y. Ahmad of AECL-RC for his approval on behalf of AECL-RC of this contract work as well as his moral support on pursuing the Master degree.

I am obliged to F. Stern of WECAN for his approval on behalf of WECAN to use the project as part of the work to fulfil the requirement of the degree, and to provide finanacial support on the degree course work.

I would like to thank R.C. Hayes of WECAN for providing professional advice on directing the research project.

I also want to thank E.R.C. Ayers of WECAN for scheduling the laboratory personnel to work on the project.

The technologists at WECAN who worked with me and helped me to make this research project successful are also gratuitously acknowledged.

Finally, to my wife, I am grateful for her patience that makes the pursuit of this Master degree on a part-time basis a worthwhile and joyful experience.

LIST OF TABLES

LIST OF FIGURES

LIST OF FIGURES (Cont'd)

LIST OF FIGURES (Cont'd)

1. INTRODUCTION

In out-reactor heat transfer experiments, fuel elements are commonly simulated by electrically heated rods which are either directly or indirectly heated. For the directly heated rods, power is applied to the sheath, and for the indirectly heated rods, power is applied to an internal heater filament which is electrically insulated from the heater sheath.

Directly heated rods are relatively simple to fabricate and can be internally instrumented in various ways to monitor the sheath temperature (fixed or movable thermocouples, etc.) and many Critical Heat Flux and Post-CHF experiments are performed with such heaters. However, their thermal time constant is small compared to nuclear reactor fuel, and local temperature variations, caused perhaps by local dryout, can perturb the local heat flux distribution. Therefore it is necessary to determine if the thermal time constant of the direct heaters would affect the CHF and the sheath temperatures after dryout in order to interpret these out-reactor experimental results for reactor design applications. So far, only limited experiments had been performed by researchers to investigate the wall thickness effect of the direct heaters on the CHF. These experiments did not cover conditions beyond CHF. Furthermore, due to the electrical current limitation of the power supply, the maximum wall thickness used in these experiments was far from

representing the thermal time constant of reactor fuels. Although more difficult to instrument, indirectly heated rods generally offer a closer simulation of reactor fuel. But, to the author's knowledge, no direct comparison on the dryout and post-dryout heat transfer have been made between the direct and indirect heaters. In the present study, CHF and Post-CHF experiments were performed in water at high pressure using two vertical, annular test sections having identical geometry. In one case, the inner rod was heated directly and in the other case the inner rod was heated indirectly. The outer flow tube (the shroud) was not heated.

The experimental results in the two cases are compared. Theoretical prediction of CHF and Post-CHF conditions are also presented in the report. The CHF prediction method is based on a physical model of the dryout mechanism in annular flow, while the Post-CHF prediction method is based on a physical model of heat transfer in the liquid deficient regime in a heated annular channel.

Similar CHF prediction methods have been used previously in tubular, annular and in rod bundle geometries. However, the Post-CHF prediction methods so far proposed, to the author's knowledge, are for tubular geometries only. For an annulus, the presence of the liquid film on the unheated shroud has to be considered and is a complicating factor. In the report, the effect of the shroud film was modelled using the same theoretical approach as in the CHF prediction method.

2. TWO-PHASE FLOW HEAT TRANSFER

Much efforts have been made by researchers to understand the fundamentals in two-phase flows and the associated heat transfer. While theoretical predictions of the physical phenomenon are far from perfect in terms of the accuracy due to the complicity in two-phase flows, a general picture of the physical phenomenon can be constructed from the qualitative understandings of various aspects of two-phase flows. Among the many references now available, References [1, 2, 3 and 4] are found to give good and comprehensive descriptions on the two-phase flows and heat transfer including CHF and Post-CHF phenomenon. The presentation given in this section is based mainly and closely on these four references.

2.1 Flow Regimes and Heat Transfer Modes

When a subcooled liquid flows in an uniformly heated, long vertical tube, vapour is generated along the heated channel after the liquid is heated to saturation temperature. If the heat flux is high, vapour may be generated when the bulk liquid is still subcooled. As the vapour velocity increases with increasing quality, the two-phase flow will go through various flow regimes and heat transfer modes when the mass flow is sufficiently high. In general, the particular flow regime depends on the conditions of pressure, flow, heat flux and channel

geometry. The transition between flow regimes is not clearly defined. Besides the flow regimes, the heat transfer coefficient and so is the wall temperature also vary along the length of the tube. The flow regimes, which have been clearly identified and generally accepted, along with the heat transfer modes, and the variations of the heat transfer coefficient and wall temperature are shown in Figure 1. In general, these flow regimes and heat transfer modes are:

(a) Single-phase liquid flow. The liquid is subcooled and heat is transferred to the liquid by forced convection. As the subcooled liquid moves along the channel, the bulk temperature of the fluid is raised to the saturation temperature. The heat transfer coefficient increases only slightly with length (or quality) as the fluid properties change with increasing bulk fluid temperature. Depending on the wall temperature gradient, nucleation may not occur at zero thermodynamic quality. When the heat flux is low, nucleation may be delayed beyond the zero thermodynamic quality and the liquid could become superheated. When the heat flux is high, nucleation may occur before zero thermodynamic quality is reached and the flow regime changes to bubbly flow with subcooled boiling.

(b) Bubbly flow with subcooled boiling. The bulk temperature of the liquid is below saturation temperature while nucleation occurs at the heated wall. Depending on the heat flux, the bubbles may collapse or detach from the heated wall as entrained bubbles in the flow. Heat is

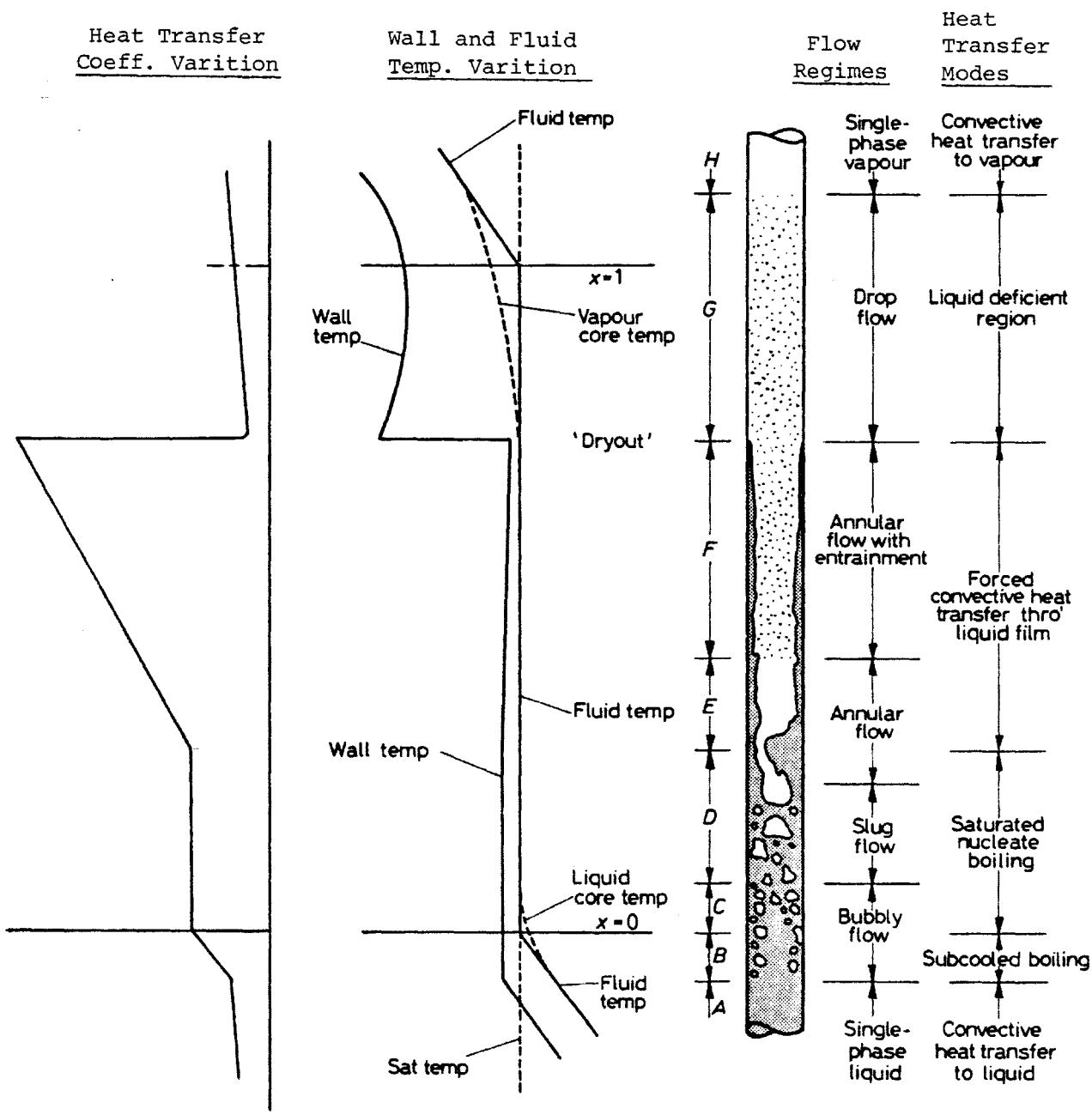

FIGURE 1 : FLOW REGIME AND HEAT TRANSFER IN CONVECTIVE BOILING (FROM COLLIER [1])

transferred to the liquid by forced convection and by nucleate boiling to the bubbles which transfer some of the heat to the liquid by condensation. Since nucleate boiling is a more efficient heat transfer mode than forced convection, the temperature difference between the wall and the bulk fluid decreases as zero thermodynamic quality is approached. And, the heat transfer coefficient increases linearly with quality along the length of the channel.

(c) Bubbly flow with nucleate boiling. The bulk temperature of the liquid is at saturation temperature. The vapour is distributed as discrete bubbles within the liquid continuum. The bubble population increases with length and coalescence takes place. Heat transfer is by nucleate boiling. The temperature difference between the wall and the fluid remains unchanged and the heat transfer coefficient remains constant.

(d) Slug flow. As more bubbles agglomerate, the vapour flows as bullet-shaped plugs which have nearly the same cross-section as the channel and are separated by slugs of liquid. At higher velocities, the vapour and liquid are mixed more homogeneously and is sometimes called churn flow. Heat is transferred by nucleate boiling.

(e) Annular flow. As quality increases, the vapour flows in the core and all the liquid flows along the wall. The vapour accelerates and the vapour velocity is greater than the liquid velocity. The interface

is not smooth and has surface waves. Further downstream, some part of the surface waves are sheared off by the vapour as entrained droplets in the core. Sometimes this is called dispersed annular flow. Besides entrainment and evaporation at the interface, mass is also transferred by droplet deposition onto the liquid film. However, the net mass transfer across the interface is such that the liquid film is depleted along the flow length. Nucleation in the liquid film is usually suppressed except at very high heat flux. Heat is transferred by forced convection from the wall to the liquid film and by evaporation of the liquid at the interface. This heat transfer mode is generally known as forced convective evaporation. As the liquid film thickness decreases gradually, the heat transfer coefficient increases with increasing quality. Thus, the wall temperature decreases along the channel.

(f) Liquid deficient flow in the film boiling region. When the liquid film is nearly depleted, the liquid film breaks down into rivulets. This phenomenon is commonly referred to as dryout and the corresponding heat flux is referred to as Critical Heat Flux (CHF). The heat transfer deteriorates due to the appearance of dry patches resulting in a sudden rise in wall temperature above the wetting temperature of the droplets. The entrained liquid can no longer contact the heated wall. The vapour is superheated. Heat is transferred to the vapour by forced convection and some of the heat is transferred from the superheated vapour to the liquid droplets by evaporation at the droplet interface. At dryout, the heat transfer coefficient suddenly drops substantially to a value close

to that expected for single-phase forced convection to dry saturated vapour. As the quality increases, the vapour velocity increases resulting in increasing heat transfer coefficient. In a temperature control system, an additional regime between the annular and the liquid deficient flow regimes can be indentified. This regime is referred to as the liquid deficient flow in the transition boiling region in which the liquid film breaks down into rivulets and small dry patches appear intermittently. When the wall temperature is low enough, the droplets can wet the wall resulting in fluctuating wall temperature.

(g) Superheated vapour. All the droplets are evaporated and the vapour is superheated. Heat transfer is by forced convection.

The boundaries of various heat transfer modes with heat flux and thermodynamic quality as parameters are shown schematically in Figure 2. The locations of the boundaries are, of course, affected by the pressure and mass flux.

The flow regimes, which are determined in experiments, are usually presented in flow regime maps. In constructing the flow regime maps, a large variety of parameters have been used. These parameters include Weber number, Froude number, mass flux, volumetric flow of each phase and quality. It is clear that there is no general agreement as to which parameters should be used in constructing flow regime maps. For application to a boiling channel, flow regime mpas with mass flux and

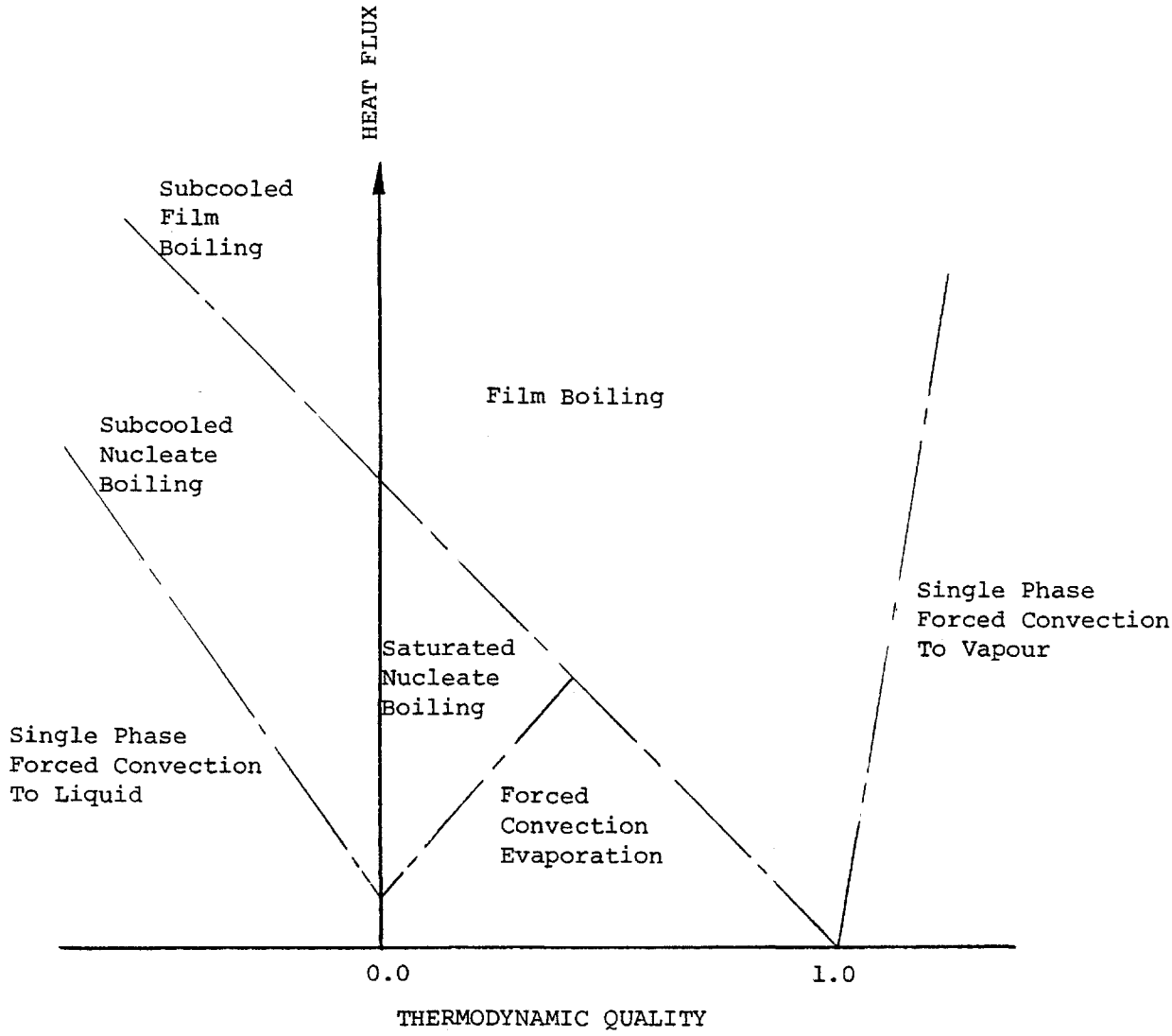

FIGURE 2: BOUNDARIES OF TWO-PHASE HEAT TRANSFER MODES (FROM COLLIER [1])

quality as parameters are probably more convenient to use. Typical flow regime map obtained by Bennett et al., [5], is shown in Figure 3. Saito, [6], in his literature survey, had found more than thirty different flow regime maps. In general, the flow regime data are not well defined due to different descriptive definitions of flow regimes, especially the flow regime boundaries which change gradually. It is therefore necessary to use the flow regime maps with caution.

In addition to flow regime maps constructed with experimental data, flow transition prediction techniques have been proposed. More recently, Taitel and Dukler [7] compared several techniques to experiments and found several discrepancies in the quantitative aspects as well as in the general trend of the transition curves. The discrepancies would be due to the subjective definition of the flow patterns, and to the rather simplistic selection of the parameters governing various transitions. Taitel and Dukler went back to physical mechanisms for the transitions and derived transition criteria defined by parameters, which are different for different flow regimes (as listed in Table 1 and shown in Figure 4).

2.2 Boiling Curve

In a diabatic system, the surface temperature and the surface heat flux are coupled. The relationship of the surface temperature and the surface heat flux can be represented by the boiling curve as shown in Figure 5. As the surface temperature is increased, heat is transferred

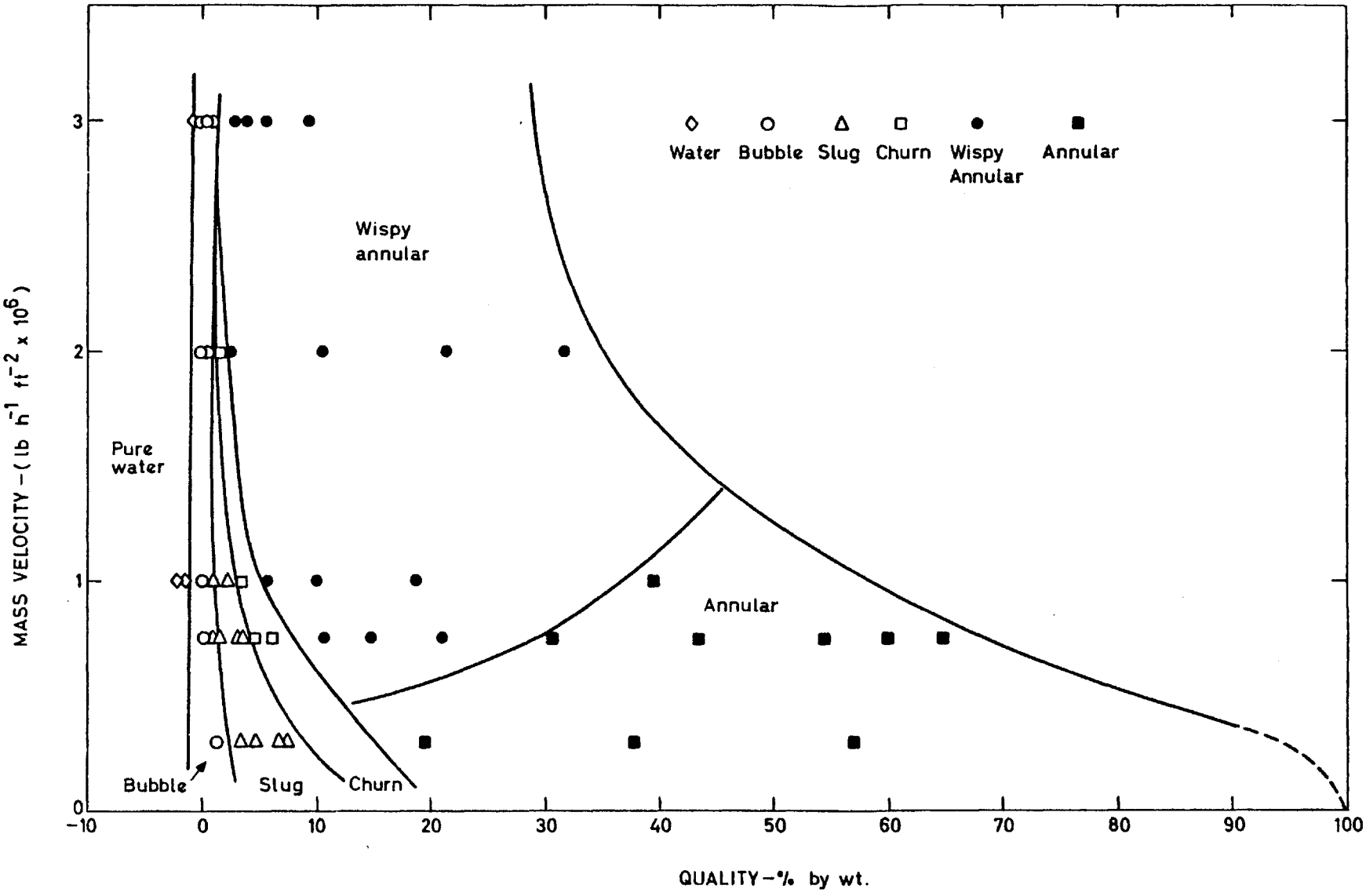

FIGURE 3 : FLOW REGIME MAP OF BENNETT (FROM [5])

TABLE 1: TAITEL AND DUKLER FLOW TRANSITION CURVES AND DEFINING PARAMETER

	Parameters		Transition Curve Defined As
	Y-axis	X-axis	
Bubbly flow to slug flow (churn flow)	$\frac{J_L}{J_G}$	$\frac{J_G \rho_L^{1/2}}{[g(\rho_L-\rho_G)\sigma]^{1/4}}$	$\frac{J_L}{J_G} = 2.34-1.07 \frac{[g(\rho_L-\rho_G)\sigma]^{1/4}}{J_G \rho_L^{1/2}}$
Slug flow to churn flow	β	$\frac{J_m}{\sqrt{gD}}$	a complex equation that involves the liquid Reynolds number, $\rho_L J_V D/\mu_L$ and the liquid kinematic viscosity, μ_L/ρ_L
Slug flow (churn flow) to annular flow	$\frac{J_G \rho_G^{1/2}}{[g(\rho_L-\rho_G)\sigma]^{1/4}}$	X	$\frac{J_G \rho_G^{1/2}}{[g(\rho_L-\rho_G)\sigma]^{1/4}} = 3.09 \frac{(1+20X+X^2)^{1/2}-X}{(1+20X+X^2)^{1/2}}$

where $J_k = \frac{x_k G}{\rho_k}$, $k=L,V$

$$X = \left[\frac{\left(\frac{dP}{dZ}\right)_L}{\left(\frac{dP}{dZ}\right)_V}\right]^{1/2}$$

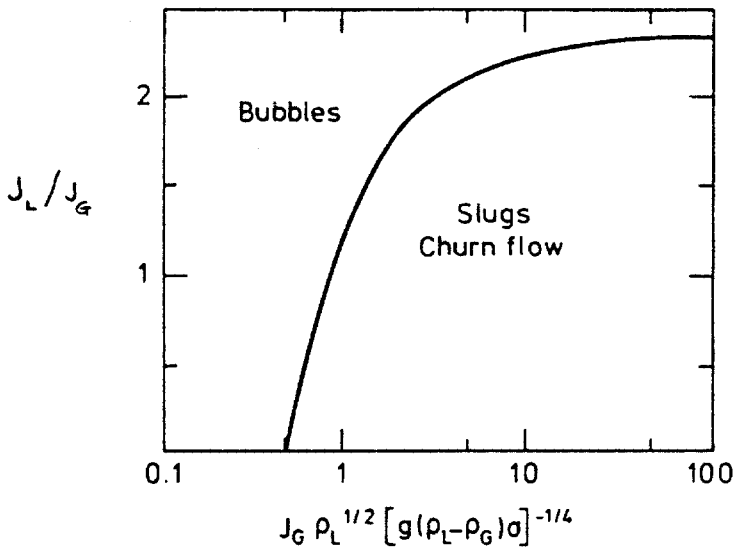

(a) Between Bubbly Flow and Slug or Churn Flow

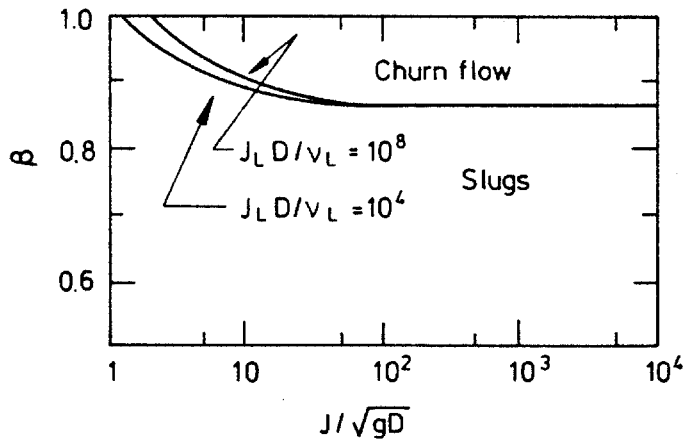

(b) Between Slug Flow and Churn Flow

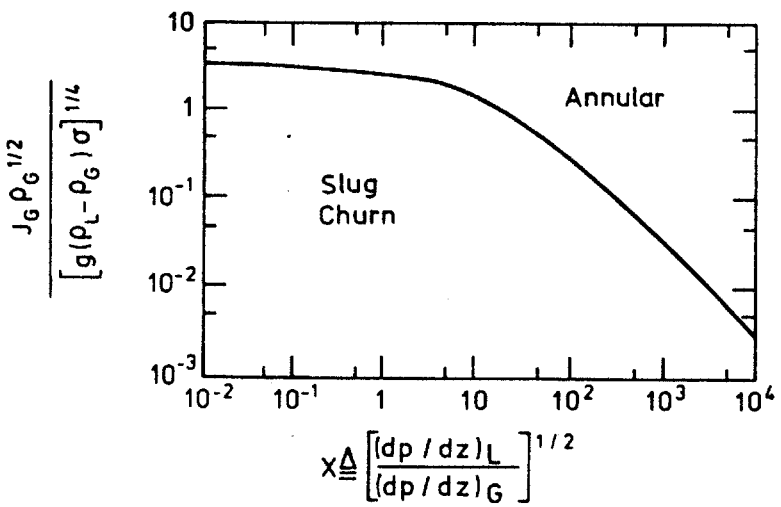

(c) Between Slug Flow or Churn Flow and Annular Flow

FIGURE 4: FLOW REGIME MAP BY TAITLE AND DURKLER PREDICTION METHOD (FROM TAITLE AND DURKLER [7])

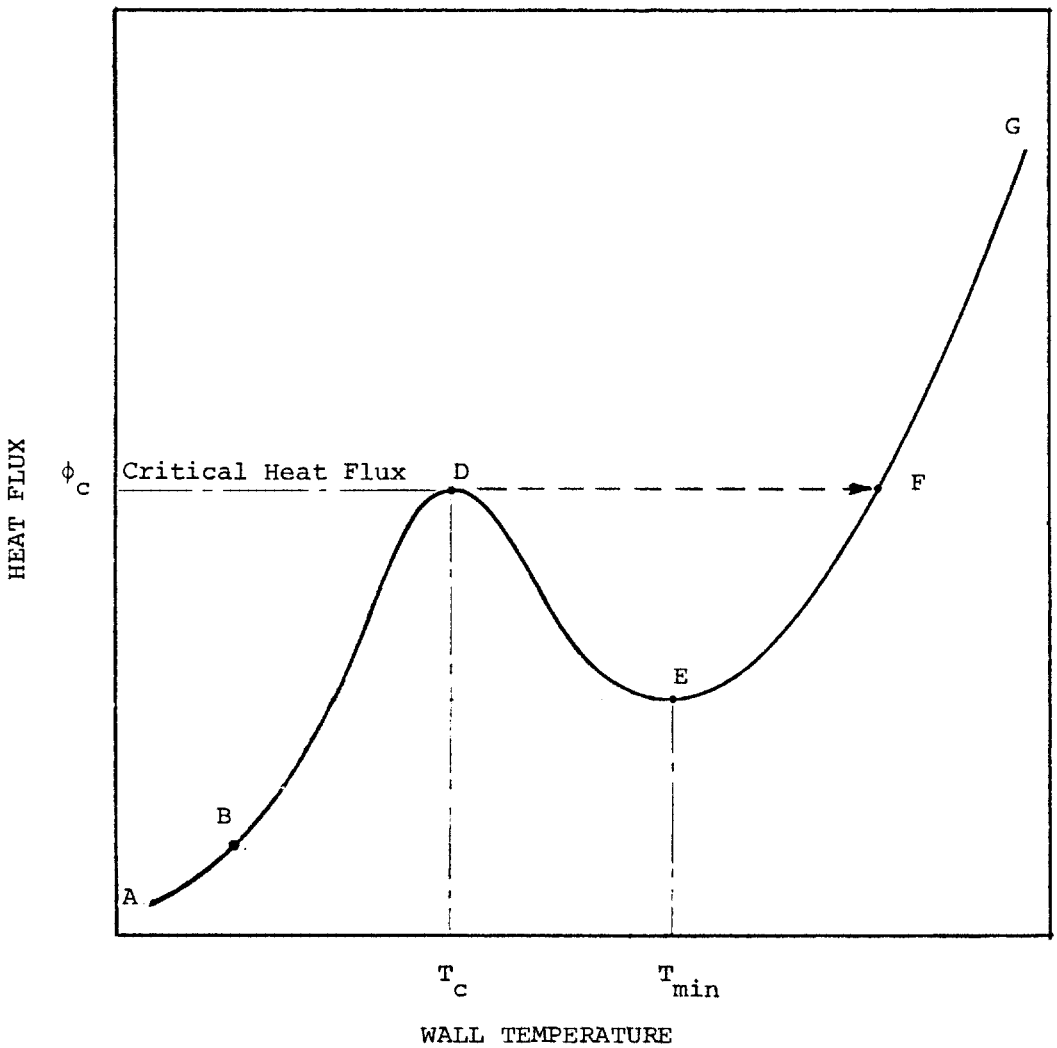

FIGURE 5: BOILING CURVE

by single-phase forced convection between points A and B. After point B, the principal mode of heat transfer is nucleate boiling or forced convective evaporation until CHF is reached at point D. Beyond CHF at point D, in a temperature controlled system, unstable film boiling occurs until point E at which the temperature exhibits a minimum. It is generally believed that above this minimum temperature, droplets cannot wet the wall and heat is transferred by film boiling.

In a heat flux controlled system, as in an electrically heated head, if the heat flux is increased, the part of the boiling curve from point A to point D is followed. Upon reaching CHF at point D, a further small increase in heat flux causes the wall temperature to jump along the dotted line to F. Sometimes the wall temperature at point F is so high that physical burn-out of the heater can result. If no physical destruction of the heater occurs, further increase in heat flux will raise the wall temperature along the path F-G.

2.3 Boiling Crisis

The phenomenon of sudden deterioration of heat transfer on the heater surface has been extensively studied. Although complete fundamental understanding of such phenomenon has not been obtained, numerous mechanisms for this boiling crisis have been proposed in the literature. The dominant mechanisms which occur under most experimental conditions and are generally accepted are summarised as:

(a) Bubble clouds. In subcooled and saturated nucleate boiling, a layer of bubbles (Tong, [8]) moves along the heated surface. The amount of liquid contacting and cooling the surface is controlled by the thickness of the bubble layer. An increase in heat flux increases the bubble layer thickness. If the bubble layer is thick enough to impede cooling liquid from reaching the surface, a vapour blanket forms over the surface and the heat transfer changes from nucleate boiling to film boiling. Such a boiling crisis is generally referred to as DNB (Departure from Nucleat Boiling). The rise in the heated surface temperature is very fast and often results in physical destruction of the heated surface.

(b) Hot spot under bubble. When a bubble grows on the heated wall, a dryspot forms as the microlayer underneath the bubble is being evaporated. The dryspot is rewetted when the bubble departs from the wall and the process repeats again. At high heat flux, the wall temperature may become too high to prevent rewetting of the dryspot, resulting in dryout. This mechanism was proposed by Kirby [9].

(c) Liquid Film Breakdown. In annular flow, the liquid film moves along the heated wall and mass transfer occurs across the liquid-vapour interface in the forms of entrainment, deposition and evaporation. If the entrainment and evaporation rate exceed the droplet deposition rate, the liquid film is depleted and its thickness decreases along the length. Eventually the liquid film breaks down into rivulets [10]. At low heat flux, the rivulets are mobile and cooling is maintained until the rivulets

are evaporated at dryout and the liquid film flow rate is very close to zero. At high heat flux, the mobility of the rivulets are restricted and wall temperature excursion occurs when the liquid film breaks down. The liquid film flow rate is small but finite. In the theoretical prediction of dryout in the annular flow, film breakdown is usually neglected and dryout is assumed to occur when the film flow rate approaches zero. When the heat flux is high and the liquid film is thin, breakdown of the liquid film may occur due to nucleation in the liquid film. Nucleation in the liquid film was noticed by Hewitt et al. [11] and also by Styrikovich et al. [12]. If the size of the vapour bubble exceeds the thickness of the liquid film, the liquid film is discontinued and a dryspot is formed. If the dryspot temperature is high enough to prevent rewetting from taking place, dryout will occur. It is also possible for the liquid film to break down if the liquid film flow rate falls below the minimum wetting rate (Groeneveld [3]).

2.4 Post-CHF Heat Transfer

As discussed in Section 2.2, heat transfer beyond CHF is represented by the region D-G of the boiling curve (Figure 5). This part of the curve includes the transition boiling (D-E) and stable film boiling* (E-G) in a temperature controlled system. Heat transfer in the transition boiling is a combination of unstable film boiling and unstable nucleate boiling. Just beyond CHF, the heater surface is covered by

* The terms "transition boiling" and "film boiling" have definite meanings in pool boiling heat transfer. However, these terms have also been commonly used in convective heat transfer although the meanings are less definite.

vapour, heat transfer has deteriorated drastically. The corresponding decreases in local vapour generation allows the liquid to rewet the heater surface momentarily. During transition boiling, the heater surface is characterized by frequently appearance of vapour patches and liquid.

In a heat flux controlled system, after dryout has occurred, the heat transfer mode is the stable film boiling which is represented by regions F-G on the boiling curve (Figure 5). In stable film boiling, heat is transferred from the heater surface by radiation, convection to the vapour and interaction of the liquid and the heater surface. The pattern of the fluid, according to Groeneveld and Gardiner [4], is believed to be:

(a) A continuum of vapour with droplets dispersed in the vapour. This is commonly known as the liquid deficient regime and usually occurs at high void fraction, $\alpha > 80\%$ (Figure 6a).

(b) An annular vapour flow with a continuous liquid core known as the inverted annular flow regime which occurs when $\alpha < 30\%$ (Figure 6b).

(c) A transition of (a) and (b) and is usually in the form of slug flow (Figure 6c).

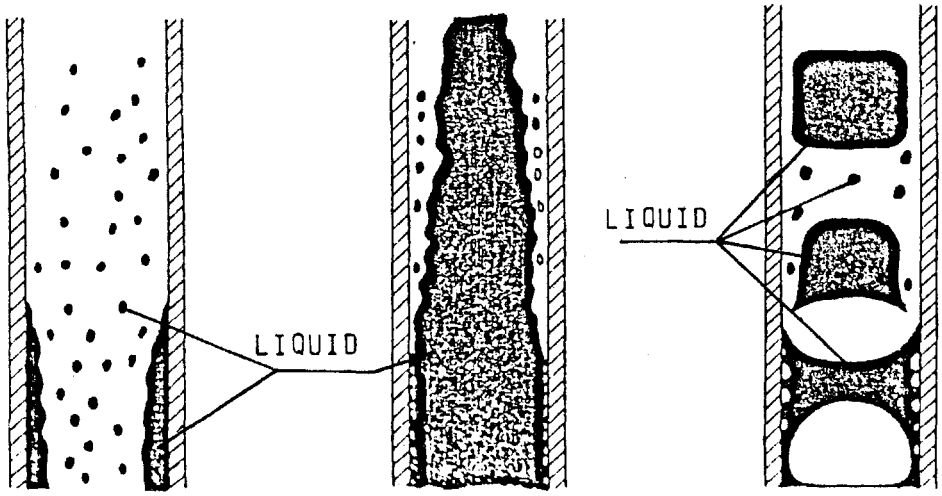

FIGURE 6: REGIMES DURING FILM BOILING
(FROM GROENEVELD AND GARDINER [4])

In the liquid deficient region of a heated tube, all the liquid are entrained in the vapour core and heat is transferred from the wall to the vapour. Just downstream of the dryout location, the vapour and the droplets are close to the saturation temperature and little heat transfer takes place between the vapour and the droplets. Further downstream where the vapour is sufficiently superheated, considerable heat is transferred to the droplet to evaporate them. With superheating of the vapour, which had been measured by Mueller [13], the actual quality becomes lower than the thermal equilibrium quality. Depending on the wall temperature, the droplets may wet the wall. As the droplets entre the vapour boundary layer, direct vapour-droplet heat transfer increases because of higher vapour temperature near the wall. In addition, the disruption of the vapour boundary by the droplets enhances vapour-wall heat transfer.

In the inverted annular flow, a layer of vapour film moves on the wall while the liquid travels as a continuous core in the centre at a slower velocity than the vapour. Heat is transferred by convection from the wall to the vapour film and by evaporation of the liquid at the interface. Since the vapour film is thin and the forced convective evaporation heat transfer is efficient, the bulk vapour temperature is assumed to be at or close to the liquid core temperature. The vapour-liquid interface is irregular. This may result in entrainment of liquid in the vapour film and subsequently enhancement of the convective heat transfer. In the liquid core, vapour bubble may be present but they have little effects except to change the core velocity.

The transition of flow regimes (a) and (b) is much less known. Groeneveld and Gardiner [4] described it to occure:

> at low flows and void fractions which are too high to support inverted annular film boiling but too low to support dispersed flow film boiling. In tubes, it is formed just downstream of the inverted annular flow region when the liquid core breaks up into slugs of liquid in an otherwise vapour matrix. ..... Kalinin [14] observed another possible mechanism for the onset of slug flow in their transient tests. Immediately after the introduction of liquid to their test section, the sudden increase in vapor volume due to vapor generation at the leading edge of the liquid caused a back pressure which decelerated the flow. The higher pressure and lower flow rate caused a decrease in vaporization and the flow surges forward. This cycle was repetitive with a liquid slug separating from the liquid core with each cycle.

3. EXPERIMENTAL APPARATUS

3.1 Test Loop

The tests were conducted in the high pressure test loop shown schematically in Figure 7. Water is circulated in the loop by two pumps, each of which is rated to provide a head of about 1.0 MPa at a flow rate of 19 $kg.s^{-1}$, which were connected in a series arrangement to give discharge pressures up to 12 MPa. The subcooled water at the pump discharge is heated to the required test section inlet temperature by an electrical preheater (up to 0.3 MW). An electric boiler (up to 3.0 MW) is also available to provide two phase conditions at the test section inlet.

The effluent from the test section goes to a separator with the steam from the separator going to a condenser through a pressure control valve to maintain the system pressure while the water is recirculated to the pumps. A high pressure feedwater pump supplies deionized make up water at the inlet of the circulating pumps to maintain subcooled conditions for the pumps.

Quick-acting valves were provided at the inlet and outlet of the test section to isolate it from the main loop, in case it ruptured due to electrical arcing during the test.

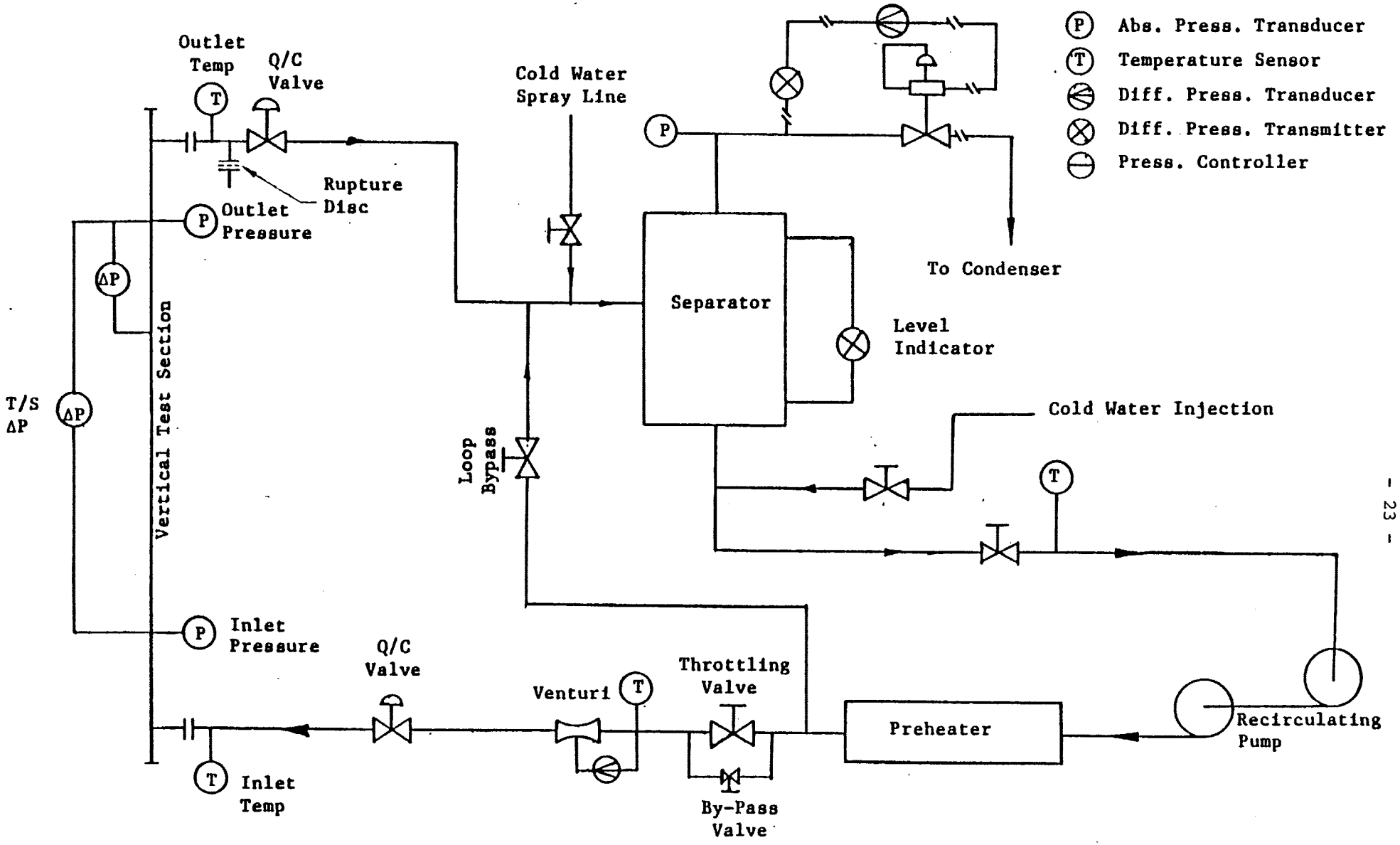

FIGURE 7: LOOP SCHEMATIC

3.2 Test Section

The annular test section, shown schematically in Figure 8, consisted of a vertically mounted, unheated shroud and a heated, concentric inner cylinder. The shroud was made of Inconel 600 and had an outside diameter of 19.1 mm, a wall thickness of 1.1 mm and an overall length between connecting flanges of 5.48 m. There were nine pressure taps, installed at an equal spacing of 0.61 m along the heated length, for measurement of pressure drop. In the present experiments, only the pressure taps at the inlet, the exit, and 0.61 m upstream of the end of the heated length, were used.

Two interchangeable inner heaters were fabricated with identical external geometry, outside diameter of 12.7 mm and heated length of 4.88 m; one directly heated and the other indirectly heated.

The direct heater, shown in Figure 9, had its heated length made of Inconel 600 tubing of 12.7 mm O.D. with a wall thickness of 0.89 mm. The heater extensions at both ends were made of Nickel 200 with the same outside diameter as the heater. A solid rod was welded to the downstream end and heavy walled tubing was brazed to the upstream end of the heater. The bore of the upstream heater extension was sufficient to allow passage of instrumentation wires.

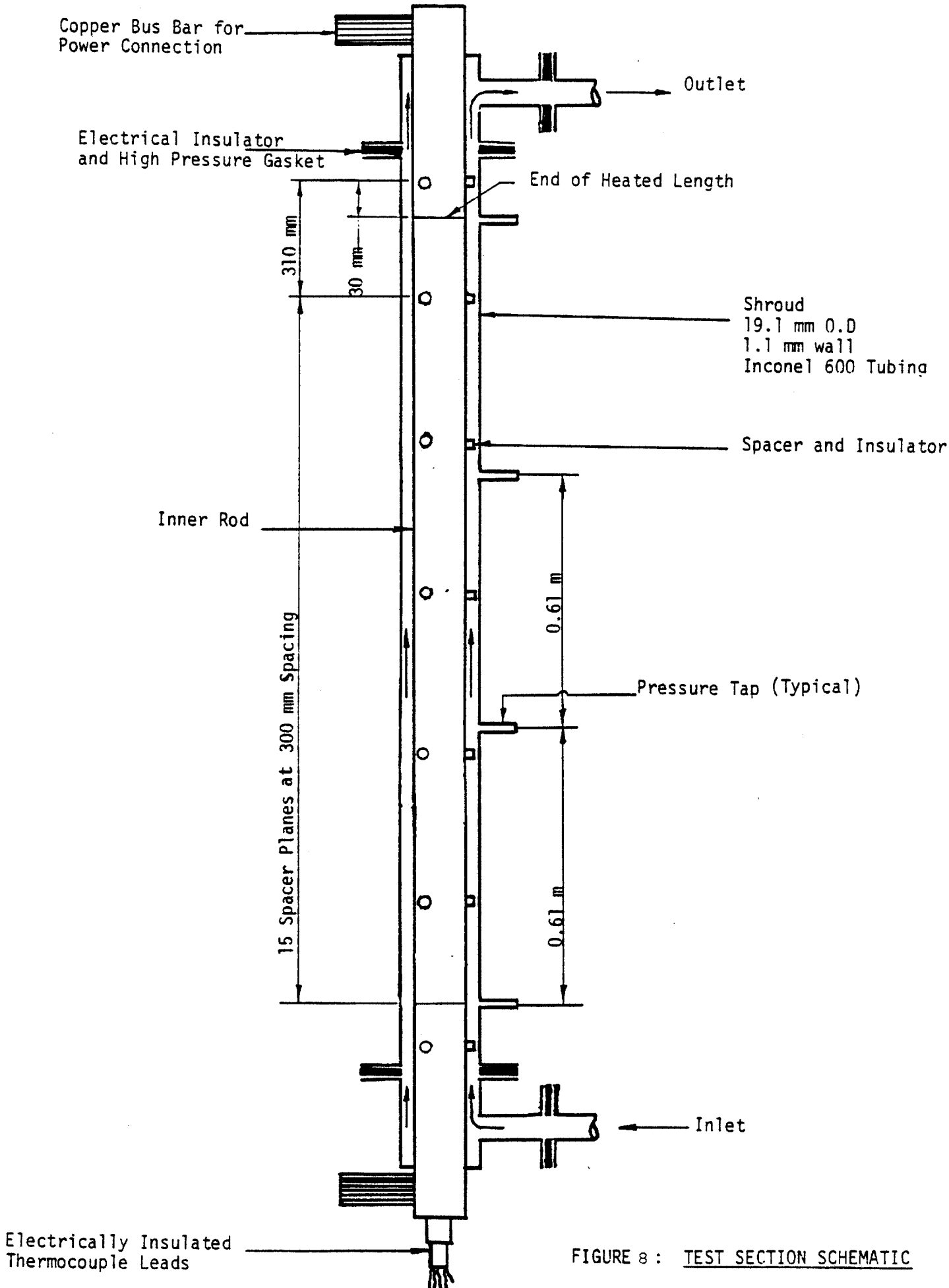

FIGURE 8 : TEST SECTION SCHEMATIC

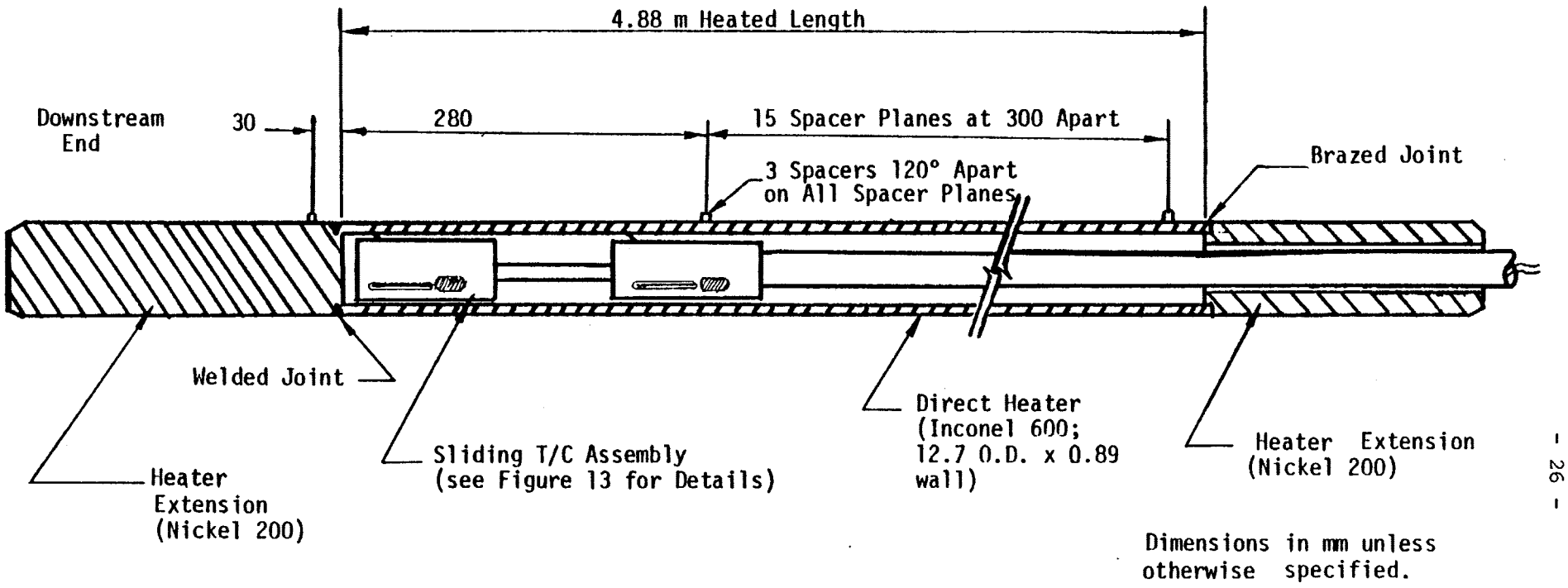

FIGURE 9: DIRECT HEATER ASSEMBLY

The indirect heater, shown in Figure 10, had an inner filament made of Inconel 600 tubing having an outside diameter of 8.72 mm and a wall thickness of 0.93 mm. The electrodes were 8.89 mm in diameter and were made of nickel plated copper rod having a short transition piece of Nickel 200 rod brazed to the copper and welded to the ends of the heater filament. Hot pressed boron nitride was machined into sleeves and used as the electrical insulation between the heater filament and the sheath. The sleeves centred the heater filament during the swaging of the sheath. An over-sized Inconel 600 tube with 15.24 mm O.D. and 0.76 mm wall was used for the sheath due to its availability. The tube was first swaged to an intermediate size of 13.72 mm O.D. and 0.89 mm wall and annealed, then assembled with the heater and swaged to the final outside diameter of 12.7 mm. Since materials grow axially during swaging, only the downstream electrode was installed before swaging. After swaging the heater was machined to the proper heated length at the upstream end and the electrode was welded to the heating filament. An Inconel 600 tube, having the same outside diameter and wall thickness as the swaged sheath, was welded to the sheath and the annular gap between the upstream electrode and the sheath was packed with boron nitride powder.

Spacers were installed on both heaters at sixteen axial planes along the inner rod as shown in Figures 9 and 10. The most downstream spacer plane was positioned at 30 mm downstream of the end of the heated length and the next upstream spacer plane was positioned 280 mm upstream of the end of the heated length. The other spacer planes were spaced 300 mm apart. At each spacer plane, three spacers were mounted at 120^{o}

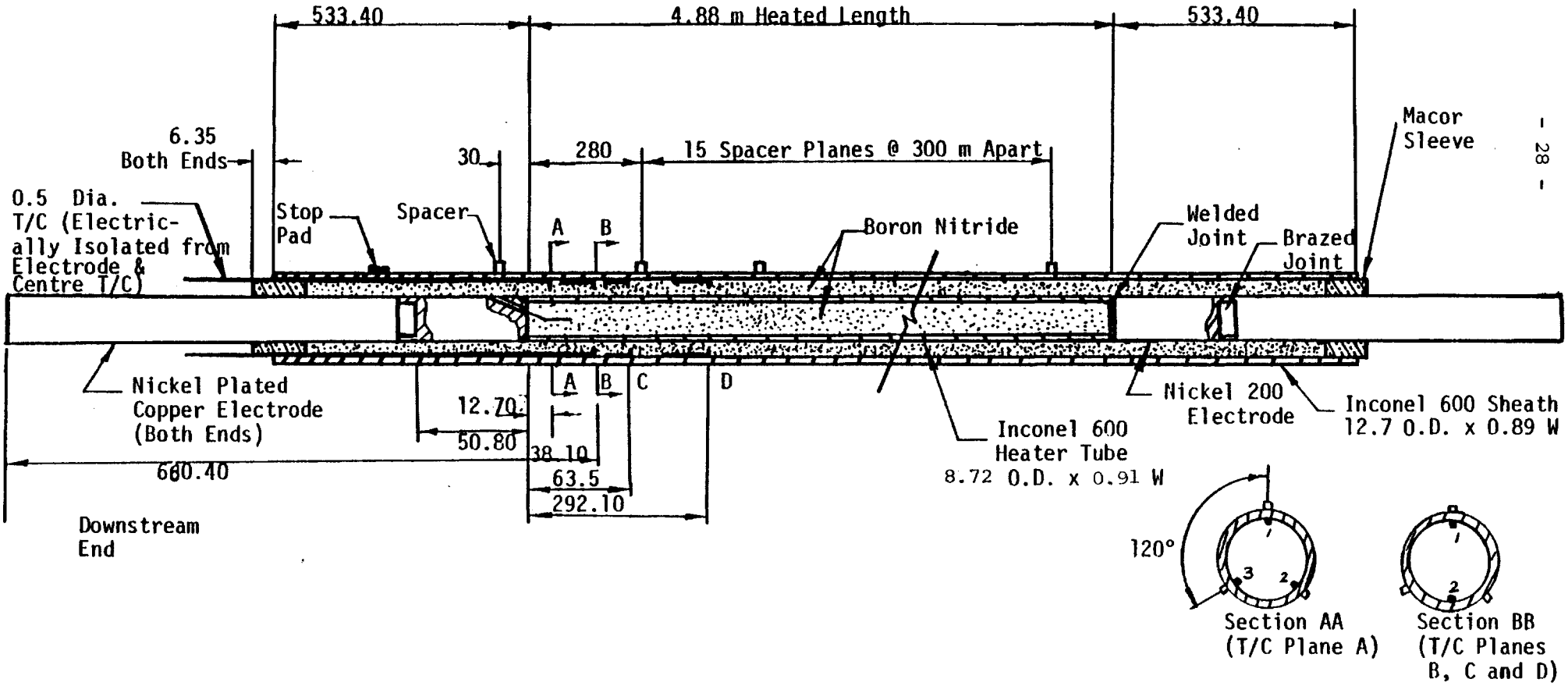

FIGURE 10: INDIRECT HEATER ASSEMBLY

around the circumference to maintain the annular gap with the shroud. For the directly heated rod, the spacers also provided the electrical isolation of the inner rod from the shroud. The spacer assembly shown in detail in Figure 11 was made by brazing a S.S 304 stud of 2.06 mm diameter onto the heater sheath. The stud was then ground to a height of 1.42 mm and a ceramic spacer cap made of Alumina HT-997 was placed onto the stud. The inner rod was circumferentially oriented in the shroud with a line of spacers opposite to the pressure taps. This line of spacers was taken to be the 0^{o} angular reference position for the angular location of the thermocoupler.

3.3 Instrumentation

The locations of the various loop instruments are shown in Figure 7. The test section flow rate was measured by a venturi meter. Water temperatures were measured using 3.2 mm diameter Chromel-Alumel thermocouples (ANSI Type K) inserted directly into the flow stream.

The pressures at both the upstream and downstream ends of the test section were measured using strain gauge pressure transducers (Viatran Model 304) and a precision Heise gauge. Pressure drop measurements across the heated length and across the 0.61 m section just upstream of the end of the heated length were made using strain gauge differential pressure transducers (Viatran Model PTB 209).

Power was supplied to the test section from a fully regulated 4 MW, three phase, AC power supply. The test section was connected

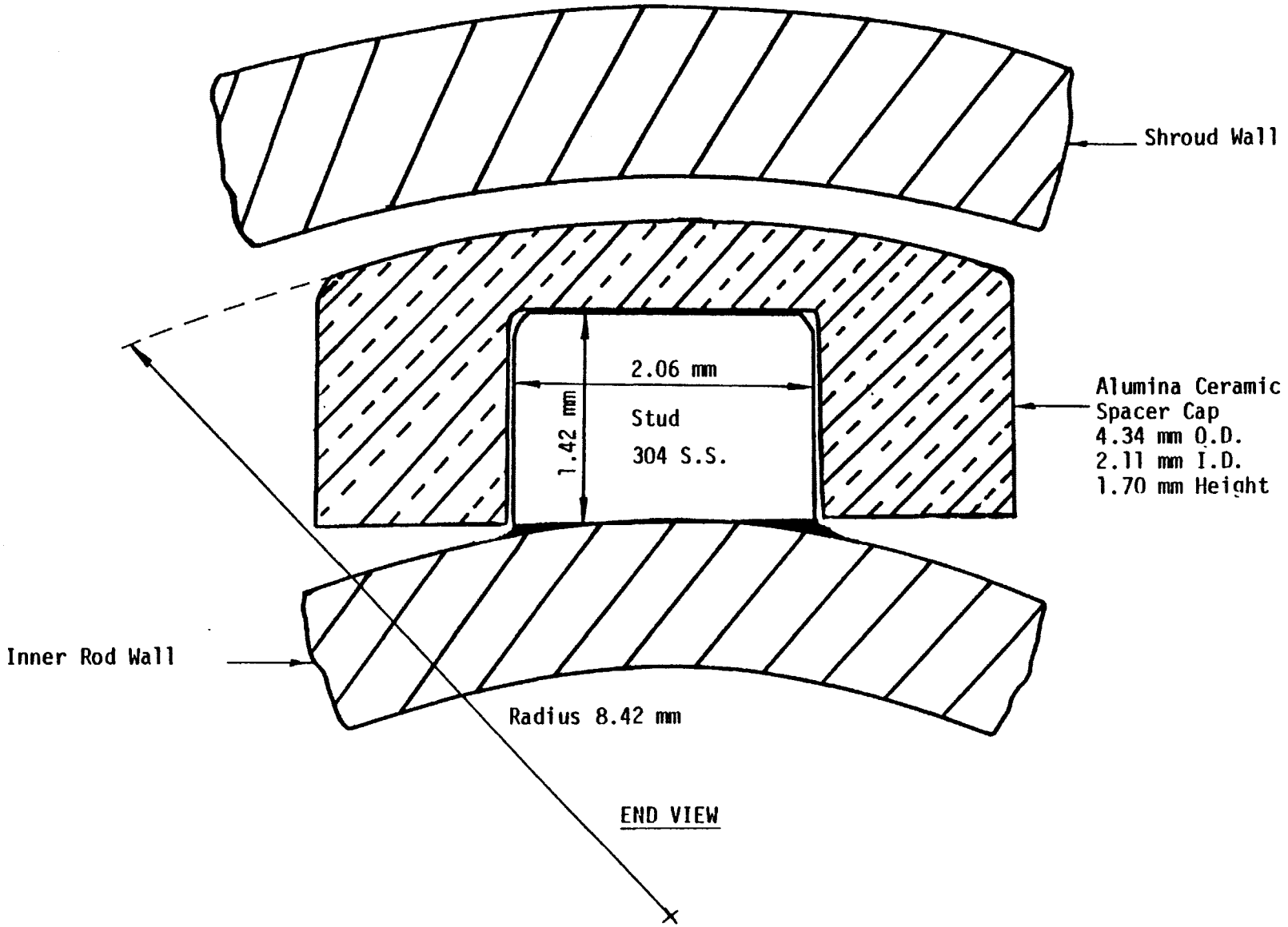

FIGURE 11: SPACER DESIGN

between one phase and neutral with the shroud floating at a potential approximately equal to the midpoint voltage of the inner rod. A ground fault detector, whose circuit is shown in Figure 12, was used to indicate the occurrence of an electrical short (contact) between the shroud and the direct heater.

The direct heater was instrumented with the sliding thermocouple assembly shown schematically in Figure 13. Three, 1.0 mm diameter, Inconel 600 sheathed, ungrounded junction, Chromel-Alumel (ANSI Type K) thermocouples were installed 120^{o} apart on a ceramic carrier. The 1.0 mm diameter thermocouples were joined to 0.5 mm diameter, Inconel 600 sheathed, thermocouple extension wires. The connections, which provided electrical discontinuity of the metal sheaths were potted in glass frit to seal off moisture. The carriers were attached by resistance welded pins to a stainless steel push rod which was insulated from the inside wall of the direct heater by ceramic fibre sleeving and centred by ceramic sleeves spaced at intervals. The thermoscouple assembly was connected to a remotely controlled actuator, supplied by CRNL, which provided up to 0.45 m of axial motion and 360^{o} of rotation in both directions. Thus, the inside wall temperature of the region extending 0.45 m upstream of the downstream end of the heated length could be monitored during the experiments.

The indirect heater was instrumented with a total of ten 0.5 mm diameter, Inconel 600 sheathed, ungrounded junction, Chromel-Alumel thermocouples (ANSI Type K), as shown in Figures 10 and 14. Nine of the

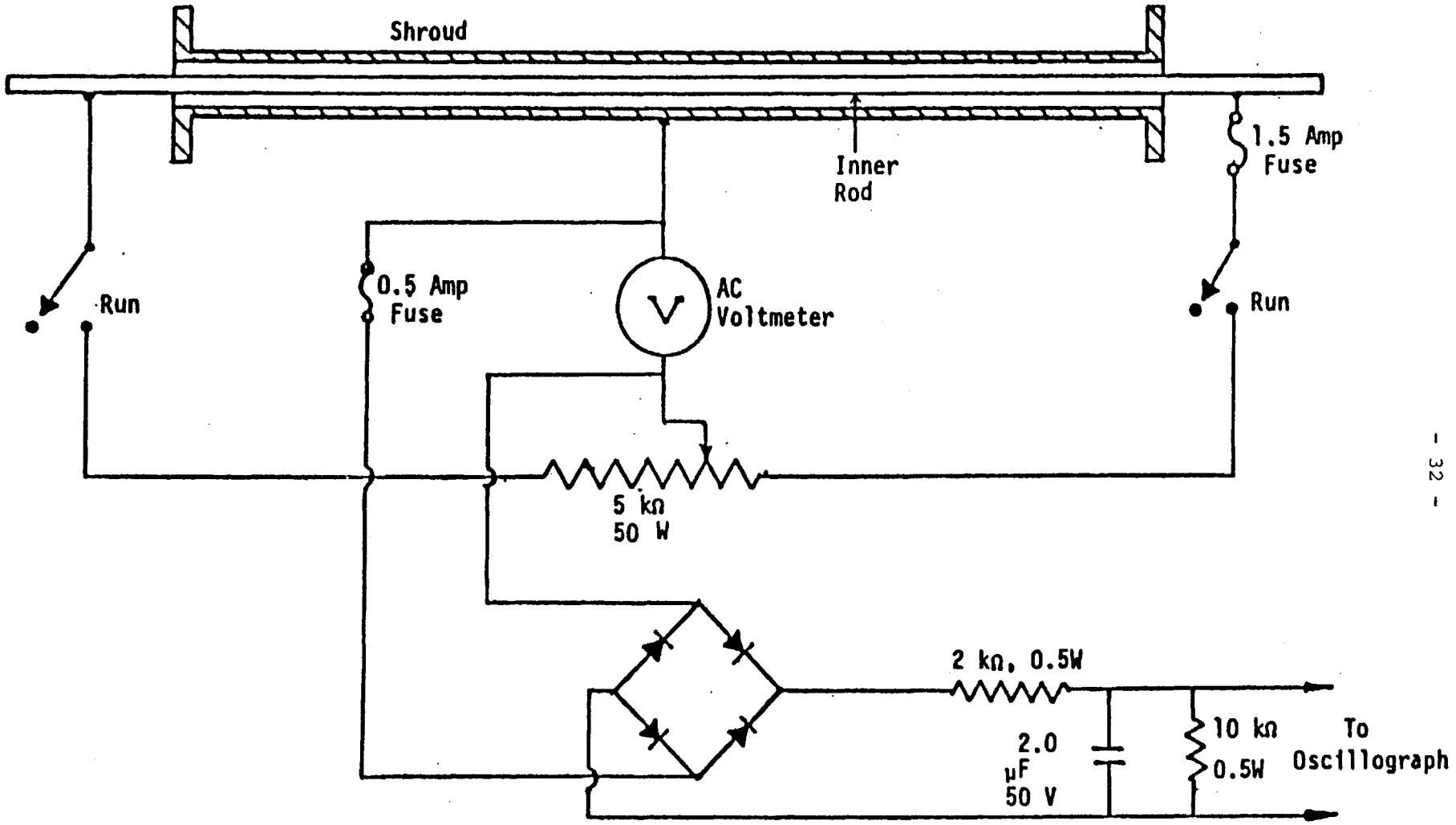

FIGURE 12: GROUND FAULT DETECTOR

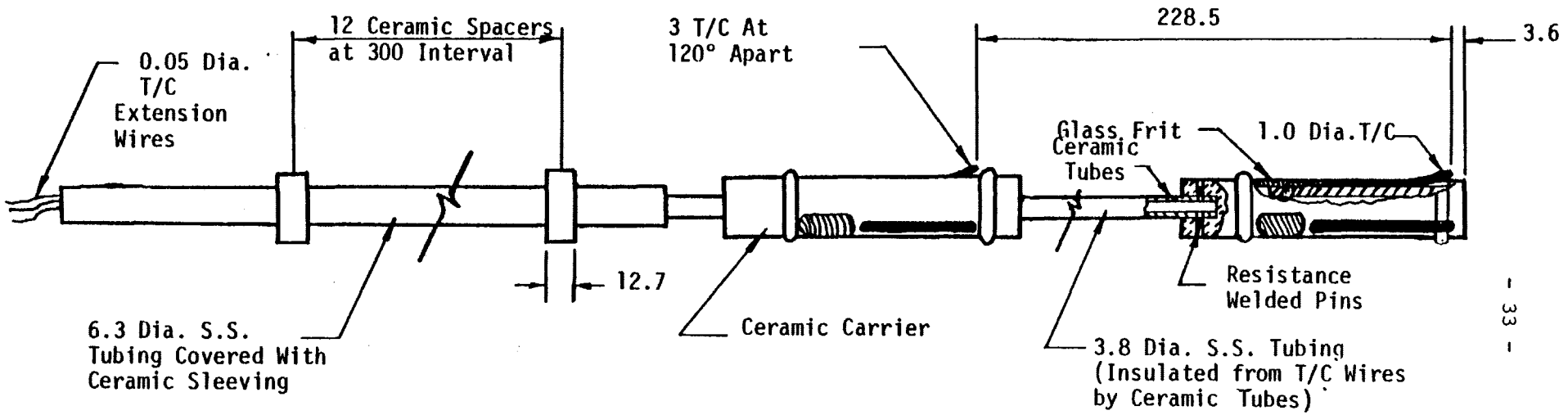

Dimensions in mm.

FIGURE 13: SLIDING THERMOCOUPLE ASSEMBLY

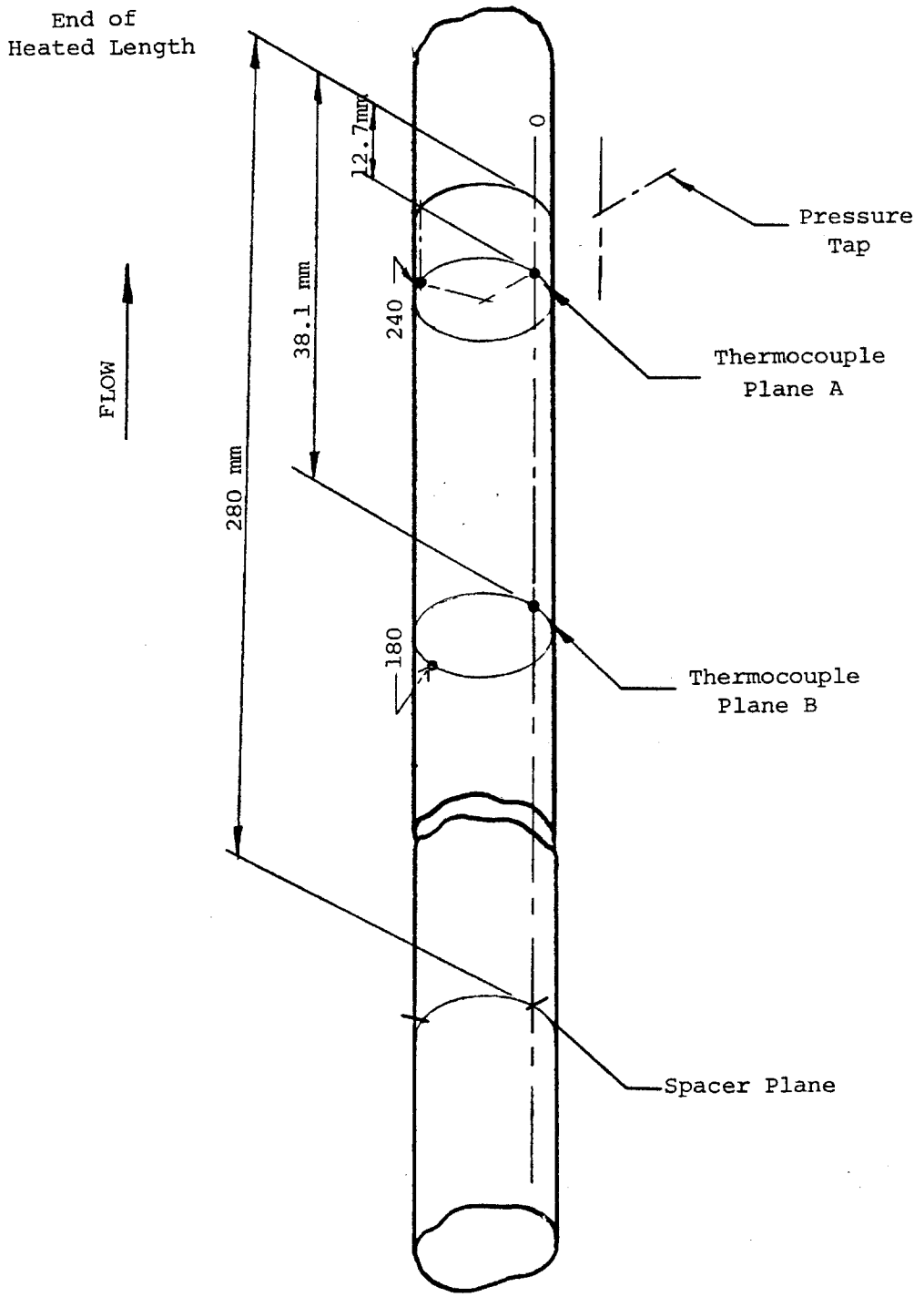

FIGURE 14: THERMOCOUPLE LOCATIONS FOR THE INDIRECT HEATER

thermocouples were mounted on the inside surface of the sheath at axial planes, A, B, C, and D, at 12.7, 38.1, 63.5 and 292.1 mm respectively from the downstream end of the heated length. Three thermocouples were mounted 120° apart on plane A and two thermocouples were mounted 180° apart on the other planes. These thermocouples were placed in grooves machined in the outer surface of the boron nitride sleeves before assembly and swaging of the sheath. One thermocouple was also installed in the centre of the heater to a depth of 38.1 mm upstream of the downstream end of the heated length.

In both heaters, all of the thermocouples were calibrated prior to assembly in a furnace over the range 250°C to 800°C prior to assembly.

4. EXPERIMENTAL PROCEDURES

The loop was warmed up to accordance with the standard loop operating procedures. After pressure and flow conditions were established, power was applied to the preheater and the test section to bring the loop up to the required temperature. When the required pressure, flow and inlet temperature conditions had been reached, the power to the test section was increased gradually in small steps. After each increment of power, and when flow conditions became steady, the test conditions were checked and, if necessary, adjusted. The test section power was increased in this manner until one or more of the rod thermocouples showed an abnormal rise in the heater surface temperature, indicating dryout. Power was then decreased slightly to bring the test section out of dryout. Test conditions were checked and adjusted if necessary, and test section power was increased slowly until dryout occurred again. Experimental data were then scanned and recorded. Some CHF tests were checked for repeatability and the data were found to be within 2%.

In the case of the direct heater, the sliding thermocouple assembly was initially in the most downstream position, and after CHF conditions were indicated, the thermocouples were moved axially and rotated to search for other dryout locations. If other dryout patches were found, the test section power was reduced until dryout disappeared and the CHF conditions were approached again. This procedure was repeated as necessary to determine the lowest power level which would

produce dryout. After CHF was determined, the power was increased gradually to levels of 2, 4, 6, 8, 10, 12 and 15% above the critical power. The test was terminated after the 15% above CHF power or when the sheath outside surface temperature reached 550°C.

In the case of the indirect heater, where the thermocouples were not movable, after CHF conditions were indicated by one or more thermocouples the power was increased gradually to above the CHF level in the same steps as used for the direct heater. The data were recorded at the specified condition and at any other condition where one or more of the thermocouples indicated fresh dryout areas. Tests were terminated after the 15% above CHF power level or when the outside wall temperature reached 550°C.

5. RESULTS AND DISCUSSION

The format codes for the Run Names of the tests conducted, the CHF and Post-CHF results for both the direct heater and the indirect heater are given in Appendix A.

The tests were conducted at the following nominal test conditions:

Pressure, MPa	9.7
Mass flux, $Mg.s^{-1}.m^{-2}$	2, 3.5, 5
Inlet Quality, %	-10, -25, -40

The direct heater failed before the tests planned for the conditions of mass flux of 2 $Mg.s^{-1}.m^{-2}$ and inlet quality of -25%, and mass flux of 5 $Mg.m^{-2}.s^{-1}$ and inlet quality of -40% could be completed.

In the direct heater tests, the locations of the dryout front at various power levels were determined with the movable thermocouple assembly. The dryout front data were analyzed and the results are presented in Section 5.4.

During the indirect heater tests, the spacers just upstream of the downstream end of the heated length failed frequently, making it possible for the annulus to become excentric. Since electrical

insulation between the sheath and the heating element was provided by the boron nitride sleeves, the ceramic spacer caps between the sheath and the shroud were not essential and were replaced by stainless steel spacer caps having identical geometry as the ceramic ones. The change in heat transfer due to the stainless steel spacers, compared to the ceramic spacers, is small and no measureable effect on CHF is postulated.

For the calculations of system conditions, the thermodynamic quality was based on the pressure measured at the downstream end of the heated length and the test section heat flux was corrected for heat dissipation in the heater extensions.

5.1 Comparisons of CHF Performance of the Headers

In the tests for both types of heater, dryout was first detected near the downstream end of the heated length (approximately 10 mm from the end). A preferential angular location of dryout was observed in the heaters generally at 0^{o*} for the direct heater and at 240^{o*} for the indirect heater. However, the thermocouples at the 0^{o} and 240^{o} locations for the same heater usually indicated dryout within a 4% difference in test section power.

---

* See end of Section 3.2 and Figure 14 for definition.

Although upstream CHF* was not measured from the dry patch spreading data, which is discussed in detail in Section 5.4, information about upstream dryout can be deduced. It appears that upstream dryout did occur at a power approximately 4 to 6% above the initial critical power for both heaters. Figures 24 and 25 (in Section 5.3) show the spreading pattern of the upstream dry patch for the direct heater. It is clear that the upstream dry patch did not spread very far downstream of the spacer plane which was 280 mm from the end of the heated length. This implies that the upstream dryout occurred in the area just upstream of the spacer plane. In Figure 25, a small upstream dry patch was evident at a power level of 4% above the critical power. This shows that the upstream dryout did not occur uniformly around the heater. For the indirect heater, upstream dry patch spreading information was not available, however, similar upstream dryout phenomenon is expected.

On a system parameter basis, it is evident from Figure 15 that the differences in CHF between the two heaters were not significant. In general, CHF was about 2% lower for the indirect heater, except at the mass flux of 3.5 $Mg.s^{-1}.m^{-2}$, and inlet quality of -25%, where the indirect heater CHF was 6% lower and at mass flux of 5 $Mg.s^{-1}.m^{-2}$ and inlet quality of -10%, where the indirect heater CHF was 4% higher, both differences were well within the expected error band for these measurements.

---

* Upstream CHF refers to the CHF at which dryout occurs some distance upstream of the end of the heated length.

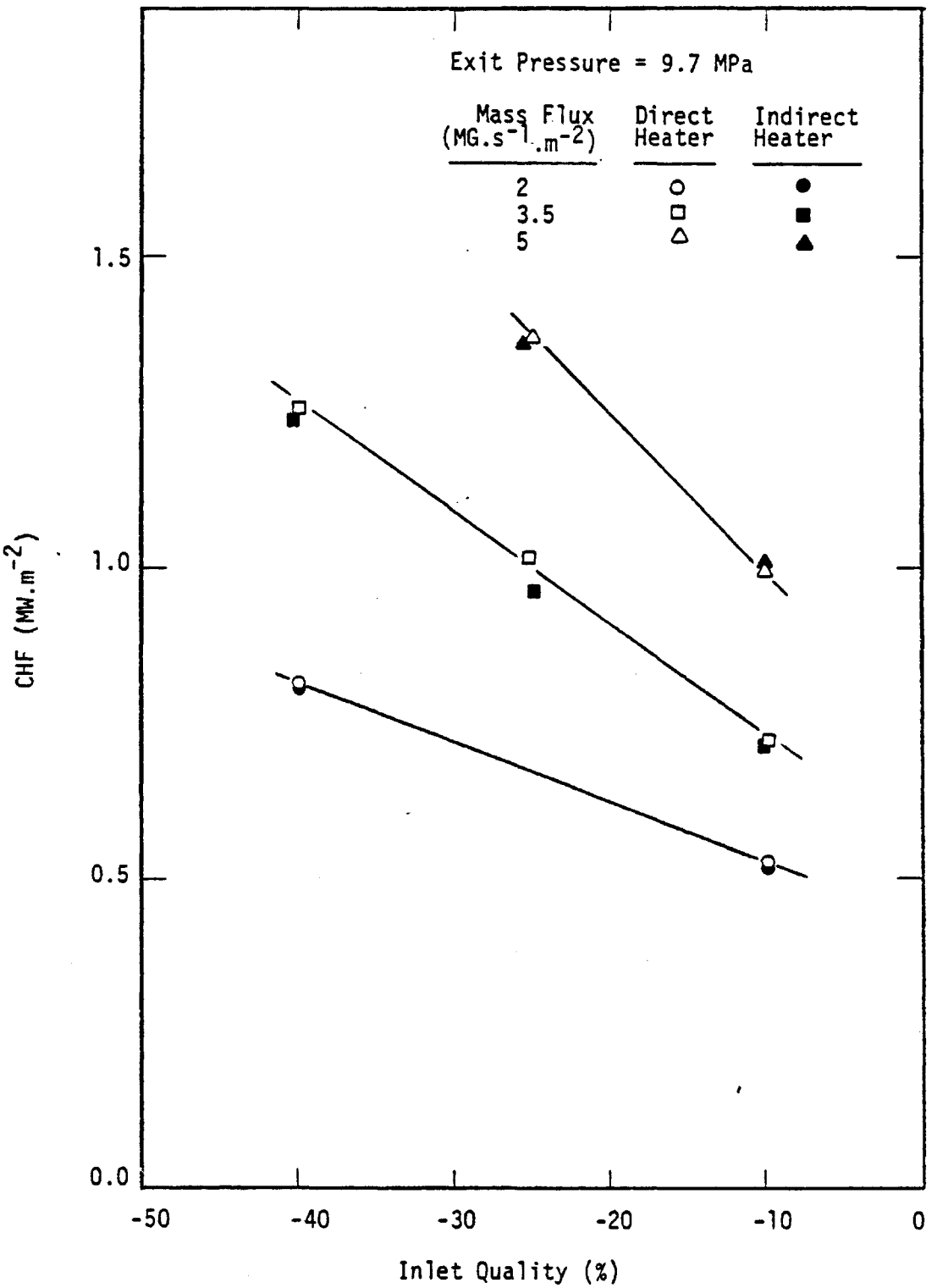

FIGURE 15: COMPARISON OF CHF DATA FOR THE DIRECT AND INDIRECT HEATER ON A SYSTEM PARAMETER BASIS

On a local conditions basis, the differences in CHF between the types of heaters appeared to be large. Figure 16 shows the comparison of CHF versus critical quality at various mass fluxes. Except at the highest mass flux, the indirect heater was lower in CHF than the direct heater, at the same quality.

5.2 Discussions of CHF Performance of the Heaters

Detailed descriptions of the construction of both the direct and indirect heaters were given in Section 3.2. The differences in the radial temperature profiles of the heaters at the same surface heat flux are shown in Figure 17. Other differences between the heaters were the surface finish and the heat generation rate at the heater extensions.

The direct heater surface finish was typical for cold drawn tubing products. The indirect heater was finished with 300 grit sand paper. Collier [1] indicates that the surface finish does not influence CHF except when it is so smooth that nucleation may become difficult. In annular flow, nucleation is usually suppressed, therefore the surface finishes of the two heaters are not expected to influence CHF.

Due to the instrumentation requirements and physical size limitations, the Joule heat generation in the upstream extension of the direct heater was about twice that of the indirect heater extension. However, this difference accounts for less than 1% error in the calculation of the local qualities. Therefore the comparison of CHF

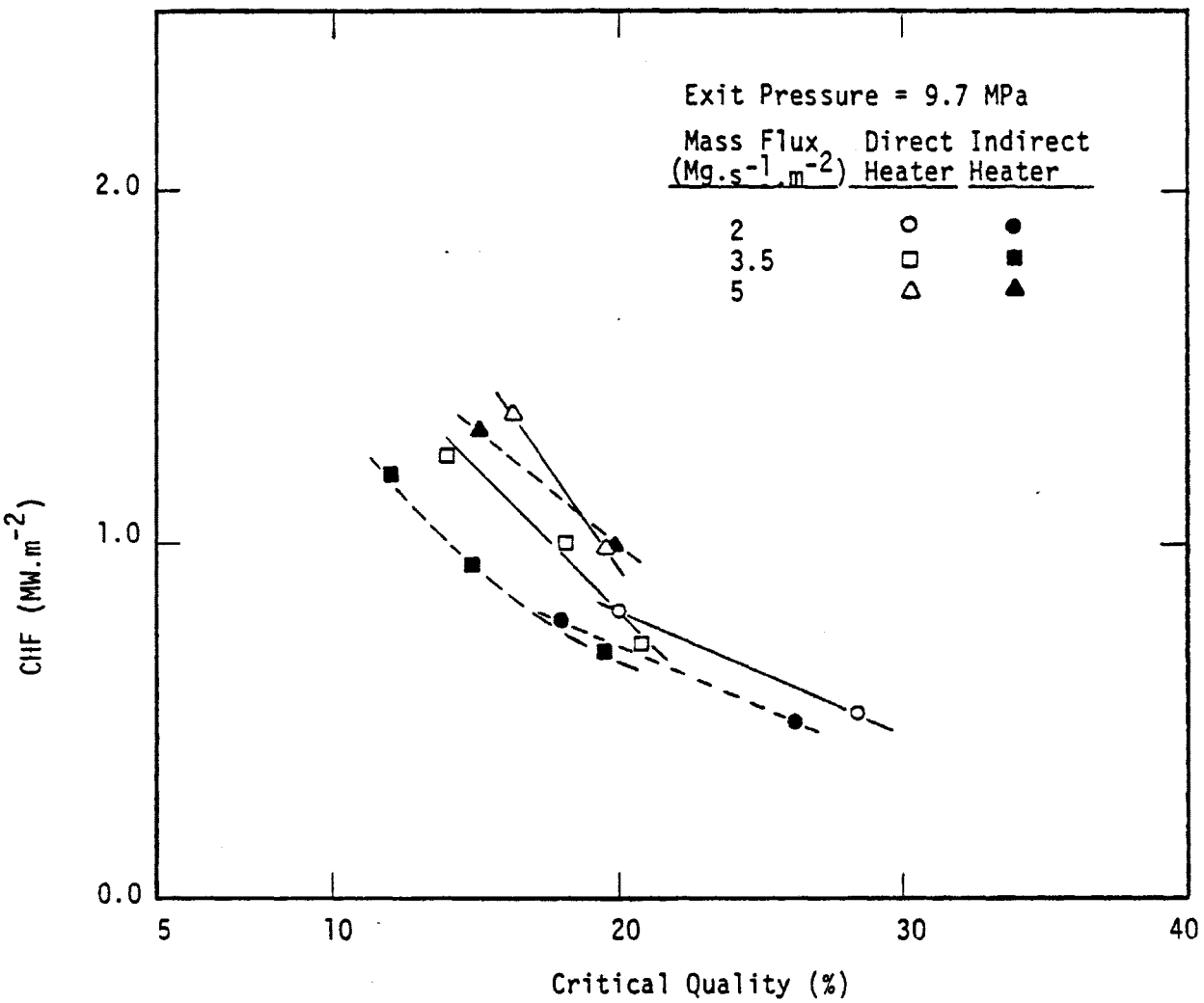

FIGURE 16: COMPARISON OF CHF DATA FOR THE DIRECT AND INDIRECT HEATER ON A LOCAL CONDITION BASIS

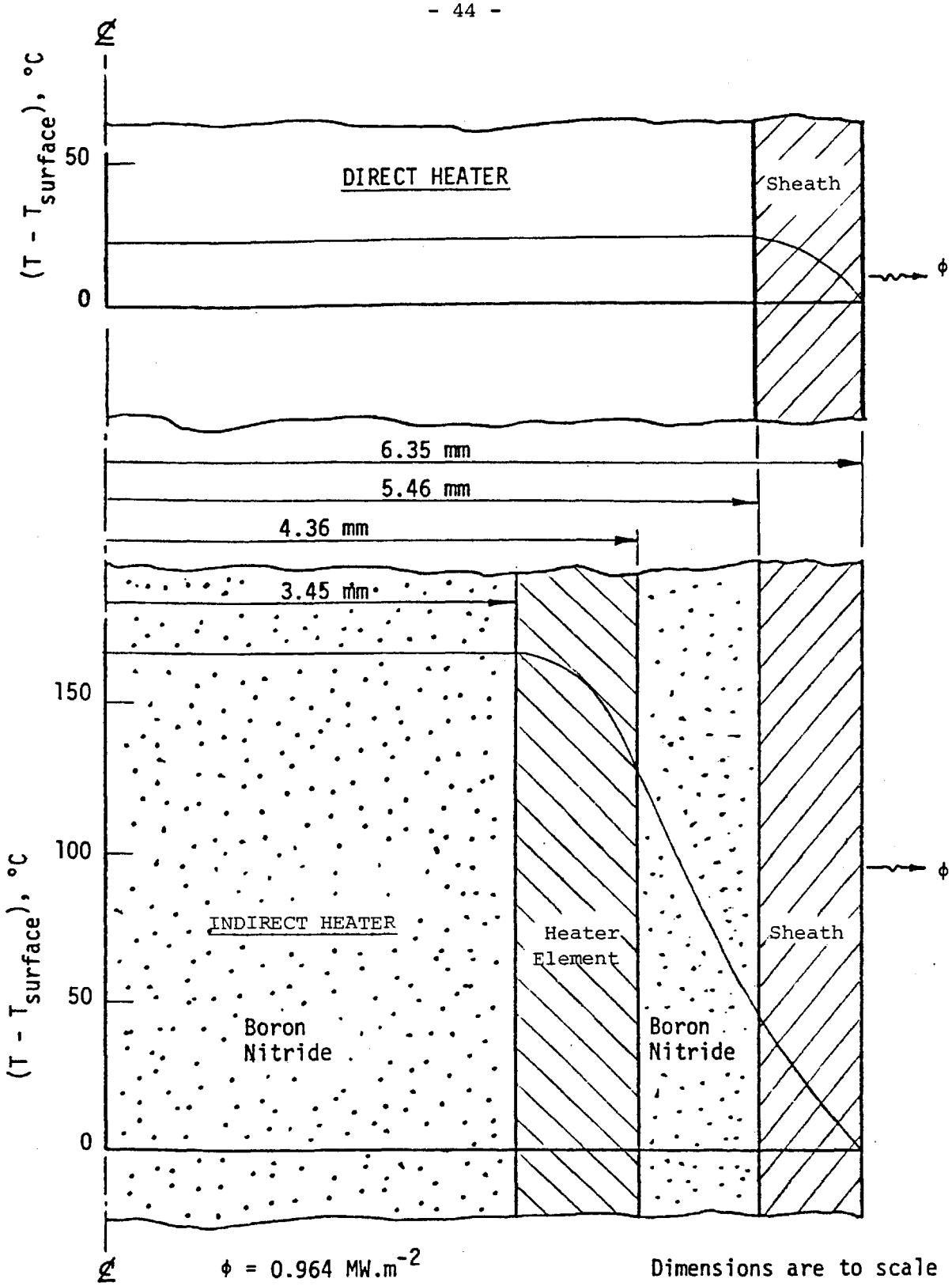

FIGURE 17: RADIAL TEMPERATURE PROFILES OF THE DIRECT AND INDIRECT HEATERS AT THE SAME SURFACE HEAT FLUX

performance of the heaters is not significantly affected by ignoring the differences in heat generation of the heater extensions.

Although the difference in CHF performance of the heaters appears to be large when the results are compared on a local condition basis (Figure 16), the difference is relatively small when compared on a system parameter basis (Figure 15). Macbeth [15] stated that the system parameters are, in fact, the independent variables affecting CHF, unlike the local conditions which are not independent. Also in annular flow, dryout depends on droplet entrainment, deposition and evaporation. Both the droplet entrainment and deposition processes, as noted by Theofanous [16], require long development lengths and strong upstream history effects would be expected. Therefore, comparison of the CHF performance using the system parameters is considered more appropriate than using the local conditions.

Despite the large differences in the wall thermal capacitance of the heaters, the CHF performance of the heaters is similar, based on the system parameter approach. The explanation for the insignificance of the wall thermal capacitance on CHF in the present experiments may be deduced from various investigations of wall thickness effects on CHF using direct heaters. The data of Lee [17] suggest that CHF is reduced slightly ($\sim$ 5%) at low inlet subcooling in forced convection boiling as the wall thickness is decreased from 2.1 to 0.9 mm for tests with the short tube (0.66 m). In the longer tube (1.73 m), no wall thickness

effect on CHF was observed. Jeffries [18] reported that in pool boiling and in cross-flow forced-convection boiling over a tube, thin walled heaters acted to reduce the dryout heat flux. He attributed the reduction in dryout heat flux to conduction in the wall. With a thin wall heater, the conduction is insufficient to damp out hot spots that may form under vapour patches. Tong [8] indicated that the effect of wall thermal capacitance on CHF can be observed when the bubble size is large and the wall temperature fluctuation period is long. In the annular flow regime, boiling is usually suppressed, and dryout occurs when the liquid film breaks down into rivulets. When the heat flux is high, the rivulets are immobilized as soon as they are formed. Conduction of heat from the dry patches to the wet regions under the rivulets will evaporate the rivulets and/or spread the dry patches upstream without affecting CHF. However, when the heat flux is low, the rivulets are mobile and can move about on the heated wall. This is reflected as fluctuations in the wall temperatures. If heat conduction is sufficient to damp out the hot spot under the dry patches and if the thermal time constant of the heater is large, as in the indirect heater, permanent rewetting may occur and higher heat flux is required to cause stable dryout. It appears that the wall thermal capacitance effect is significant when boiling heat transfer occurs and may be observed when liquid film dries out at low heat fluxes. In the present experiments, liquid film appeared to dry out under high heat flux situations since the thermocouple traces of the wall temperatures showed sudden temperature excursion without fluctuation.

Therefore, for the present long annular test section, the CHF performance of the two types of heater is similar. Also Jeffries [18] and Tolubinskiy [19] noticed a critical wall thickness existed in their studies on wall thickness effects. Above a critical wall thickness, dryout heat flux was not affected by the wall thickness. In the present experiments, if the wall thickness of the direct heater exceeded the critical wall thickness for the test conditions, no difference in CHF between the heaters would be observed.

5.3 Comparisons of Post-CHF Performance of the Heaters

When the power level was raised above CHF, the dry patch which had formed at CHF, tended to spread both upstream and around the circumference of the heaters. In general, heat fluxes of more than 6% above CHF were required to spread the drypatch completely around the circumference of the direct heater. In the case of the indirect heater, the heat flux required to spread the drypatch around the circumference appeared to be lower than for the direct heater. The spreading of the drypatch is discussed in detail in Section 5.4. In either heater type, the dryout front did not occur uniformly around the heater. Therefore the maximum wall temperature measurements were used to compare the behaviour of the heaters. In general the temperature measurements used were made on Plane A for the direct heater, and were made on Plane A at 0° and on Plane B at 180° for the indirect heater. The locations of the thermocouple planes are shown schematically in Figure 14.

The maximum wall temperatures of the heaters in Post-CHF are compared in Figures 18, 19 and 20. With other things being equal, the wall temperatures in the dryout region of both heaters are affected by the critical heat flux. As such, the ratio of CHF, ψ*, for each test condition, is indicated in the graphs. It is evident that, at similar test conditions in Post-CHF, the wall temperatures generally increased at a similar rate with heat flux for both heaters.

At mass fluxes of 2.0 and 3.5 $Mg.s^{-1}.m^{-2}$ (Figures 18 and 19) with $\psi > 0.97$ the indirect heater appeared to have slightly lower wall temperatures. However, it should be noted that, because of the limited instrumentation to measure the wall temperatures of the indirect heater, the indicated maximum wall temperatures in the experiments may not be the true maximum wall temperatures. However, since the heaters had similar CHF values and for similar reasons to those discussed in Section 5.2 the true maximum wall temperatures are not expected to be much higher than the indicated maximum wall temperatures. Therefore the differences in the wall temperatures between the heater types in Figures 12 and 13 are negligible.

At mass flux of 2.0 $Mg.s^{-1}.m^{-2}$ and inlet quality of -25%, the indirect heater was 6% lower in CHF and had higher wall temperatures for a given heat flux above CHF than the direct heater. The indirect heater appears to have inferior heat transfer. Such an interpretation is misleading. In fact, at a given heat flux, the heat flux above CHF for

---

* $\psi = \frac{CHF_{indirect}}{CHF_{direct}}$

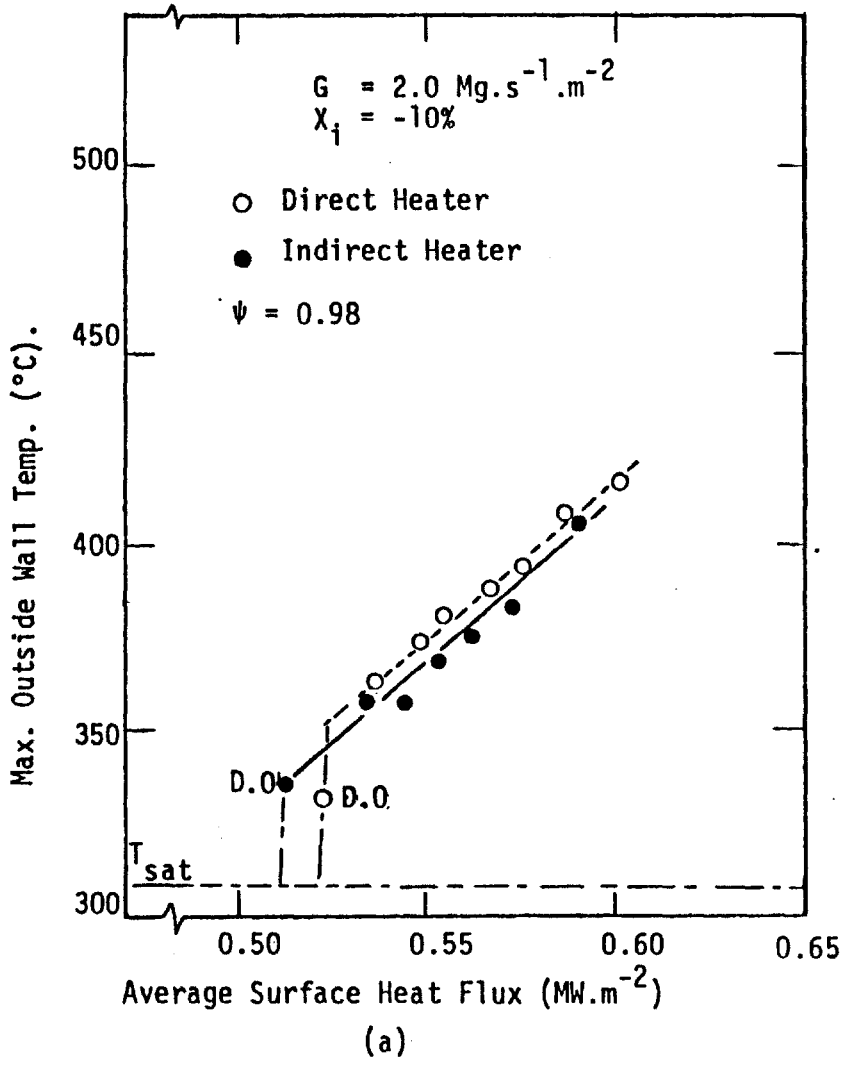

(a)

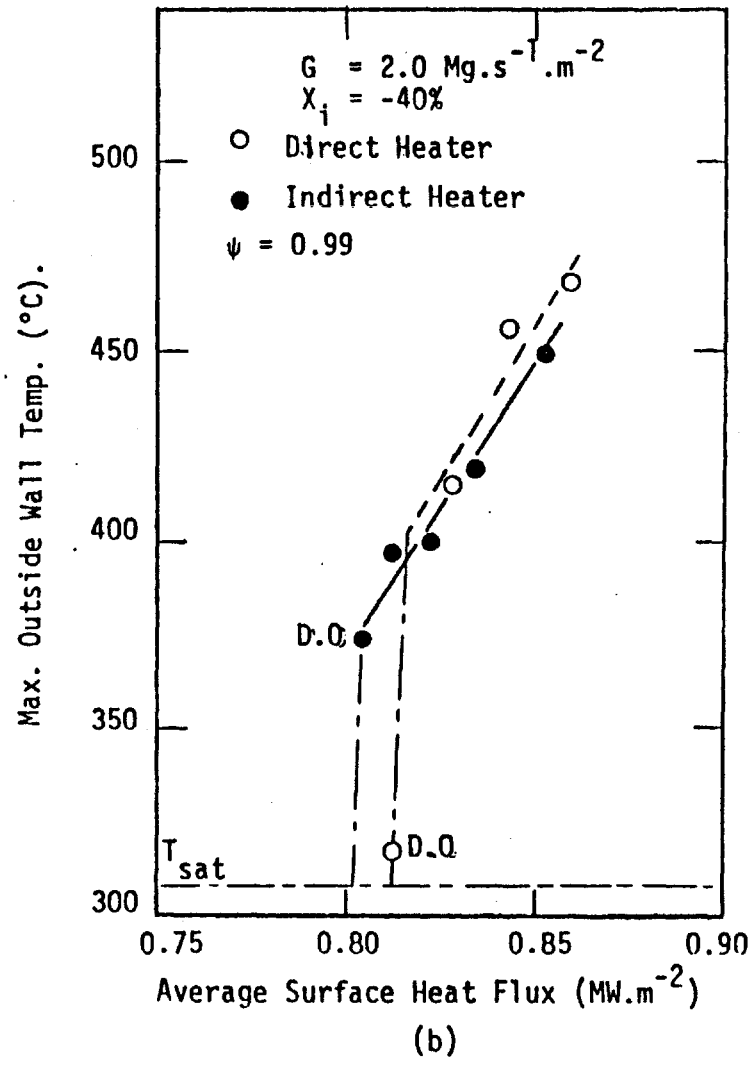

(b)

FIGURE 18: COMPARISONS OF THE MAXIMUM WALL TEMPERATURES OF THE DIRECT AND INDIRECT HEATERS, BASED ON AVERAGE SURFACE HEAT FLUX AT EXIT PRESSURE OF 9.7 MPa AND MASS FLUX OF 2.0 Mg.s^{-1}.m^{-2}

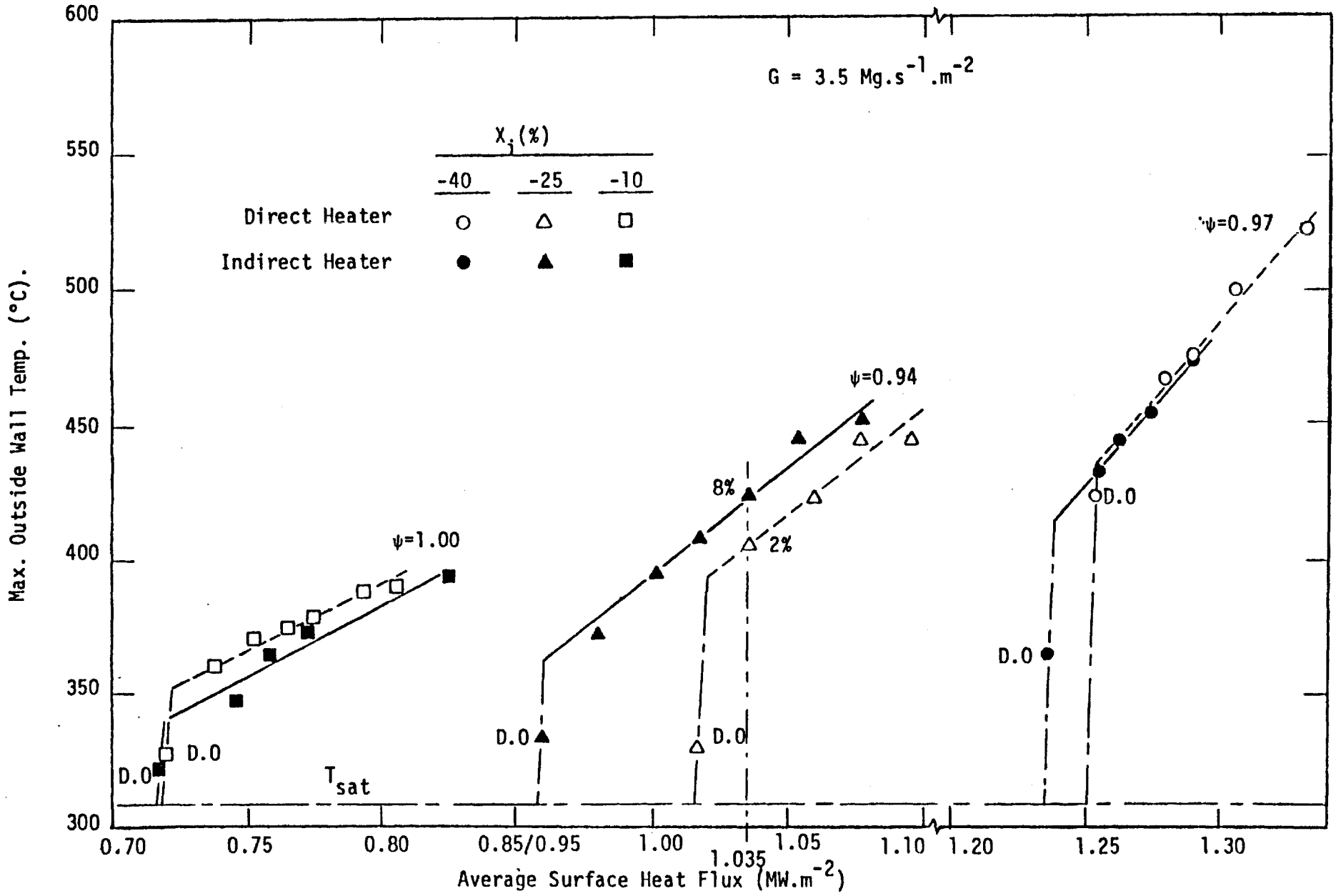

FIGURE 19: COMPARISONS OF THE MAXIMUM WALL TEMPERATURES OF THE DIRECT AND INDIRECT HEATERS, BASED ON AVERAGE SURCACE HEAT FLUX AT EXIT PRESSURE OF 9.7 MPa AND MASS FLUX OF 3.5 Mg.s^{-1}.m^{-2}

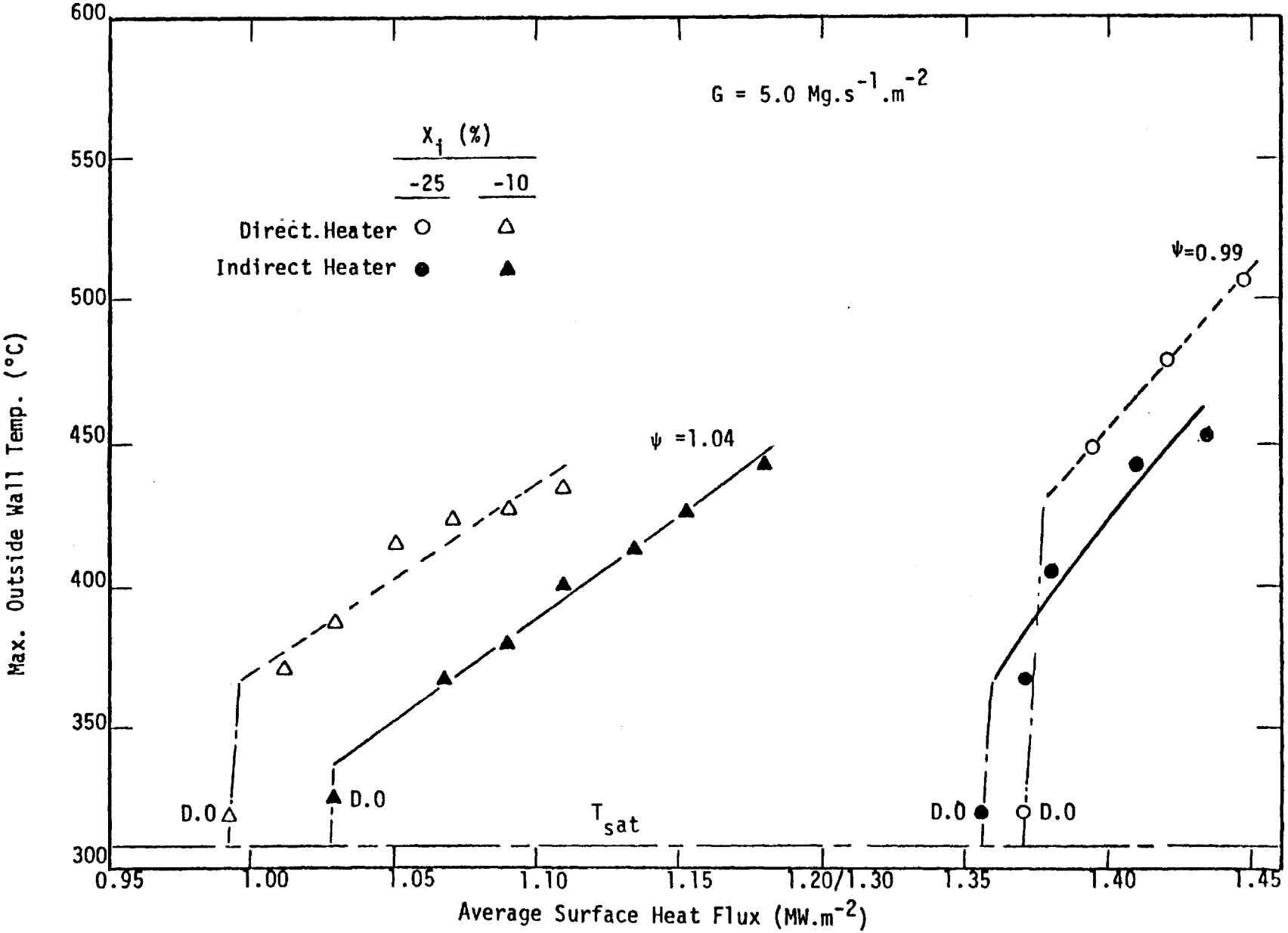

FIGURE 20: COMPARISONS OF THE MAXIMUM WALL TEMPERATURES OF THE DIRECT AND INDIRECT HEATERS, BASED ON AVERAGE SURFACE HEAT FLUX AT EXIT PRESSURE OF 9.7 MPa AND MASS FLUX OF 5.0 Mg.s^{-1}.m^{-2}

the indirect heater was higher than for the direct heater (e.g. 8% versus 2% above CHF at a heat flux of 1.035 $MW.m^{-2}$). Therefore, the wall temperatures of the indirect heater were higher in spite of having lower CHF. When this difference in heat flux above CHF is discounted, the wall temperature difference would probably be less than that indicated.

At mass flux of 5.0 $Mg.s^{-1}.m^{-2}$, the wall temperatures were lower for the indirect heater (Figure 20). It should be noted that, in the case of the indirect heater with inlet quality of -25%, the A-plane thermocouple at 240° indicated dryout. But at heat fluxes higher than 2% above CHF, the thermocouple on Plane B at 180° indicated the highest temperature. Similarly with inlet quality of -10%, the Plane A thermocouple at 0° indicated dryout, but the Plane B thermocouple at 180° indicated the highest temperatures at heat fluxes higher than 6% above CHF. Possible explanations for the lower wall temperatures in the direct heater are presented in Section 5.4.

The spacers between the heater and the shroud tube served to promote turbulence and improve the heat transfer downstream of the spacer planes. In the Post-CHF regime, the upstream spreading of the dry patch from the downstream end of the heated length was limited, by these effects of the spacers, to less than 15 cm, event at heat fluxes 15% above CHF. Similar limitations, or spreading of the dry patch upstream of the spacer plane was also observed. The variation of the minimum heat transfer coefficient h_{min}†, which corresponds to the indicated maximum

† The calculation of h_{min} was based on the saturation temperature,

i.e. $$h_{min} = \frac{\phi}{(T_w - T_{sat})}$$

wall temperature, is shown in Figures 21 and 22. The value of h_{min}, which decreases as the heat flux increases, was compared with the correlation developed by Groeneveld and Moeck [20] for fully developed film boiling heat transfer coefficient in vertical annuli. It is evident that the film boiling in the present tests was not fully developed because of the short length in dryout due to the effects of the spacers. An indication of the fully developed value of h_{min} may be obtained by extrapolating the curves of the experimental data to higher heat flux region. The fully developed values of h_{min} then obtained, are similar for both heater types and are similar to those predicted by the correlation. At the mass flux of 5.0 $Mg.s^{-1}.m^{-2}$, (Figure 22) the value of h_{min} for the indirect heater was higher than for the direct heater, but both the heaters appeared to have similar fully developed values of h_{min}. This implies that it takes a longer length for the film boiling heat transfer coefficient to develop as a result of better heat transfer observed in the case of the indirect heater at high mass flux.

The typical axial profiles of wall temperature for the direct heater, with the normallized heat flux as a parameter, are shown in Figure 23. As the heat flux increased, the wall temperatures increased and the dry patches spread upstream. The spreading pattern of the upstream dry patch indicates the effects of the spacers. The upstream dry patch spread upstream but only spread slightly downstream beyond the spacer plane. At high heat flux levels, the maximum wall temperature of the upstream dry patch could be higher than that of the dry patch near

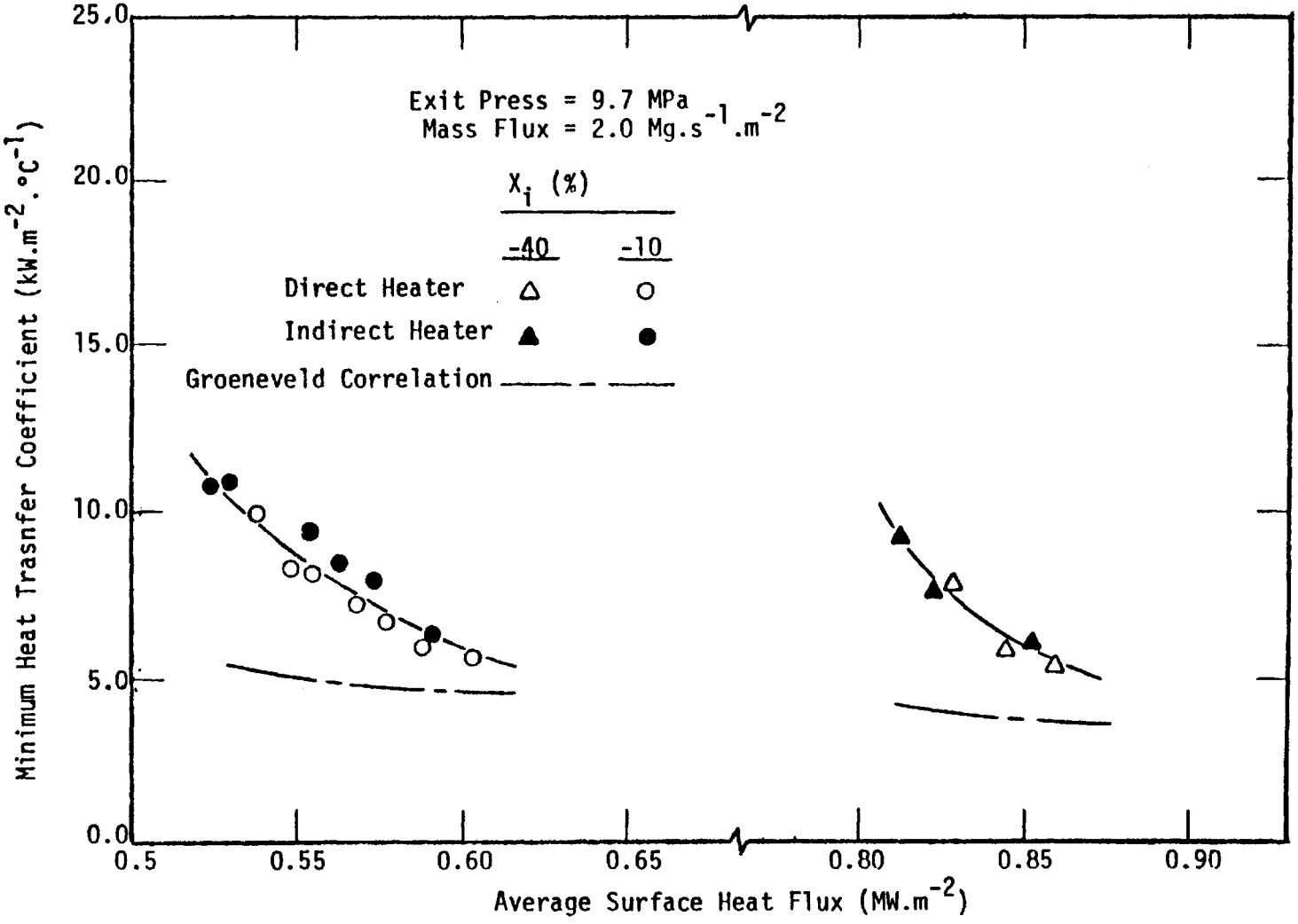

FIGURE 21: COMPARISONS OF MINIMUM HEAT TRANSFER COEFFICIENTS OF THE DIRECT AND INDIRECT HEATERS, BASED ON AVERAGE SURFACE HEAT FLUX

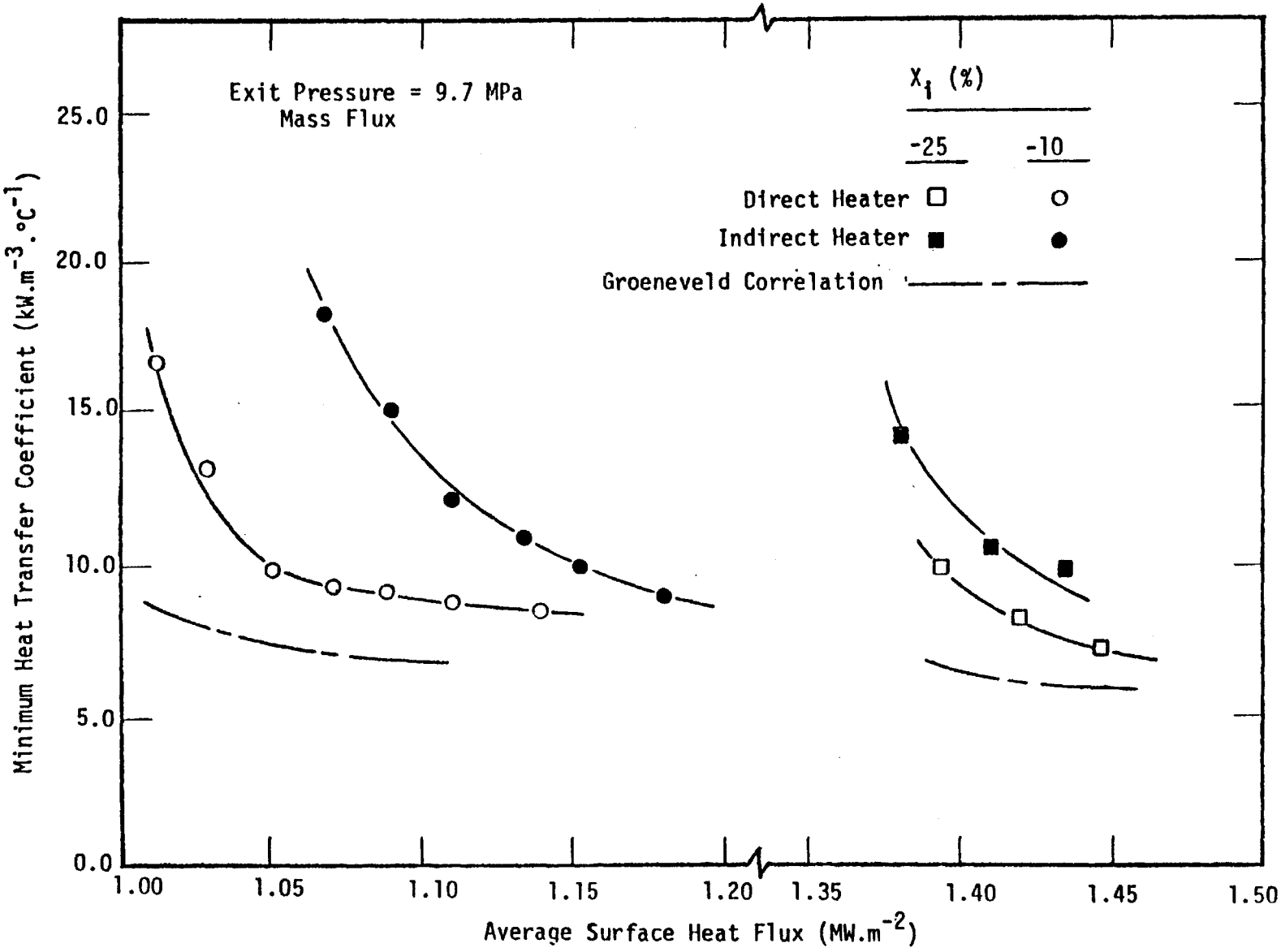

FIGURE 22: COMPARISONS OF MINIMUM HEAT TRANSFER COEFFICIENTS OF THE DIRECT AND INDIRECT HEATERS, BASED ON AVERAGE SURFACE HEAT FLUX

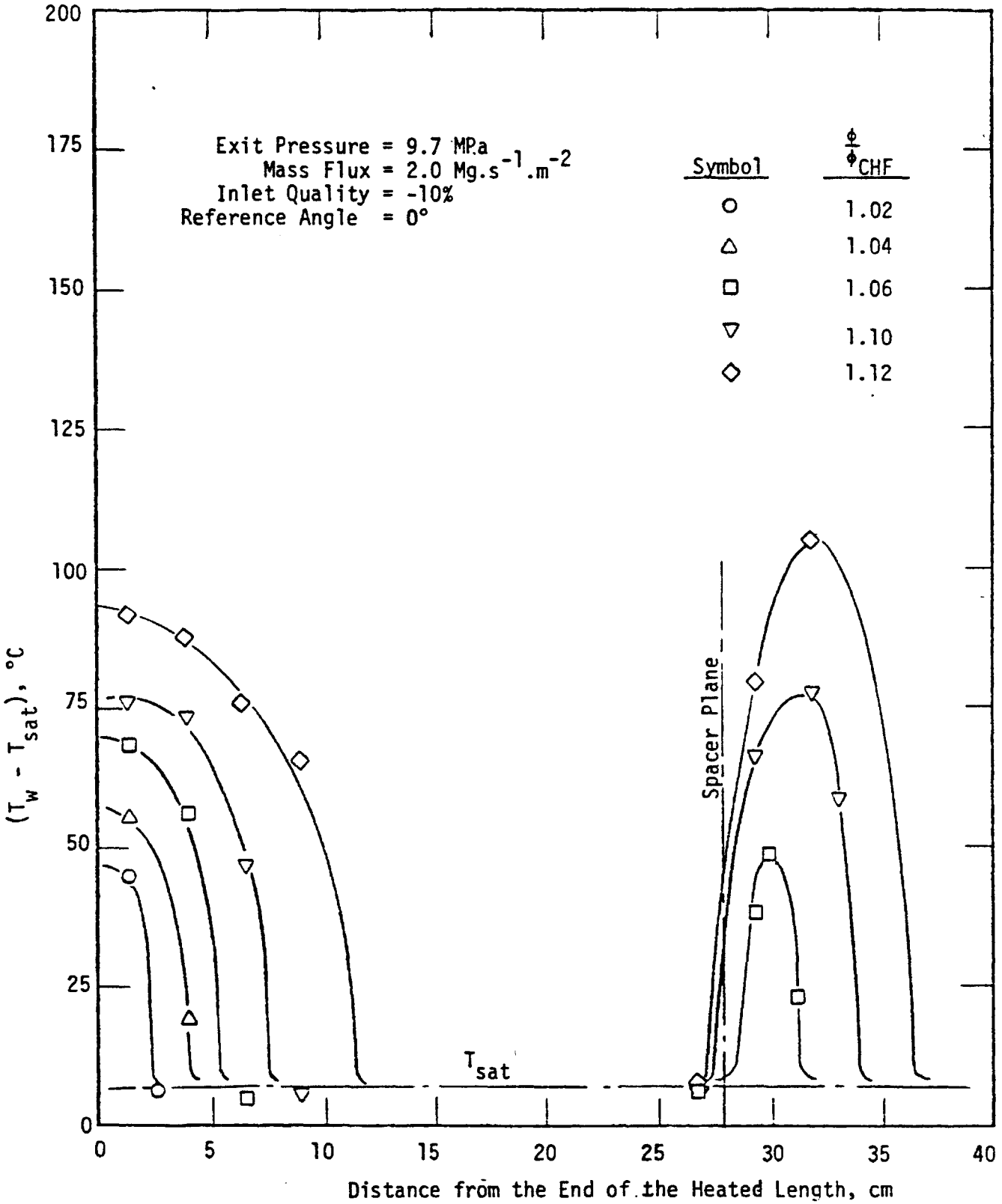

FIGURE 23 : TYPICAL AXIAL WALL TEMPERATURE PROFILE

the end of the heated length. The higher wall temperatures in the upstream portions of the dry region are probably attributable to the lower quality than was on the downstream portions. At lower quality, the vapour velocity and the droplet velocity are lower and there is less turbulence and less droplet-wall interaction. Therefore, the heat transfer is worse and the wall temperatures could be higher in the upstream portions of the dryout regions.

More detailed mappings of the dryout front as the heat flux was varied are shown in Figures 24 and 25. Again, the effects of the spacers are clearly indicated.

It should be noted that the dryout front positions are approximate. At a given heat flux level, it might have taken as long as 30 minutes to complete the recording of the measurements of wall temperatures at the various locations due to the limited speed of printing out the computer scans. During this period the flow conditions generally fluctuated within small limits and the dryout front probably fluctuated slightly. From the figures, it is clear that the dryout front did not occur uniformly around the direct heater. Although dryout front data were not available in the case of the indirect heater, a few data points from the indirect heater were plotted in Figures 24 and 25. These data points correspond to wall temperatures which were less than $30^{\circ}C$ above the wet wall temperatures. Therefore, they should indicate the approximate locations of the dryout front.

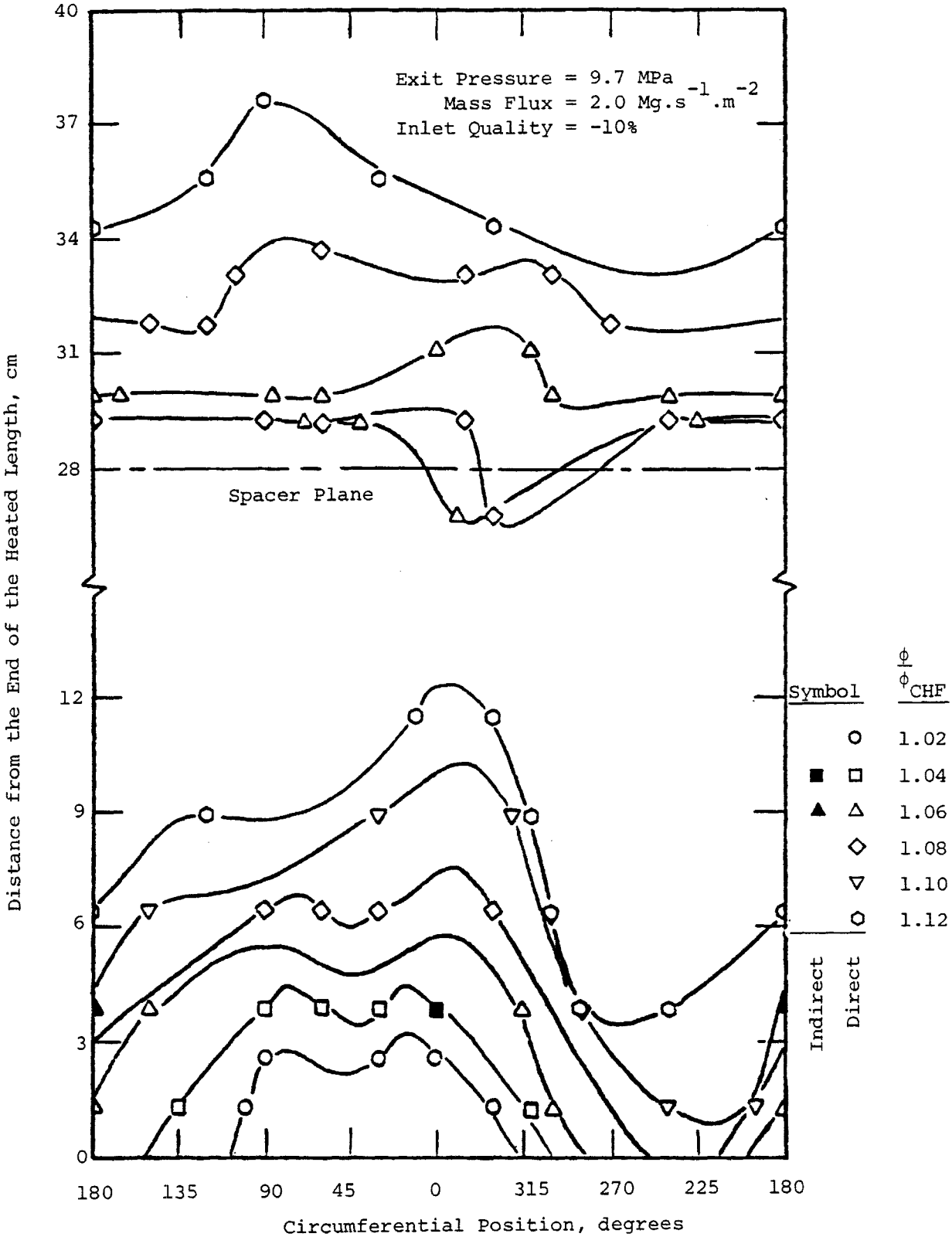

FIGURE 24: DRYOUT FRONT MAP OF THE DIRECT HEATER AT 2.0 Mg.s^{-1}.m^{-2}

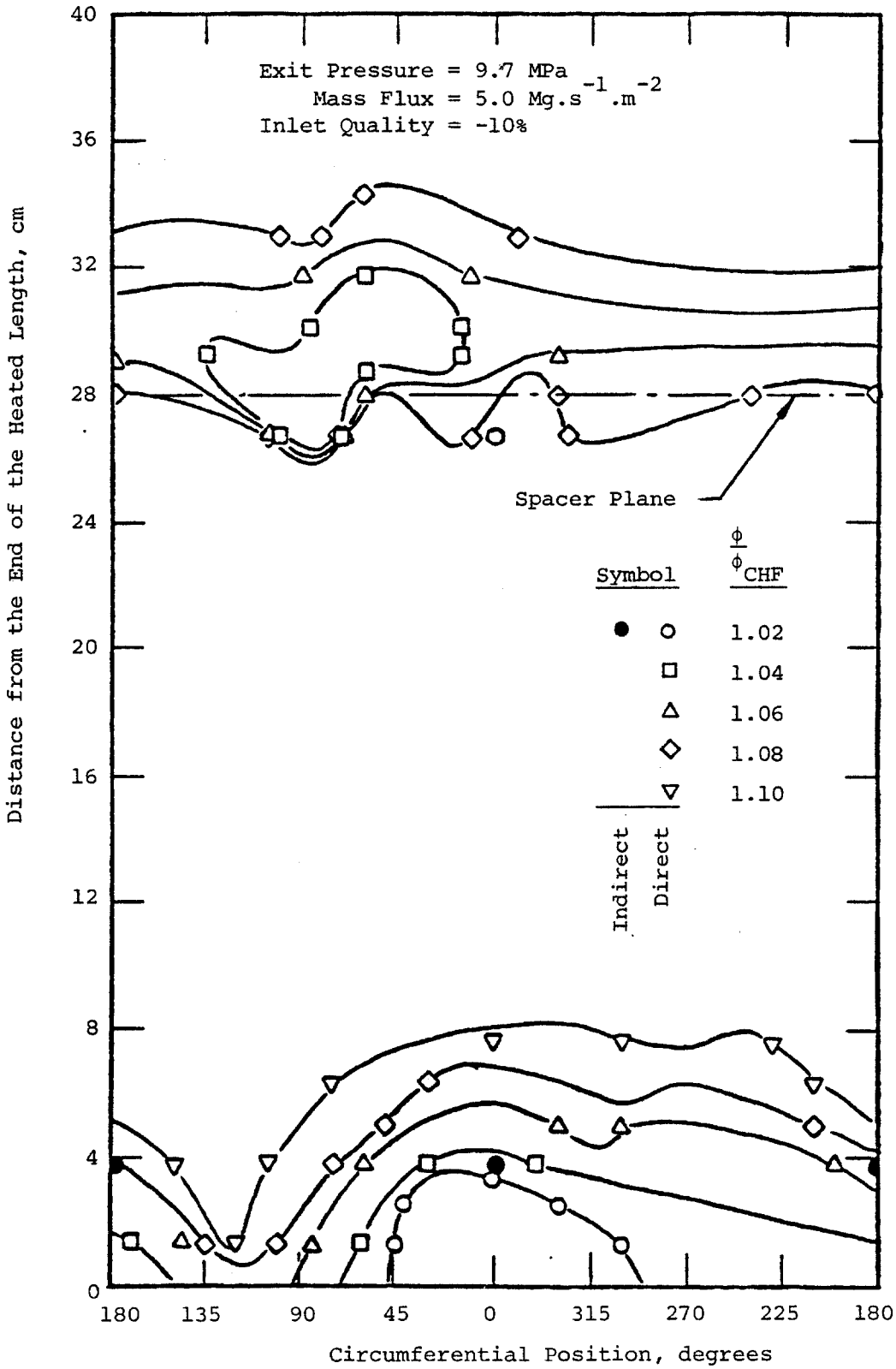

FIGURE 25: DRYOUT FRONT MAP OF THE DIRECT HEATER AT 5.0 Mg.s^{-1}.m^{-2}

Circumferential spreading of the drypatch may be infered from Figure 24 for the indirect heater. At the heat flux of 6% above CHF and at the location 38 mm from the downstream end of the heated length, a dryout front was indicated at 180°. However the heater wall was dry at 0° (because a dryout front was indicated at 4% above CHF) and at 240° (because initial dryout was indicated at 240° near the end of the heated length). It implies that the dry patch spread around the indirect heater at a heat flux of less than 6% above CHF. For the direct heater, complete circumferential spreading of the dryout patch occurred at a heat flux of 10% above CHF. With similar reasoning, in Figure 25, complete circumferential spreading of the dryout patch might have occurred at a heat flux just 2% above CHF in the indirect heater while for the direct heater, complete spreading of the dryout patch occurred at a heat flux of about 8% above CHF. In summary, comparison of the results of the dryout front information of the heaters is not conclusive due to limited data for the indirect heater but is indicative that circumferential spreading of the downstream dryout patch is easier for the indirect heater. Possible explanations are given in Section 5.4 in terms of better internal conduction in the indirect heater.

5.4 Discussions on Post-CHF Performance of the Heaters

At the mass flux of 5.0 $Mg.s^{-1}.m^{-2}$, the wall temperatures of the indirect heater in post dryout were lower than those of the direct heater at a given heat flux (Figures 18, 19 and 20). The difference in wall temperatures may be due to the differences in internal thermal conduction and thermal response of the heaters.

When CHF is exceeded. The temperatures of the dry wall became higher than the wet wall and internal axial conduction of heat from the dry wall region to the wet wall region occurs. While the wall thickness is the same for both heater sheaths, the indirect heater provides additional heat conduction paths in the isulation and in the heater filament. In the case where the heat flux above CHF is low and the dryout patch has not spread completely around the heater, heat is also conducted circumferentially in the sheath of the direct heater. For the indirect heater, conduction of the heat can also occur across the cross-section from the higher temperature region underneath the dryout patch to the lower temperature region underneath the wet wall. In comparison, the indirect heater offers better redistribution of the heat by internal conduction than the direct heater.

Consider when consecutive water droplets impinge on the hot surface of a plate, the heat transfer beneath the hot surface may be viewed as a local transient phenomenon. When the first drop of water falls on the hot surface, the surface temperature is lowered. After a period of time, depending on the thermal response of the hot plate, additional heat reaches that point of the surface and returns it to the initial temperature. If the time period is longer than the time interval of the water droplets hitting the surface, each water droplet will lower the surface temperature further and the surface temperature at the point is not able to return to the previous temperature. Eventually the surface temperature at that point will be reduced until the time period required for the surface temperature to return to the previous temperature

equals the time interval of the impinging water droplets. Rohsenow et al. [21], in an investigation of rewetting in film boiling flow, suggested that during a period of liquid contacting the heater surface, a depression in the temperature in this region occurs. The magnitude depends on the rate at which heat is conducted from the surrounding heater material to the contact region. A high thermal conductivity material may supply heat at a sufficiently high rate so as to retard any wetting that might produce a lower temperature, while the contrary is true for a poor conductor. Similar phenomenon might have occurred in these experiments.

In the Post-CHF region, heat is removed from the heated surface by forced convection to the superheated vapour and also by droplet-wall interaction. With high mass flux, the turbulence is high and the doplets have high velocity. The disturbance effect of the droplets is increased in the vapour layer separating the droplets and the surface. Pedersen [22] concluded that, for a droplet impinging upon a dry heated surface, the approach velocity is the dominant variable affecting the droplet heat transfer. Therefore at the highest mass flux in the experiments (5.0 $Mg.s^{-1}.m^{-2}$), the droplet-wall interaction may be significant and the heater wall temperature was lowered after droplets interacted with the wall. In the direct heater, the heat is generated instantaneously in the sheath and the wall temperature was returned to the initial wall temperature almost immediately. In the indirect heater which has much slower thermal response than the direct heater, the wall temperature was lowered due to the above mentioned local transient phenomenon after droplet wall interactions. Therefore the indirect

heater should have lower wall temperatures (Figure 20) than the direct heater.

Internal conduction is always present when there is a temperature gradient in the heaters and the amount of heat conduction is proportional to the temperature gradient. The axial temperature profiles of the direct heater, as shown in Figure 23, reveals that the temperature gradient is very small at the maximum wall temperature. Therefore the axial conduction near the region of maximum wall temperature is insignificant. When complete spreading of the dry patch around the heater did not occur, circumferential conduction, and in the case of the indirect heater, conduction across the cross-section will occur. Incomplete spreading of the dryout patch around the heater occurs at low Post-CHF. The dry wall temperatures are moderately higher than the wet wall temperatures. Therefore heat conduction is small.

In summary, the internal conduction of heat does not significantly affect the maximum wall temperature achieved but only affects the wall temperatures of the regions in the proximity of the dryout patch. This is indicated by the experimental data which show that lower maximum wall temperatures, in the indirect heater, were observed only at the highest mass flux rather than in situations in which the wall temperatures were high. The limited effect of axial conduction was also reported by Groeneveld [23]. The distribution of heat transfer parameters along the directly heated tubular test section of [23] is reproduced in Figure 26. Due to axial conduction, the heat flux just upstream from the dryout

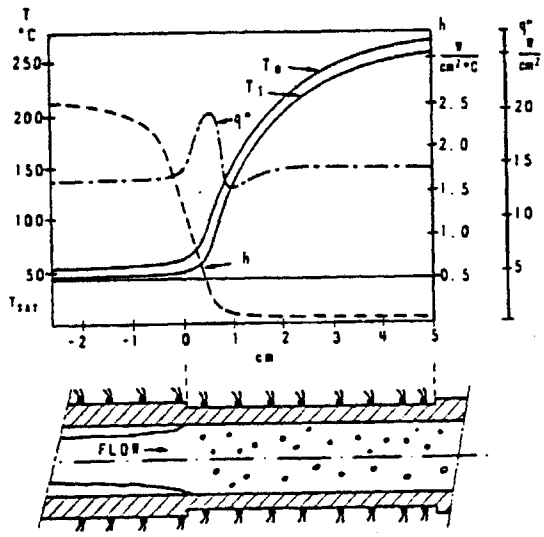

FIGURE 26: DISTRIBUTION OF HEAT TRANSFER PARAMETER
$P=10.7$ bar, $G=67\ g.s^{-1}.cm^{-2}$, $x_{DO}=0.626$
(FROM GROENEVELD [23]

location was increased while the heat flux just downstream from the dryout location was reduced. Further downstream, the heat flux remained the same as the average heater heat flux. The effect of axial conduction is local.

6. THEORETICAL ANALYSIS OF CHF AND POST-CHF HEAT TRANSFER

Various analytical models, based on physical phenomena, to predict the CHF and Post-CHF heat transfer have been proposed. These CHF prediction models have been applied to tubes, annuli and rod bundles. However, for Post-CHF heat transfer, the available prediction models have only been applied to tubular geometries. In annular geometries, the presence of the liquid film on the shroud in the post dryout region have to be modelled.

In this section, a multifluid CHF prediction model is presented and the prediction capability is tested against the experiments in Section 6.3.

Also presented in this section, is a Post-CHF prediction model suitable for vertical annular geometry. The prediction results were compared to the direct heater experiments in Section 6.4. Furthermore, the sensitivity of the calculated results to changes in some of the assumptions was also determined to check whether the model had the correct prediction trends.

6.1 Analytical Model For CHF Prediction

In annular two-phase flow, the liquid phase flows as a film along the walls of the channel. The vapour phase flows in the central

core. The liquid-vapour interface is characterized by disturbance waves. Liquid, in the form of droplets, is continuously torn off the wavy liquid film, probably from the large disturbance waves, and are carried along with the vapour. These entrained droplets are subsequently redeposited onto the liquid film. With heat addition to the fluid, evaporation takes place at the liquid-vapour interface resulting in net depletion of the liquid film. At dryout conditions in annular flow, it had been found by Hewitt et al. [11] that the liquid film flow rate was nearly zero. In the prediction model, the gradients of the liquid film flow rate along the test section are evaluated by considering the deposition rate, the entrainment rate and the evaporation rate at the interface of the inner rod liquid film and the vapour. CHF occurs when the liquid film flow rate of the inner rod becomes zero at the downstream end of the heated length.

The theoretical calculation treats the annulus as two subchannels. A schematic diagram of the typical geometry of annular flow is given in Figure 27. The surface of zero shear stress, of radius r_s, forms the boundary of the two subchannels. The subscript 1 of the symbols refers to regions inside r_s and the subscript 2 of the symbols refers to regions outside r_s. The entrainment and deposition rates are treated empirically. The asymmetric liquid film flow, which is typically found in annular test sections, is also treated empirically. The triangular relationship between the liquid film flow rate, the shear stress and the liquid film thickness is established by assuming Prandtl's universal, turbulent two-layer velocity profile in the liquid film and the turbulent logarithmic

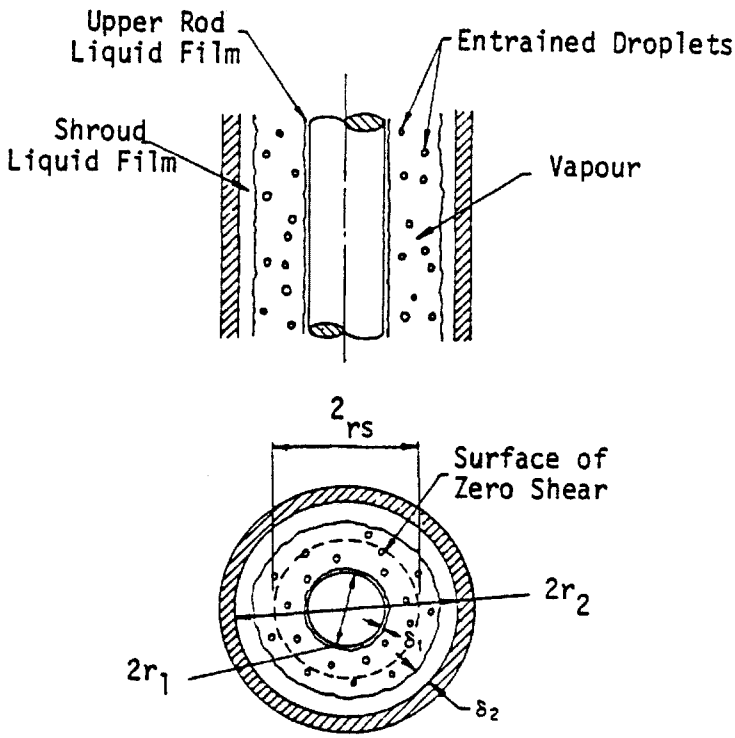

FIGURE 27: ANNULAR FLOW GEOMETRY SCHEMATIC

velocity profile in the vapour core. The heated portion downstream of the onset of the annular flow regime, is divided into small sections. The gradient of the liquid film flow is derived for each section. For given initial conditions at the onset of the annular flow, the liquid film flow and the liquid film thickness are evaluated at the end of each section which, in turn, are used as the initial conditions for the next section. The calculations are performed for each section along the length, until, by varying the heat flux, the liquid film flow rate becomes zero at the end of the heated length. The imposed heat flux is the CHF value.

6.1.1 CHF Prediction Model Formulation

Basically, the model considers the variation of the liquid films. The general volume averaged conservation of mass for the liquid films are:

$$\frac{\partial}{\partial t}(\alpha_{LFj}\rho_{LFj}) + \frac{\partial}{\partial z}(\alpha_{LFj}\rho_{LFj}U_{LFj}) = \Gamma_{LFj} \quad ; \; j=1,2 \tag{1}$$

where Γ_{LFj} = net interfacial mass exchange rate for liquid film j per unit volume

To simply the physical process in annular flow, thus reduces the general formulation to a particular one, the following assumptions are made:

(a) The pressure drop along the annular flow region is small compared to the system pressure such that flashing is neglected.

(b) The fluid properties are constant and are evaluated based on the exit pressure.

(c) Gravity effects on CHF are neglected.

(d) Bouyancy effects are neglected.

(e) The flow is steady and one dimensional.

(f) The liquid and vapour are at saturation conditions.

(g) Viscous dissipation is neglected.

(h) The locations of zero shear stress coincide with the locations of the maximum velocity of the vapour in the vapour core.

(i) The shear stress is constant across the liquid film.

(j) Near the zero shear region, the Prandtl's mixing length hypothesis, on which the fluid velocity profiles are based, also applies.

(k) The effect of curvature on the velocity profiles in the liquid film is neglected.

(l) Spacer effects are neglected.

With assumptions (e) and (f) the conservation of mass, equation (1), reduces to:

$$\frac{d}{dz}\left(\alpha_{LF1}\rho_{LF1}U_{LF1}\right) = \frac{G_{D1}}{dz} - \frac{G_{E1}}{dz} - \frac{G_{evap}}{dz} \qquad (2)$$

for the rod film. The right hand side of equation (2) is the net interfacial mass exhange rate for the rod film per unit volume, Γ_{LF1}, in which

G_{D1} = droplet deposition mass flux onto the rod film

G_{E1} = liquid entrainment mass flux of the rod film

G_{evap} = evaporation mass flux of the rod film at the liquid-vapour interface

and

$$\frac{d}{dz}\left(\alpha_{LF2}\rho_{LF2}U_{LF2}\right) = \frac{G_{D2}}{dz} - \frac{G_{E2}}{dz} \qquad (3)$$

for the shroud film. Again, the right hand side represents the net mass exchange for the shroud film where

G_{D2} = droplet deposition flux onto the shroud film

G_{E2} = liquid entrainment flux of the shroud film.

6.1.2 Constitutive Equations

For the closure of the conservation of mass equations, constitutive equations are required to describe the interaction between the fluids which are represented by G_{D1}, G_{D2}, G_{E1}, G_{E2} and G_{evap} in

equations (2) and (3) as well as the initial conditions at the start of the annular flow region. The constitutive relations for the entrainment mass fluxes, G_{E1} and G_{E2}, are generally correlated as a function of the liquid film thickness, δ. In annular film flow, the film thickness may be calculated from the triangular relationship between the liquid film flow rate, pressure drop and the liquid film thickness. The triangular relationship, which gives any one of the three variables when the other two are known, is also derived in this section.

6.1.2a Initial Conditions

Although the onset of annular flow is dependent on the pressure, the mass flux and the quality (or void fraction), various simplified transition criteria have been used by researchers in the theoretical prediction of CHF. Würtz [24] assumed the void fraction α = 80% in both tubular and annular geometries. Hewitt et al [25] used x = 1% in tubes and Whalley [26] also used x = 1% but in bundle geometries. Saito [6] reviewed various flow regime maps and annular flow transition criteria and determined that the transition to annular flow for high pressure water steam flows can be taken to occur at x = 5%. Although the transition criteria and other initial conditions varried widely, the predictions agreed well with experimental data. It appears that the prediction results are relatively insensitive to initial conditions provided the channel is long. In the present model, the criteria for annular flow transition x = 5% is used. This agrees with the annular flow transition predicted by Taitel and Dukler [7] (Section 2.1) as shown

in Figure 28. Although Taitel and Dukler's flow transition prediction was for tubes, it is expected that it would give some indication of the flow transitions in annuli. Other assumptions at the onset of the annular flow regime are:

(i) The velocity of the entrained droplet equals the vapour velocity.

(ii) The film thickness of the rod and shroud are equal.

(iii) The ratio of the area occupied by the entrained liquid to the area occupied by the liquid, F_s, is 0.15. This is an emperial factor. Saito [6] obtained $F_s = 0.10$ by comparing the prediction results of his model to the experimental film flow data.

It should be emphasised that these assumptions are made to aid the calculations of the initial conditions and only affect the first iteration step. In the subsequent interation steps, the parameters in the assumptions are calculated in the model. Assumption (i) is justifiable because at the transition from slug or churn flow to annular flow, the flow is rather chaotic and homogeneous flow velocity may be approximated. The rod and shroud film thicknesses have been observed in experiments to be different because of different interfacial shear stresses. However the transition to annular flow of the unequally thick films are gradual. Assuming equal film thickness at the onset of the annular flow (assumption (ii)) is probably not to far off. Saito [6] also made similar assumptions at the onset of the annular flow.

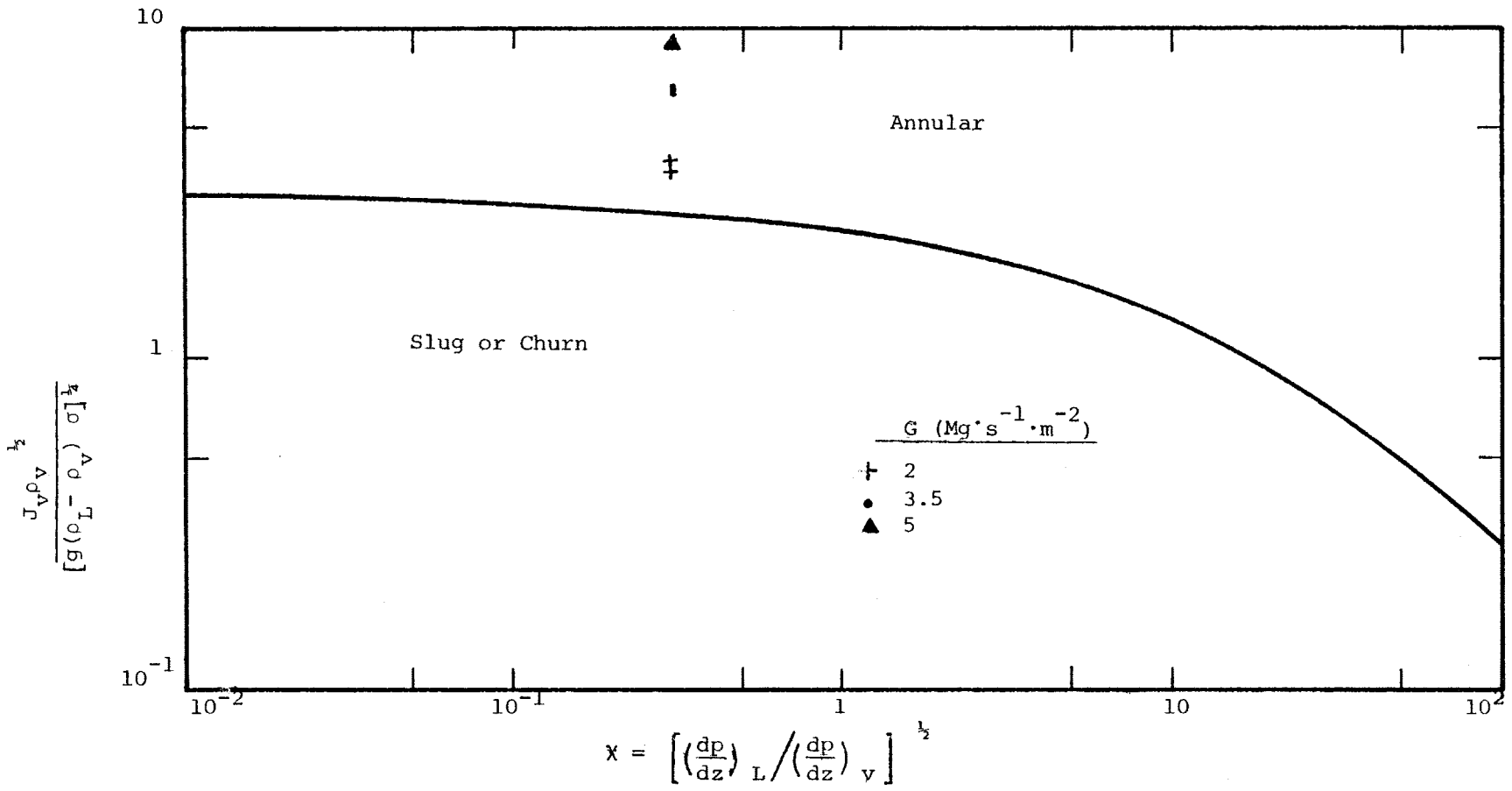

FIGURE 28: ANNULAR FLOW TRANSITION BASED ON TRANSITION CRITERIA OF TAITEL AND DUKLER [7]

The initial liquid film flow rates and film thickness are then evaluated as in the following:

Average gas velocity is

$$\bar{U}_G = \frac{GX}{\rho_G \alpha} \tag{4}$$

where α is the void fraction given by Ahmad's [27] void-fraction correlation,

$$\alpha = \frac{X}{X + \frac{\rho_G}{\rho_L} S(1 - X)} \tag{5}$$

where the slip ratio is

$$S = \left(\frac{\rho_L}{\rho_G}\right)^{0.205} \left(\frac{G.D_e}{\mu_L}\right)^{-0.016} \tag{6}$$

The average entrained droplet velocity is

$$\bar{U}_E = \bar{U}_G \tag{7}$$

and the entrained droplet mass flow rate is

$$M_E = \rho_L \bar{U}_E (1 - \alpha) F_s A \tag{8}$$

The total liquid film mass flow rate becomes

$$M_{LF} = (1 - X)M - M_E \tag{9}$$

The average liquid film velocity is then

$$\bar{U}_{LF} = \frac{M_{LF}}{\rho_L(1 - \alpha)(1 - F_s)A} \tag{10}$$

The liquid film flow rate can also be expressed as

$$M_{LF} = \rho_L \bar{U}_{LF} \pi[(r_1 + \delta)^2 - r_1^2 + r_2^2 - (r_2 - \delta)^2] \tag{11}$$

Rearranging, the liquid film thickness can be expressed as

$$\delta = \frac{M_{LF}}{2(r_1 + r_2)\rho_L \bar{U}_{LF} \pi} \tag{12}$$

which can be simplified with equation (10) and becomes

$$\delta = \frac{(1 - \alpha)(1 - F_s)(r_2 - r_1)}{2} \tag{13}$$

Finally, the initial rod and shroud films are, respectively,

$$M_{LF1} = \rho_L \bar{U}_{LF} \pi[(r_1 + \delta)^2 - r_1^2] \tag{14}$$

and

$$M_{LF2} = \rho_L \bar{U}_{LF} \pi[r_2^2 - (r_2 - \delta)^2] \tag{15}$$

6.1.2b Frictional Pressure Gradient

The frictional pressure gradient is estimated by the correlation of Thom [28], in which the frictional two-phase multiplier is

$$\phi_f^2 = \frac{(\frac{dP}{dz})_{TP}}{(\frac{dP}{dz})_L} \tag{16}$$

The two-phase multiplier is given in [28] with system pressure and quality as parameters.

Since pressure drop data along the test section were not taken during these experiments the total pressure drop of the test section was used to check the prediction results of Thom's correlation. In general, the prediction of the total pressure drop is in good agreement, as shown in Table 2. The frictional pressure drop cannot be measured directly in the experiments and the accuracy of predicting the two-phase frictional pressure drop by any prediction methods cannot be confirmed. El-shanawany et al. [29] used the Lockhart-Martinelli [30] correlation to estimate the frictional pressure gradient in the prediction of dryout in gas-water flow and obtained acceptable results. This provides some confidence in using this correlation approach to calculate the two-phase frictional pressure gradient.

6.1.2c Shear Stress

The shear stress at the walls are

$$\tau_{wj} = \left(\frac{dP}{dz}\right) \frac{|r_s^2 - r_j^2|}{2r_j} \quad , \quad j=1,2 \tag{17}$$

and the interfacial shear stresses are

$$\tau_{ij} = \left(\frac{dP}{dz}\right) \frac{|r_s^2 - r_{ij}^2|}{2r_{ij}} \quad , \quad j=1,2 \tag{18}$$

TABLE 2 : RESULTS OF TOTAL PRESSURE DROP PREDICTION BY THOM'S CORRELATION

Mass Flux ($Mg.s^{-1}.m^{-2}$)	Inlet Quality (%)	Actual Total ΔP (kPa)	Predicted Total ΔP (kPa)	$(1-\frac{\Delta P_{Pred}}{\Delta P_{Act}})\times 100$ (%)
2.0	-40	177.1	161.7	8.7
2.0	-10	242.7	210.5	13.3
3.5	-40	351.3	349.3	0.6
3.5	-25	418.1	403.8	3.4
3.5	-10	488.9	468.1	4.3
5.0	-25	723.4	731.4	1.1
5.0	-10	860.7	879.7	2.2

6.1.2d Velocity Profile in the Liquid Films

Hewitt and Hall Taylor [10] noted that satisfactory predictions of film flow rate and film thickness can be obtained by applying single-phase turbulent flow theories to give analogous equations for annular flow systems. One of the commonly used turbulent flow theories is Prandtl's universal, turbulent two-layer model. In the present model, the velocity profiles in the films are described by the universal velocity profile.

The dimensionless velocity,

$$U_{Lj}^{+} = \frac{U_{Lj}}{U_{Lj}^{*}} \quad , \qquad j=1,2 \tag{19}$$

where U_{Lj} is the velocity in the film and

$$U_{Lj}^{*} = \sqrt{\frac{\tau_{wj}}{\rho_L}} \quad , \qquad j=1,2 \tag{20}$$

is the shear velocity and is related to the dimensionless wall distance

$$Y_j^{+} = \frac{\rho_L \, Y_j \, U_{Lj}^{*}}{\mu_L} \quad , \qquad j=1,2 \tag{21}$$

where the distance from the wall is

$$Y_j = |r_j - r| \quad , \qquad j=1,2 \tag{22}$$

by the two-layer model

$$U_{Lj}^{+} = \begin{cases} Y_j^{+} \ , \ Y_j^{+} < 11.5 \ \text{(laminar)} \\ \\ \frac{1}{\kappa} \ln Y_j^{+} + B, \ Y_j^{+} > 11.5 \ \text{(Turbulent)} \end{cases} \tag{23}$$

where $\kappa = 0.4$, von Karman constant (24)

$B = 5.5$, value for roughness function B of smooth tubes (25)

$j = 1,2$

Integrating the velocity profile gives the triangular relationship:

$$M_j^{+} = \frac{M_{LFj}}{2\pi r_j \mu_L} = \int_0^{\delta_j^{+}} U_{Lj}^{+} \, dY_j^{+} \tag{26}$$

therefore

$$M_j^{+} = \begin{cases} \frac{1}{2} (\delta_j^{+})^2 \quad , \quad \delta_j^{+} \leq 11.5 \\ \\ 8.5 \, \delta_j^{+} + 2.5 \, \delta_j^{+} \ln \delta_j^{+} - 214, \ \delta_j^{+} > 11.5 \end{cases} \tag{27}$$

where $\delta_j^{+} = \dfrac{\rho_L \, \delta_j \, U_{Lj}^{*}}{\mu_L}$ (28)

δ_j = film thickness (29)

and $j = 1,2$ (30)

6.1.2e Velocity Profile in the Vapour Core

The velocity profiles of the vapour in both zones are assumed to be given by the turbulent logarithmic profile which was also used by Würtz [24] in his CHF prediction model. That is

$$U_{Gj}(r) = U_{ij} + U^*_{Gj}\left(\frac{1}{\kappa}\ln\frac{|r_{ij} - r|}{k_s} + B\right) \tag{31}$$

where $\kappa = 0.4$, von Karman constant (32)

$B = 8.5$, value for roughness function B or rough walls (33)

and k_s denotes the equivalent sand roughness and is correlated with the film thickness δ:

$$k_s = 0.57\delta + 21.73 \times 10^3\delta^2 - 38.30 \times 10^6\delta^3 + 55.68 \times 10^9\delta^4 \tag{34}$$

the interfacial velocity, U_{ij}, is given by equation (23) at $Y_j^+ = \delta_j^+$ and the friction velocity for the gas core is

$$U^*_{Gj} = \sqrt{\frac{\tau_{ij}}{\rho_G}} \tag{35}$$

To satisfy the continuity of the velocity at the radius of zero shear, r_s, which coincides with the maximum velocity by assumption (h),

$$U_{G1}(r_s) = U_{G2}(r_s) \tag{36}$$

Equation (36) along with equation (27) for j = 1 and 2 allows the evaluation of the three unknowns, r_s, δ_1 and δ_2, when the film flow rates and the frictional pressure gradients are known.

6.1.2f Entrainment From Liquid Film

In the annular flow regime, nucleation in the liquid film is generally suppressed. So the effect of heat flux on the entrainment process is assumed to be small and the entrainment rate can be developed from that under adiabatic conditions. In the present work, the correlation method of Hutchinson and Whalley [31] is used to correlate the steam-water data at 69 bars of Singh et al. [32] and Keeys et al. [33], as shown in Figure 29, by the entrainment parameter

$$S_\delta = \frac{\tau_i \delta}{\sigma} \tag{37}$$

The same correlations were also used by Saito, [6]. With a polynominal fit, which has been performed by Saito, the entrainment mass flux is given by

$$G_E = -2.695 \times 10^{-5} - 1.104 \times 10^{-2}\, S_\delta + 4.444 \times 10^{-1}\, S_\delta^{\,2} + 1.241 \times 10\, S_\delta^{\,3} - 3.775 \times 10\, S_\delta^{\,4} + 4.077 \times 10\, S_\delta^{\,5} - 1.510 \times 10\, S_\delta^{\,6}, \quad \text{for } S_\delta \leq 1 \tag{38}$$

when G_E becomes negative as S_δ approaches zero from equation (38), G_E is set equal to zero. Outside the correlation range,

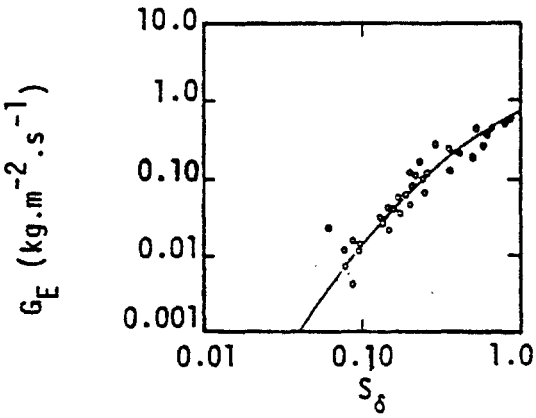

∘ Steam-Water Data (69 bars) from Singh [32]

• Steam-Water Data (69 bars) from Keeys [33]

FIGURE 29 : ENTRAINMENT CORRELATION BASED ON LIQUID FILM THICKNESS: HUTCHINSON AND WHALLEY [31]

$$G_E = -4.504 \times 10^{-1} + 1.824\ S_\delta - 6.828 \times 10^{-1}\ S_\delta^2 + 1.343 \times 10^{-1}\ S_\delta^3 - 1.268 \times 10^{-2}\ S_\delta^4 + 4.519 \times 10^{-4}\ S_\delta^5 \quad \text{for } 1 < S_\delta < 5 \tag{39}$$

$$G_E = 4.670 \times 10^{-1} + 4.725 \times 10^{-1}\ S_\delta - 4.534 \times 10^{-2}\ S_\delta^2 + 1.518 \times 10^{-3}\ S_\delta^3 \quad \text{for } 5 < S_\delta \leq 10 \tag{40}$$

and

$$G_E = 0.01\ \rho_L\{1 - \exp[-4.605(S_\delta - 10)]\} \quad \text{for } S_\delta > 10 \tag{41}$$

6.1.2g Deposition of Entrained Droplets

For small particles or droplets in a turbulent gas stream, it is reasonable to assume the particles or droplets interact with the turbulent eddies. The path followed by the droplets across the gas stream is therefore random. Hutchinson et al. [34] characterized the motion of a large number of droplets by a deposition coefficient.

Under adiabatic conditions, the deposition mass flux is

$$G_D = k_D\ C_{eq} \tag{42}$$

where k_D is the deposition coefficient and C_{eq} is the homegeneous concentration of the droples in the vapour core. For homogeneous flow, in the core,

$$C_{eq} = \frac{M_E}{\frac{M_E}{\rho_L} + \frac{M_G}{\rho_G}} \tag{43}$$

Various investigators have found that the deposition coefficient is a weak function of vapour velocity, tube diameter, drople concentration and pressure. The deposition coefficient is assumed to be a function of pressures only and its values are taken from data reported by Würtz [24] and listed in Table 3.

Under diabatic conditions, evaporation of liquid at the interface would reduce the deposition rate. This effect is accounted for by reducing the deposition coefficient in the adiabatic situation by the radial velocity of the evaporating steam at the interface, [24]

$$V_G = \frac{q''}{h_{fg}\rho_G} \tag{44}$$

which is assumed to decrease exponentially with the distance from the wall, Y. The deposition mass flux becomes:

$$G_D = \begin{cases} (k_D - V_G e^{-\delta/Y_D})\ C_{eq} & , \text{ when } V_G e^{-\delta/Y_D} < k_D \\ 0 & , \text{ when } V_G e^{-\delta/Y_D} \geq k_D \end{cases} \tag{45}$$

where Y_D was estimated from the diabatic film flow data of and reported by Würtz [24] to be

$$Y_D = 50\ \mu m \tag{46}$$

TABLE 3: DEPOSITION COEFFICIENT (FROM WÜRTZ [24])

P (bar)	30	50	70	90
k_D (m/s)	0.021	0.013	0.010	0.006

Film flow experiments in annuli show that the shroud film carries more liquid than the rod film. Würtz [24] reasoned that the curvature effect on the entrainment rate is small, therefore the asymetric film flow is due to a reduction of deposition coefficient of the rod film. That is

$$k_{D1} < k_{D2} \tag{47}$$

from his film flow data, he estimated that

$$k_{D1} = 0.4\ k_{D2} \tag{48}$$

which is used in the present analysis.

6.1.2h Evaporation Mass Flux

In annular flow, heat is transferred by convection from the wall to the rod film and by evaporation from the rod film to the vapour core. This heat transfer mode is efficient, thus the liquid and vapour are considered as in thermal equilibrium (assumption (f)). Hence the evaporation flux at the rod film-vapour interface is well defined by classical thermodynamics as:

$$G_{evap} = \frac{q''}{h_{fg}} \tag{49}$$

6.2 Post-CHF Physical Model

Theoretical methods to predict the wall temperature in the liquid deficient region at high pressures for turbular geometrics were proposed

by Bennett et al. [35], Keeys et al. [36], and Groeneveld [3]. These theories were based on physical models of flow in the dry regions in which the axial variations of drople diameter, quality, vapour velocity, droplet velocity and vapour temperature were considered. The predicted results agreeded well with experiments. In Groeneveld's model, effects due to pressure drop, flashing, and conversion of enthalpy into kinetic energy and potential energy were also included. In the case of annular geometrices the physical model of flow in the dry region is further complicated by the presence of a liquid film on the shroud. The shroud film continues to contribute droplets to the vapour flow which desuperheat the vapour. Thus the variations of the mass transfer, at the liquid-vapour interface of the shroud film along the dry region has to be considered. In this section, a theoretical model to predict the dry wall temperatures for annular geometries is proposed based on the theoretical approach of Bennett, Keeys and Groeneveld [35,36,3].

The physical picture of the flow and heat transfer considered in the post dryout region in an annulus are shown in Figure 30. The liquid film on the heated rod vanishes at the dryout location while the liquid on the shroud advances onto the post dryout region. Mass transfers by deposition and entrainment continue at the vapour-liquid interface of the shroud film. Heat from the heated wall is transferred by forced convection to the vapour ($q"_{W-S}$). Some of this heat is, in turn, transferred from the vapour to the entrained droplets ($q"_{S-D}$). In the process, the vapour is superheated and the droplets are being evaporated.

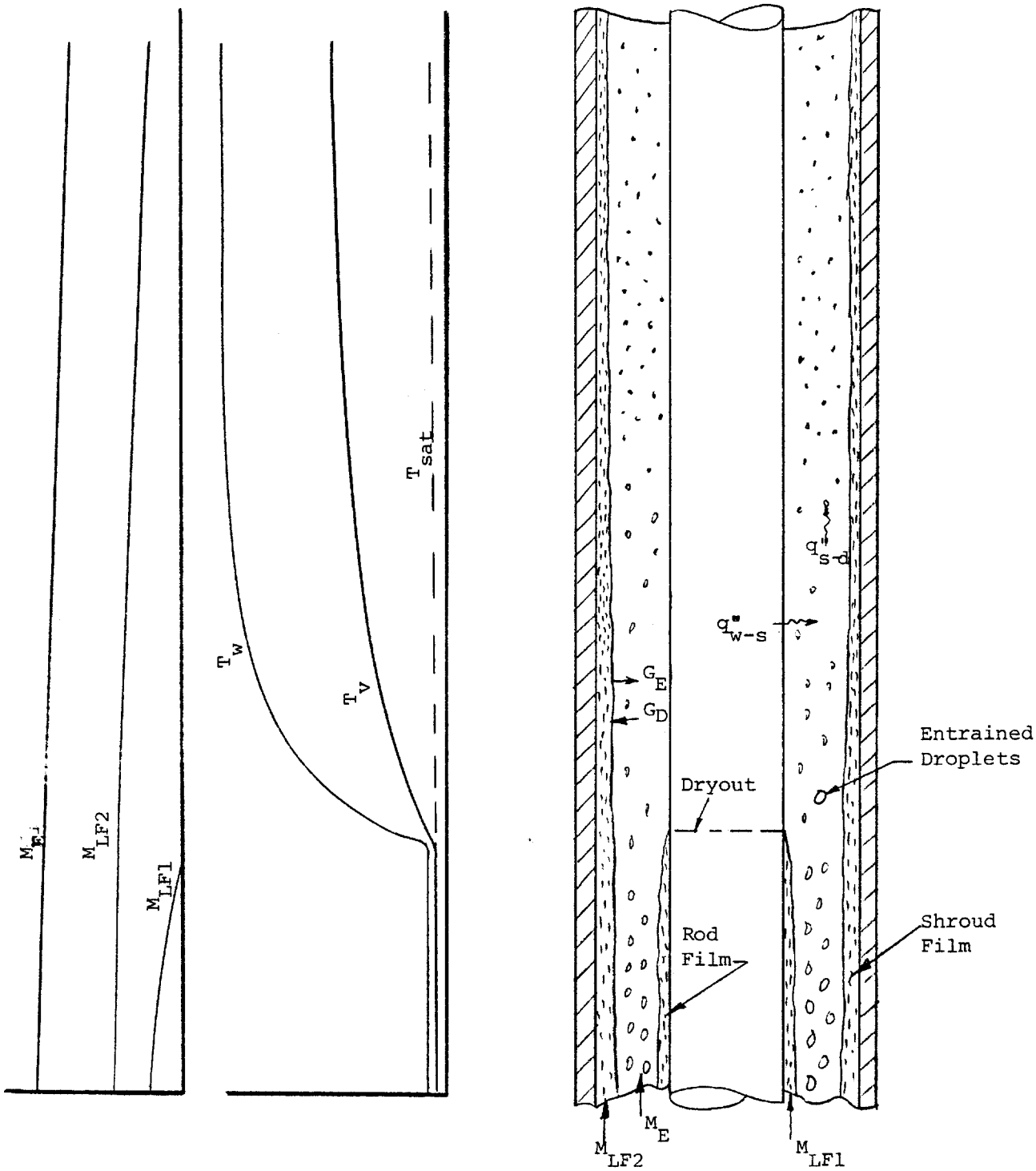

q''_{w-s} - heat transfer from wall to steam

q''_{s-d} - heat transfer from superheated steam to droplets

FIGURE 30: PHYSICAL PICTURE OF HEAT TRANSFER IN POST-DRYOUT REGION

Some of the heat is also transferred from the superheated vapour to the shroud film, however this is expected to be insignificant. The vapour, adjacent to the heated wall is highly superheated. But further away from the wall, the vapour loses most of the superheat to the droplets. Therefore the temperature of the vapour adjacent to the shroud film is close to the saturation temperature and little heat is transferred to the shroud film. The heat transfer from the superheated vapour to the droplets depends, among other things, on the number of droplets in the core. The presence of the liquid film is to contribute fresh liquid to the core, increasing the number of droplets available for evaporation, and hence reduce the superheating of the vapour, lowering the wall temperatures.

To calculate the liquid film conditions and the mass transfer at the liquid-vapour interface in the region downstream of the dryout location, the annular space was treated as two subchannels with the surface of zero shear defining the boundary as in the case of the CHF model (Section 6.1). For the droplet and vapour flow conditions, the annular space was treated as a whole and cross-sectional average quantities were used.

Downstream of the dryout location, the dry region is divided into small sections. Given the initial conditions at dryout, the flow conditions and the vapour temperature are evaluated at the end of each section, which in turn, are used as the initial conditions for the next section. The wall temperature at the end of each section is then found

from the vapour temperature and a single phase heat transfer coefficient.

6.2.1 Assumptions of Post-CHF Model

The following simplifying assumptions are made:

(a) Assumptions given in Section 6.1.1 (except (e)) for the CHF model apply to the shroud film analysis here.

(b) Cross-sectional average values of the conditions of the droplets and steam are used in the thermal calculations.

(c) Heat transfer by radiation is ignored.

(d) Heat transfer from the superheated steam to the shroud film is ignored.

(e) The droplet size is constant at any cross-section of the channel but allowed to vary along the channel.

(f) The liquid just torn off from the shroud film at any axial position breaks up into droplets having a diameter equal to the droplets entrained in the vapour core at the same axial position.

(g) Any effects of the heat capacity of the heater on the wall temperatures are not considered.

Assumption (b) is made such that the single phase heat transfer coefficient, which is based on cross-sectional average conditions, can be used to evaluate the wall temperatures.

The radiation heat transfer in the dry region at the conditions tested was inferred from [35] to be negligible (hence assumption (c)). Bennett et al. [35] estimated that radiant heat which is transferred to the droplets to be less than 10% even with the walls and droplets taken as black bodies. In the present experiments, the experimental wall temperatures were similar to those of [35], but the system pressure was 9.7 MPa compared to 6.9 MPa. Therefore the temperature difference between the wall and droplets would be smaller in the present analysis and the radiation heat transfer would be smaller as well.

Assumption (d) is reasonable because the temperature of the steam adjacent to the shroud film is expected to be close to that of the shroud film for the reasons given in Section 6.2.

At any cross-section, droplets with various sizes are present. However assumption (e) is justified by the work of Bennett et al. [35] in which the predicted wall temperatures were found to be insensitive to the droplet size. Bennett et al. and Groeneveld [3] also assumed constant droplet size at any cross-section in their analysis. With similar argument, the droplets just entrained from the shroud film, although having a wide spectrum of sizes, are assumed to be the same size as those of the droplets in the core (assumption (f)).

In the experiments, the heat capacity of the heater was found to be significant at high enough mass fluxes. Thus with assumption (g), the applicability of the model is limited to direct heaters and to indirect heaters at low mass fluxes.

6.2.2 Initial Conditions

In order to calculate the flow conditions at the dryout location, assumptions in addition to those listed in Section 6.2.1 are required:

(i) The vapour and liquid phases are in thermal equilibrium.

(ii) The droplet diameter at dryout is equal to the critical droplet diameter defined by the Weber number.

At the dryout location, superheating of the vapour phase is possible. This may result from flashing in which the saturated vapour upstream of the dryout location becomes superheated when the vapour reaches the dryout location. In most application, especially in high pressure systems, flashing effect is insignificant. Therefore assuming thermal equilibrium between phases (assumption (i)) is reasonable.

In the prediction method of Bennett et al. [35], a constant droplet size was assumed at dryout for all the test conditions. The starting droplet size was determined by varying the droplet diameter at dryout until optimum agreement between the predicted and experimental

results was found. In Groeneveld's model, [3], the initial droplet diameter was calculated by the critical Weber number. This is adapted here (assumption (ii)).

It should be noted that the above assumptions affect the first interation only. Further downstream of the dryout location, thermal non-equilibrium between the phases and the droplet diameter are calculated by the model.

6.2.2a Dryout Quality and Dryout Length

When the critical heat flux is known, as in the case here, the dryout length, and hence the dryout quality, can be estimated from CHF correlations using inlet conditions and heated length as parameters. In the present work, the experimental dryout quality was used and the dryout length was obtained from substracting the length of the dry region from the heated length. The dry region length was obtained from the wall temperature profile graph. The dryout location is taken as the point on the temperature profile graph where the wall temperature deviates from the wet wall temperature. Knowning the dryout location, the length of the dry region is obtained.

6.2.2b Pressure

The pressure at the dryout location can be estimated from two-phase pressure drop correlations. If the length in dryout is short and

the pressure drop is small, the outlet pressure can be taken as the dryout pressure.

Here, the dryout pressure drop was interpolated from the experimental pressure drop across the dryout region since this pressure drop measurement was available.

6.2.2c Droplet and Vapour Velocity

In annular flow, the liquid films have lower velocities than the entrained droplets in the vapour core. At dryout, almost all the rod film is entrained in the vapour core, therefore the cross-sectional average liquid velocity is increased. The slip ratio,

$$S = \frac{U_V}{U_L} \quad , \tag{50}$$

calculated by correlations for slip before dryout, will be larger than the actual slip ratio. Therefore, the slip ratio at dryout is assumed, as in [3], to be midway between the homogeneous flow and that predicted by the slip correlations.

In the present analysis, the slip correlation,

$$S = \left(\frac{\rho_L}{\rho_G}\right)^{0.205} \left(\frac{G\, D_e}{\mu_L}\right)^{-0.016} \tag{51}$$

in Ahmad's, [27], void fraction correlation

$$\alpha = \frac{x}{x + \frac{\rho_G}{\rho_L} S(1 - x)} \tag{52}$$

is used.

Then the vapour velocity is

$$U_V = \frac{Gx_{DO}}{\rho_G \alpha_{DO}} \tag{53}$$

and the droplet velocity is assumed to be

$$U_d = \frac{U_V}{S_{DO}} \tag{54}$$

6.2.2d Droplet Diameter

The droplets entrained in the vapour core have various droplet sizes. Here, at dryout, the droplet diameter is represented by an 'effective' diameter calculated from the critical Weber number,

$$W_c = \frac{\rho_G (U_V - U_L)^2 d}{\alpha g_c} \tag{55}$$

The critical Weber number, W_c, was measured by Isshiki [37] for water droplets breaking up in an accelerating air stream and was found to be

$$W_c = 6.5 \tag{56}$$

This value of W_c was used by Groeneveld [3], who obtained good post-dryout prediction results, and is used in the present analysis.

6.2.2e Liquid Film Flow Rate

When dryout occurs, the liquid film flow on the rod vanishes and the liquid film on the shroud continues. The mass flow rate of the shroud film at dryout can be obtained from an annular film flow model when the dryout location is known. If the dryout location is not known, a CHF model which accounts for the film flow, [6,24,25,29], can be used to predict the shroud film flow rate at dryout. In the present analysis, the CHF model presented in Section 6.1 was used to calculate the shroud film flow rate.

6.2.3 Film Flow in Post-Dryout Region

At the dryout location, the liquid film on the inner rod vanishes while the liquid film on the shroud continues to move forward. A film flow model similar to the one used in the CHF prediction model was derived for the post-dryout region. Knowing the velocity profiles in the shroud film and in the vapour core, the triangular relationship between the film flow rate, shear stress and the film thickness was derived. The droplet entrainment and deposition were obtained from entrainment and deposition correlations. The net mass transfer across the liquid-vapour interface was obtained from a mass balance.

The annular space was considered as two subchannels with the surface of zero shear, r_s, separating the subchannels. In the analysis, the subscript 1 refers to the symbols inside r_s and subscript 2 refers to the symbols outside r_s.

6.2.3a Shear Stress

The shear stress at the walls are

$$\tau_{wj} = \left(\frac{dP}{dZ}\right) \frac{|r_j^2 - r_s^2|}{2r_j} \quad , \quad j=1,2 \tag{17}$$

and the interfacial shear stresses at the shroud film interface is

$$\tau_{i2} = \left(\frac{dP}{dZ}\right) \frac{r_{i2}^2 - r_s^2}{2r_{i2}} \tag{57}$$

The frictional pressure gradient, $\left(\frac{dP}{dZ}\right)$, in the post dryout region is difficult to evaluate. Since there are no verified theoretical prediction methods or correlations to predict frictional pressure drops in the post dryout region the two-phase frictional multiplier approach using Thom's correlation, [28], was used in the present analysis. This approach was also used in the CHF prediction model and was found to be satisfactory in predicting the frictional pressure drop in annular flow before CHF was reached. In the post dryout region, the frictional pressure drop is expected to be lower than that in the annular flow regime before dryout. This is because in the liquid deficient regime:

(a) There is one liquid film-vapour interface instead of two. The frictional pressure drop due to the wavy liquid film-vapour interface which increases turbulence in the core, would be lower.

(b) The viscosity of the vapour is lower than the viscosity of the liquid. The wall friction on the dry heater surface would be smaller.

Any frictional pressure drop prediction method, which is suitable to be applied to the annular flow regime, is expected to overpredict the frictional pressure drop in the liquid deficient regime at the same flow conditions.

6.2.3b Velocity Profiles in the Shroud Film

As in the CHF model in Section 6.1.2d, Prandtl's universal, turbulent two-layer model is assumed for the velocity profile in the shroud film. Integrating the universal velocity profile gives the triangular relationship for the shroud film,

$$M_2^+ = \begin{cases} \frac{1}{2} (\delta_2^+)^2 , & \delta_2^+ \leq 11.5 \\ 8.5\ \delta_2^+ + 2.5\ \delta_2^+ \ln \delta_2^+ - 214 , & \delta_2^+ > 11.5 \end{cases} \quad (58)$$

6.2.3c Velocity Profiles in the Vapour Core

Downstream of the dryout location, a layer of laminar vapour moves along the heated wall. The vapour moving in the core becomes turbulent at some distance from the wall. The velocity profile in the vapour core in zone 1 is assumed to be expressed by the Prandtl's universal, turbulent two-layer model. Therefore, in zone 1,

$$U_{V1}^+ = \begin{cases} Y_1^+ , & Y^+ \leq 11.5 \\ \frac{1}{\kappa} \ln Y_1^+ + B , & Y_1^+ > 11.5 \end{cases} \quad (59)$$

where $$U_{V1}^{+} = \frac{U_{V1}}{U_{V1}^{*}} \tag{60}$$

$$U_{V1}^{*} = \frac{\tau_{w1}}{\rho_V} \tag{61}$$

$$Y_1^{+} = \frac{\rho_V \, Y_1 \, U_{V1}^{*}}{\mu_V} \tag{62}$$

$$Y_1 = |r - r_1| \tag{63}$$

and $B = 5.5$ for smooth walls (64)

In zone 2, the velocity profile in the core is assumed to be given by the turbulent logarithmic profile as in the CHF model in Section 6.1.2e. That is

$$U_{V2}(r) = U_{i2} + U_{V2}^{*} \left(\frac{1}{\kappa} \ln \frac{|r_{i2} - r_s|}{k_s} + B\right) \tag{65}$$

where $\kappa = 0.4$ von Karmon constant (66)

$B = 8.5$ for rough walls (67)

Assuming the maximum velocity coincides the radius of zero shear, then at r_s,

$$U_{V1}(r_s) = U_{V2}(r_s) \tag{36}$$

$$\text{i.e.} \quad U^{+}_{V1} \cdot U^{*}_{V1} = U_{i2} + U^{*}_{V2} \left(\frac{1}{\kappa} \ln \frac{|r_{i2} - r_s|}{k_s} + B\right) \tag{68}$$

Equation (68) along with equation (58) allow the evaluation of the radius of zero shear, r_s, and the shroud film thickness, δ_2, when the film flow rate and the frictional pressure gradient are known.

6.2.3d Entrainment and Deposition at Shroud Film Interface

In the post dryout regime, the droplet concentration in the vapour core is reduced as evaporation takes place at the surface of the droplets. The deposition of droplets onto the shroud film, which is proportional to the droplet concentration in the vapour core, is also reduced. Equilibrium between droplet deposition and entrainment would not occur resulting in net mass transfer from the shroud film. The entrainment and deposition correlations, which were described in Sections 6.1.2f and 6.1.2g, will be used to evaluate the entrainment and deposition masss fluxes for the shroud film in the post dryout region.

For the entrainment mass flux, the correlating parameter is

$$S_\delta = \frac{\tau_i \delta}{\sigma} \tag{37}$$

and the correlations for various ranges of S_δ are given by equations (38) to (41).

Under adiabatic conditions, the deposition mass flux is

$$G_D = k_D C_{eq} \tag{42}$$

The homogeneous concentration of droplets in the core is

$$C_{eq} = \frac{M_E}{\frac{M_E}{\rho_L} + \frac{M_V}{\rho_V}} \tag{43}$$

The deposition coefficient, k_D, is listed in Table 3 as a function of pressure.

6.2.3e Mass Balance on Shroud Film

From the continuity of mass across the liquid-vapour interface of the shroud film, the net mass transfer is

$$\frac{d M_{LF2}}{dZ} = 2\pi r_2 (G_{D2} - G_{E2}) \tag{69}$$

In the model, it is assumed that, at any location, the mass transfer from the shroud film to the vapour core is in the form of droplets having the same diameter as the droplets in the vapour core at the same location. Therefore, the net entrainment effect is to increase the number of droplets in the core. This increases the total surface area of droplets for heat transfer from the superheated steam, resulting in lower vapour temperatures and hence, lower wall temperatures. This is in contrast to other post-dryout models for tubes, [35,36,3], in which, the number of droplets remains unchanged if there is no droplet breakup.

6.2.4 Droplet-Vapour Flow in Post-Dryout Region

To evaluate the flow conditions of the droplets and the superheated vapour, the model considers the annular space as a whole and cross-sectional average valves are used in the analysis.

6.2.4a Droplet Velocity Gradient

In vertical up flow, each droplet experiences a drag force and a gravitational force. The drag force is

$$F_D = \frac{\pi}{4} d^2 C_D \rho_V \frac{(U_V - U_d)^2}{2} \tag{70}$$

and the gravitational force is

$$F_{grav} = \frac{\pi}{6} d^3 (\rho_L - \rho_V) g \tag{71}$$

Therefore, the acceleration of the droplet is

$$\frac{dU_d}{dt} = \frac{(F_D - F_{grav})}{\frac{\pi}{6} d^3 \rho_L}$$

$$= \frac{3C_D \rho_V (U_V - U_d)^2}{4d\rho_L} - (1 - \frac{\rho_V}{\rho_L}) g \tag{72}$$

Ingebo, [38], had studied particle acceleration in accelerating air stream and has correlated a wide range of data for the drag coefficient, C_D:

$$C_D = \frac{27}{Re_d^{0.84}} \tag{73}$$

where $$Re_d = \frac{\rho_V (U_V - U_d) d}{\mu_V} \tag{74}$$

The same expression for C_D was also used by Bennett et al. [34]. Minimum value of $C_D = 0.4$ was used by other researchers and is used in the present model. The velocity gradient is thus given by equations (70), (71) and (72) as follows:

$$\frac{dU_d}{dZ} = \frac{1}{U_d} \frac{dU_d}{dt}$$

$$= \frac{3C_D \rho_V (U_V - U_d)^2}{4 d U_d \rho_L} - (1 - \frac{\rho_V}{\rho_L}) \frac{g}{U_d} \tag{75}$$

6.2.4b Droplet Diameter Gradient

The droplets reduce the diameter as a result of heat transfer from the superheated steam to the droplets and mass transfer of water vapour from the droplet surface to the superheated steam.

The rate of change of the droplet diameter can be obtained from an energy balance:

$$\frac{d}{dt} (\frac{\pi}{6} d^3 \rho_L) = \frac{\pi d^2 q''_{S-D}}{h_{fg}} \tag{76}$$

$$\therefore \quad \frac{d(d)}{dt} = - \frac{2q''_{S-D}}{h_{fg}\rho_L} \tag{77}$$

For a sphere in a still fluid, the Nusselt number for heat transfer and the Sherwood number for mass transfer are both equal to 2.0. That is

$$q''_{S-D} = \frac{2k_V}{d} (T_V - T_i) \tag{78}$$

Combining equations (77) and (78), the rate of change of droplet diameter becomes,

$$\frac{d(d)}{dt} = - \frac{4k_V(T_V - T_i)}{h_{fg}\rho_L d} \tag{79}$$

The water vapour diffusing into the superheated steam depends on the pressure of the droplet at the interface and the pressure of the superheated steam. Alternatively, the rate of change of droplet diameter can be obtained from a mass balance at the droplet interface, according to Ryley as reported by Bennett et al. [35]:

$$\frac{d(d)}{dt} = - \frac{4K_D(P_i - P_V)}{\rho_L R\theta_V d} \tag{80}$$

where θ_V is the absolute vapour temperature, and K_D, as suggested by Ryley, is:

$$K_D = \frac{k_V(\gamma - 1)}{\rho_V R} \tag{81}$$

where γ is the index for isentropic expansion.

From equations (79) and (80), Bennett derived an iterative method to evaluate P_i and T_i and Groeneveld, [3], derived an expression for P_i which is more suitable at high pressures than Bennett's method. Groeneveld also suggested that it is realistic to assume that, at high turbulence level, the diffusive resistance $(P_i - P_V)$ can be neglected and $T_i = T_{sat,P_V}$ which is the saturation temperature at P_V. This assumption is adapted in the present analysis and equation (79) becomes

$$\frac{d(d)}{dt} = - \frac{4k_V(T_V - T_{sat,P_V})}{h_{fg}\rho_L d} \tag{82}$$

When there is relative motion between the droplets and the superheated vapour, the heat and mass transfer are enhenced. The Froessling ventilation factor F is introduced (Bennett et al. [35]) and the actual rate of $\frac{d(d)}{dt}$ is:

$$\frac{d(d)}{dt} = \left(\frac{d(d)}{dt}\right)_{still} \cdot F \tag{83}$$

where $$F = 1 + 0.276\ Re_d^{1/2} \left(\frac{\mu_G}{K_D \rho_V}\right)^{1/3} \tag{84}$$

The droplet diameter gradient can then be obtained:

$$\frac{d(d)}{dZ} = \frac{1}{U_d} \frac{d(d)}{dt}$$

$$= - \frac{4k_V(T_V - T_{sat,P_V})}{U_d h_{fg}\rho_L d} \cdot F \tag{85}$$

If the pressure gradient along the post dryout region is large, evaporation of the droplet will occur as a result of flashing. Also,

evaporation of droplet will be increased due to dry wall collision by the droplets. Groeneveld derived expressions for the droplet diameter gradient due to flashing and dry wall interaction. In the experiments, the qualities in the post-dryout region were low (below 30%) and the length in dryout was short (less than 15 cm). The pressure gradient along the dryout length was small. The change of droplet diameter due to flashing is insignificant and is therefore neglected. The expression, which was suggested by Groeneveld to estimate the extra amount of heat transfer to the droplets due to dry collision for a tube is:

$$q''_d = k_{V,f}(1 - \alpha) \frac{T_w - T_{sat}}{\delta} \exp\left(- \frac{2D}{Z - Z_{DO}}\right) \qquad (86)$$

where $(1 - \alpha)$ is the fraction of wall facing a liquid mass

$\exp - \frac{2D}{Z - Z_{DO}}$ is estimated to account for the reduced wall-droplet interaction just beyond dryout

and δ_V is an equivalent minimum vapour film thickness which also accounts for the effects of increased convection.

To determine δ in equation (86), q''_d is initially estimated from the experimental values of the total heat flux, q", and the measured wall temperatures:

$$q''_d = q'' - H(T_w - T_V) \qquad (87)$$

where

$T_V \simeq T_{sat}$ just beyond dryout.

Once q''_d is known, δ_V can be estimated from equation (86). But, as stated by Groeneveld, q''_d is the difference of two nearby equal quantities, the uncertainty in δ_V will be large. And, in equation (86), the fraction of wall facing a liquid mass is given by the liquid fraction, $(1 - \alpha)$, which is not true for annuli since some of the liquid remain on the shroud wall. In the present model, the extra heat transfer due to droplet-wall interaction is neglected.

It should be noted that droplet breakup may occur if the effective droplet diameter exceeded the critical diameter,

$$d_c = \frac{We_c \sigma g_c}{\rho_V (U_V - U_d)^2} \tag{88}$$

Therefore, at each node, the effective droplet diameter should be compared to the critical diameter. If droplet break up occurred, the effective diameter in equation (85) is taken to be equal to d_c.

6.2.4c Actual Quality Gradient

At dryout, the droplet mass flux can be found from

$$G_d = G(1 - x_{DO}) - G_{LF} \tag{89}$$

where the mass flux of the liquid film on the shroud is defined as

$$G_{LF} = \frac{M_{LF}}{\pi(r_2^2 - r_1^2)} \tag{90}$$

Therefore, the droplet flux is

$$N_d = \frac{G_d}{\frac{\pi}{6} d_c^3 \rho_L}$$

$$= \frac{G(1 - x_{DO}) - G_{LF}}{\frac{\pi}{6} d_c^3 \rho_L} \tag{91}$$

Differentiating equation (91), assuming ρ_L is constant, the variation of quality can be expressed as

$$dx = -\frac{1}{G}\left[\frac{\pi}{2} \rho_L d^2 N_d d(d) + \frac{\pi}{6} \rho_L d^3 \cdot dN_d + dG_{LF}\right] \tag{92}$$

The second and the third terms on the R.H.S. of equation (92) represent the conversion of complete droplets into vapour and the evaporation of the shroud film respectively. Since it is assumed that the change of quality is due to the evaporation at the droplet vapour interface only,

$$\therefore \quad dN_d = dG_{LF} = 0 \tag{93}$$

and the quality gradient becomes

$$\frac{dx}{dZ} = -\frac{\pi \rho_L d^2 N_d}{2G} \frac{d(d)}{dZ} \tag{94}$$

As discussed in Section 6.2.3d, due to the net entrainment of the shroud film, the droplet flux in the vapour core will change. Assuming the freshly entrained liquids at any axial location are in the form of droplets having the same diameter as the droplets in the gas core at the same axial location, the change of droplet flux can be related to the change in the film mass flux as:

$$dN_d = - \frac{dG_{LF}}{\frac{\pi}{6} d^3 \rho_L} \tag{95}$$

where $$dG_{LF} = \frac{dM_{LF}}{\pi(r_2^2 - r_1^2)} \tag{96}$$

Therefore at each node, a new value for N_d should be calculated and used in equation (94):

$$(N_d)_n = (N_d)_{n-1} - \frac{dG_{LF}}{\frac{\pi}{6} d^3 \rho_L} \tag{97}$$

If there is droplet break up at anyone node, new values for d and N_d have to be used in equation (94) from

$$d = d_c = \frac{We_c \sigma g_c}{\rho_V (U_V - U_d)^2}$$

and $$N_d = \frac{G(1 - x_a) - G_{LF}}{\frac{\pi}{6} d^3 \rho_L}$$

6.2.4d Vapour Temperature Gradient

The change of the temperature of the vapour is due to the heat transfer from the heated wall to the vapour and heat transfer from the vapour to evaporate the droplets. Therefore, from a heat balance,

$$C_{P_V} x_a M dT_V = 2\pi r_1 dZ q'' - (h_V - h_L) M dx \tag{98}$$

Rearranging,

$$\frac{dT_V}{dZ} = \frac{1}{x_a C_{P_V}} \left[\frac{2\pi r_1 q''}{M} - (h_V - h_L) \frac{dX}{dZ} \right] \tag{99}$$

6.2.4e Wall Temperature

Finally, the wall temperature is obtained from:

$$T_w = T_V + \frac{q''}{H} \tag{100}$$

where H is the heat transfer coefficient for dry steam. In the present work, the heat transfer coefficient correlation of Collier-Bennett, [39], for high pressure single-phase superheated steam in an annulus, is used,

$$\text{i.e.} \quad Nu = \frac{HD_e}{k} = 0.0173 \left(\frac{\rho U D_e}{\mu} \right)_v^{0.821} \left(\frac{C_P \mu}{k} \right)_v^{0.3} \tag{101}$$

and all the fluid properties are evaluated at the film temperature.

With the presence of the spacers, turbulent level and hence the heat transfer downstream of the spacer is significantly enhanced. Therefore in the present experiments, the post-dryout length is short (less than 15 cm) and the heat transfer coefficient was not fully developed. Although the effects of spacers have been observed and studied by researches, systematic investigations on this subject are still lacking. More recently, literature survey of the spacer effects by Groeneveld and Yousef [40] revealed that spacing devices increase turbulence and hence heat transfer downstream, the magnitude of improvement, with other things being equal, depends very much on the geometry of the spacing devices. This suggests that it is best to account for the spacer effects for individual cases. Since there are no theories or correlations available in literature to predict the spacer effects, it is attempted here to correlate the spacer effects. The increased turbulence level downstream of the spacers decreases as the distance from the spacer increases. The resulting post-dryout heat transfer coefficient downstream of the spacer probably behaves similarly to the developing heat transfer coefficient at the entrance region of a conduit. In the entrance region, the Nusselt number is given by:

$$Nu_{\substack{\text{entrance}\\\text{region}}} = F_d \, Nu_{\substack{\text{developed}\\\text{region}}} \tag{102}$$

where the developing factor, F_d, can be correlated in the general form, [41]:

$$F_d = 1 + Re^a \left(\frac{L}{D_e}\right)^b \tag{103}$$

The same functional form is employed in the present analysis, and F_d is correlated by:

$$F_d = 1 + \frac{6}{\left(\frac{Re_V}{10^5}\right)^2 \left(\frac{\ell}{D_e}\right)^{0.7}} \tag{104}$$

The local Nusselt number at ℓ is then:

$$Nu_\ell = F_d \; 0.0173 \left(\frac{\rho U D_e}{\mu}\right)_V^{0.821} \left(\frac{C_p \mu}{k}\right)_V^{0.3} \tag{105}$$

6.3 CHF Prediction and Discussion

Since direct heaters are commonly used in CHF experiments, the predicted CHF results were compared to the CHF data from the direct heater. As summarized in Table 4, the predicted results are in good agreement with the experimental results. At inlet qualities of -25% and higher, the experimental data were predicted to within 13%. The error trend is shown in Figure 31 in which the predicted and experimental CHF were compared. In general, for a given mass flux, the model under predicted CHF at high inlet qualities (low inlet subcoolings) and over predicted CHF at low inlet qualities (high inlet subcoolings). At low inlet qualities (high inlet subcoolings), the errors increased as mass flux increased.

It is interesting to note that the error trend which substantially over predicts CHF at high inlet subcoolings is consistent with the

TABLE 4: CHF PREDICTION RESULTS

Mass Flow ($Mg.s^{-1}.m^{-2}$)	Inlet Quality (%)	Inlet Subc. (°C)	Exit Quality (%)	CHF_{Exp} ($MW.m^{-2}$)	CHF_{Pred} ($MW.m^{-2}$)	$(1-\frac{CHF_{Pred}}{CHF_{Exp}})\times 100$ (%)
2.0	-40	106	20.0	0.812	.925	-13.9
2.0	-10	23	28.3	0.522	.473	9.3
3.5	-40	106	13.7	1.245	1.494	-20.0
3.5	-25	64	18.1	1.016	1.102	- 8.5
3.5	-10	23	20.8	0.720	.664	7.8
5.0	-25	64	16.3	1.366	1.536	-12.5
5.0	-10	23	19.6	0.992	.928	6.5

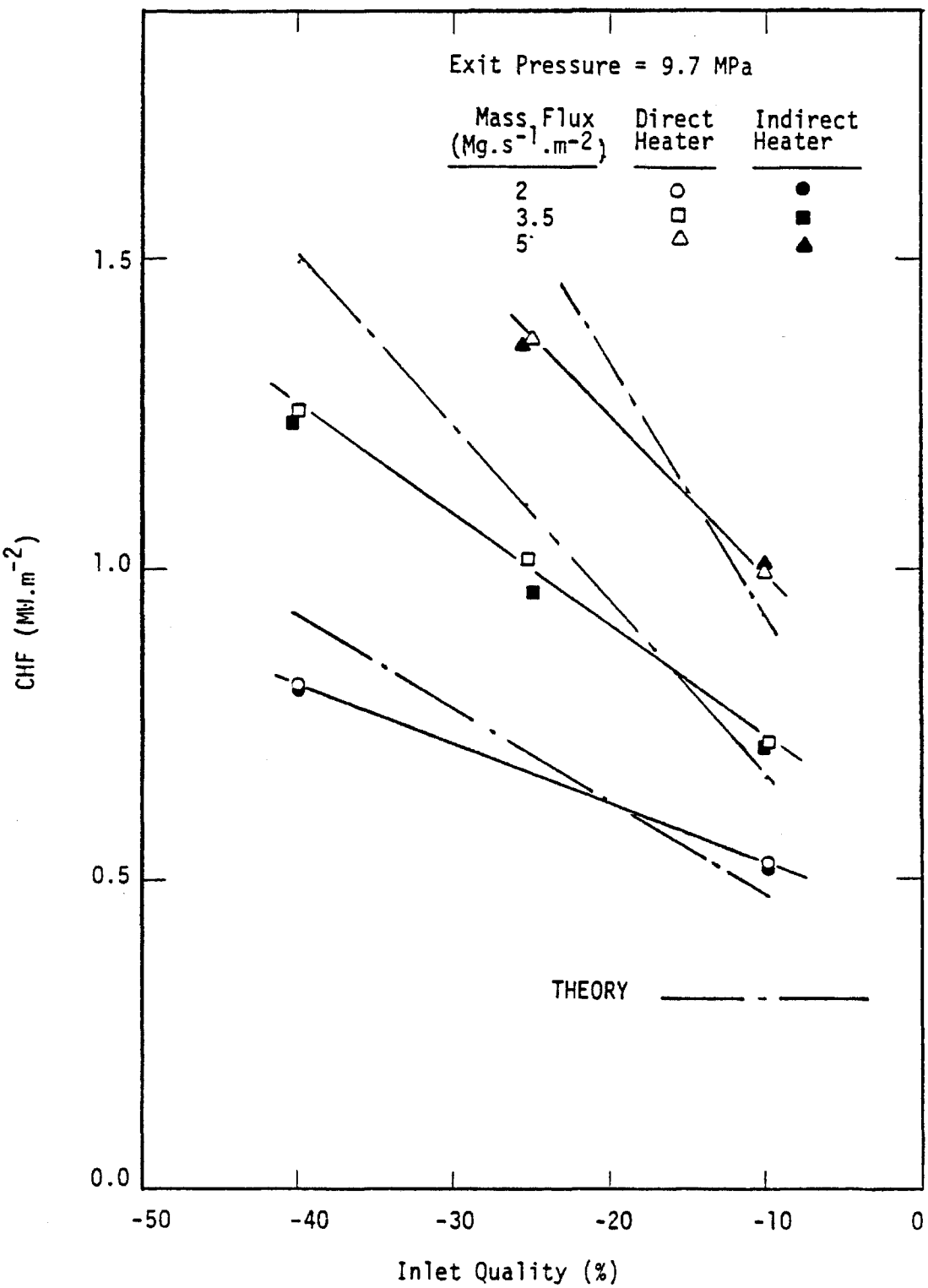

FIGURE 31 : COMPARISON OF PREDICTED CHF AND EXPERIMENTAL CHF DATA

predicted results of Saito [6] and Würtz [24]. The predicted results of Saito are listed in Table 5 for comparison. Saito suggested that the error trend may be due to nucleation in the liquid film. With nucleation in the liquid film, the bursting of bubbles at the interface should increase the entrainment. Also the friction at the heated surface would be increased, leading to the thickening of the rod film and resulting in higher entrainment. Indeed, simplified heat transfer calculations showed that, when the heat flux was high, nucleation occurred in the liquid film in regions just downstream of the onset of the annular flow region where the quality was low and suppression of nucleation was weak. Simplified analysis was performed to account for the effect of increased entrainment on CHF. The results showed that when entrainment was increased just downstream of the annular flow transition, then further downstream the droplet concentration was increased resulting in an increase of deposition. Overall CHF prediction were not improved to any significant degree and the effect of nucleation in the liquid film on CHF prediction is negligible. Other uncertainties such as the effects of heat flux on deposition and entrainment might in general have attributed to the observed error trend. The entrainment correlations used in the present model, as in the models of Saito [6] and Würtz [24], are based on adiabatic entrainment data for tubes. Probably it is more appropriate to use entrainment data for annuli if they are available. Also the deposition model for droplets is probably valid only for a limited range of sizes since recent photographic evidence [42] suggests that the large droplets move in straight lines with velocities near those at which they were entrained. Any one (or

TABLE 5: CHF PREDICTION RESULTS OF SAITO [6] FOR ANNULI

Experimental data								Prediction		
Experiment no.	Press. (bar)	Mass flux ($kg/m^2 \cdot s$)	Inlet subc. (°C)	Heat flux (MW/m^2)	Critical power (kW)	Boiling length (m)	Quality at CHF (–)	CHF (MW/m^2)	Critical power (kW)	Error (%)
1	69.2	354	32.3	0.83	92.6	2.20	0.615	0.67	75.3	–18.7
3	69.4	758	29.1	1.18	132.1	2.06	0.381	1.20	134.3	1.7
8	69.0	1295	37.9	1.62	180.1	1.74	0.259	1.77	198.2	9.7
9	69.8	1006	82.5	1.62	181.0	1.21	0.231	1.95	217.8	20.3
11	69.1	1573	32.5	1.65	184.5	1.70	0.213	1.97	220.2	19.2
69	68.9	564	41.1	1.09	121.9	1.99	0.448	1.04	116.6	–4.3
73	68.9	967	29.3	1.31	146.2	1.98	0.310	1.37	153.5	5.0
75	69.2	1397	24.2	1.43	159.9	1.92	0.228	1.65	184.2	15.2
94	68.9	797	69.4	1.52	170.1	1.60	0.351	1.56	173.7	2.1
107	69.1	1086	146.1	2.37	264.5	0.86	0.209	2.76	308.4	16.6
155	68.9	1533	55.4	2.00	222.9	1.42	0.212	2.33	260.2	16.7
192	68.9	2089	5.5	1.57	175.7	2.38	0.208	1.77	198.1	12.7
193	68.9	1146	5.0	1.36	151.4	2.47	0.339	1.22	135.4	–10.4
353	68.6	722	22.3	1.55	127.4	2.18	0.285	1.60	131.5	3.2
355	69.4	731	68.8	2.02	165.7	1.41	0.236	2.25	184.6	11.4
358	69.4	743	150.3	2.98	245.0	0.91	0.215	3.34	273.9	11.8

some combination) of these mechanisms could be used to rationalize the differences between experiments and predictions.

As in the present work, the prediction models of Saito [6] and Whalley [26] were based on the physical model of mass transfer across the interface by entrainment, evaporation at the interface and by deposition. All of these models did not include spacer effects, have widely different initial conditions and use different approaches to analyze the film flow rate and film thickness, yet all the prediction results are encouraging and have errors comparable to the correlations. Saito [6] and Whalley [26] extende the theory to calculate CHF in rod bundles with good results, and it is expected that the present model could be extended to the prediction of CHF in rod bundles also.

6.4 Post-CHF Prediction and Discussion

Since the heat capacity of the heater is not modelled, the predicted results are compared to the direct heater experiments only. In Figures 32 to 34, the predicted wall temperatures along the dry wall are comapred to the experimental wall temperatures*. Because initial dryout did not occur uniformly around the heater, implying the flow conditions were not perfectly uniform around the heater, the circumferential dry wall temperatures at any axial location were not

---

* Experimental wall temperature refers to the outside wall temperature obtained by substracting from the measured inside wall temperature, the temperature drop across the wall thickness which is estimated from a heat conduction calculation.

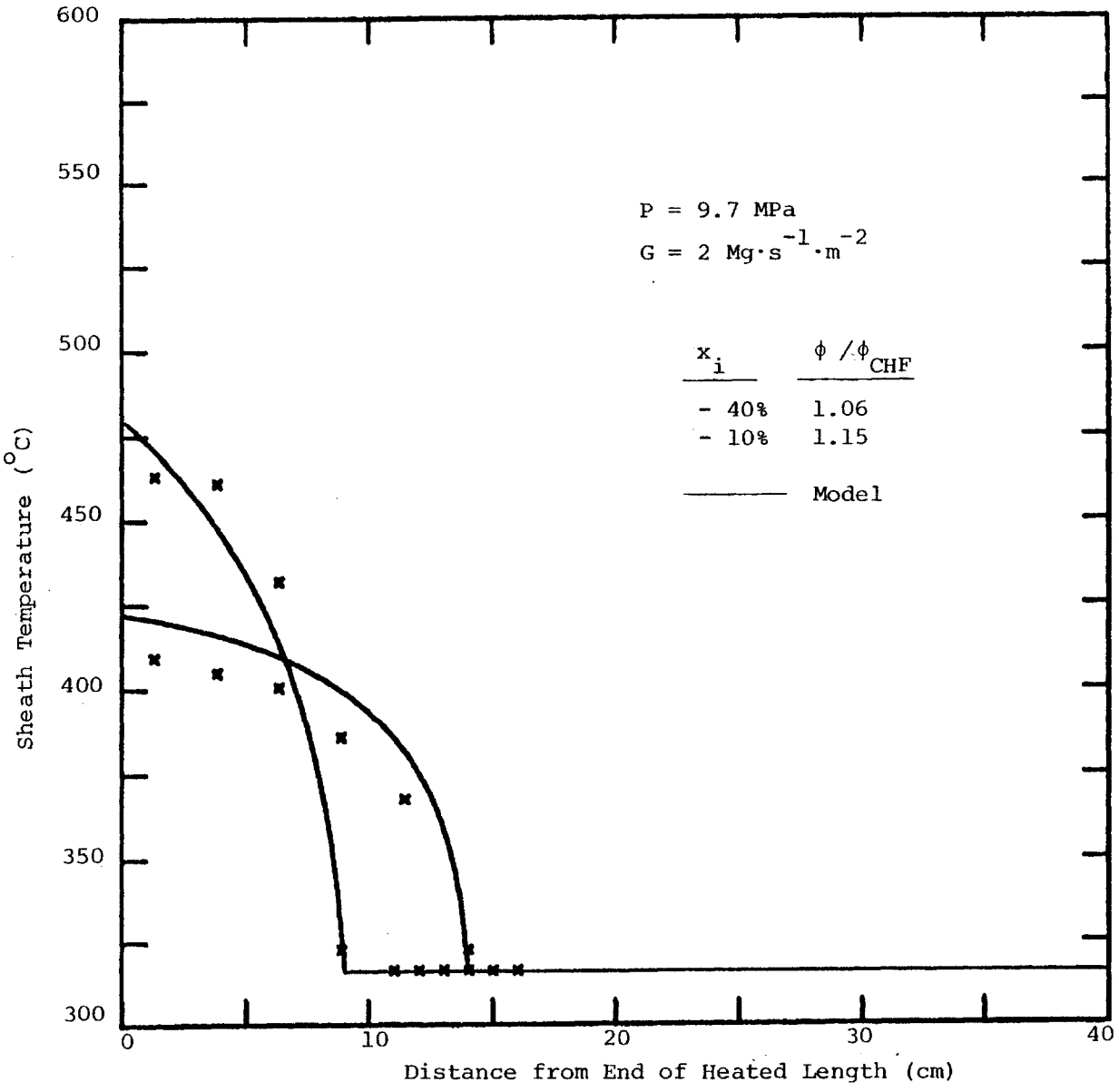

FIGURE 32: COMPARISON OF PREDICTED AND EXPERIMENTAL WALL TEMPERATURES AT G = 3.5 $Mg \cdot s^{-1} \cdot m^{-2}$

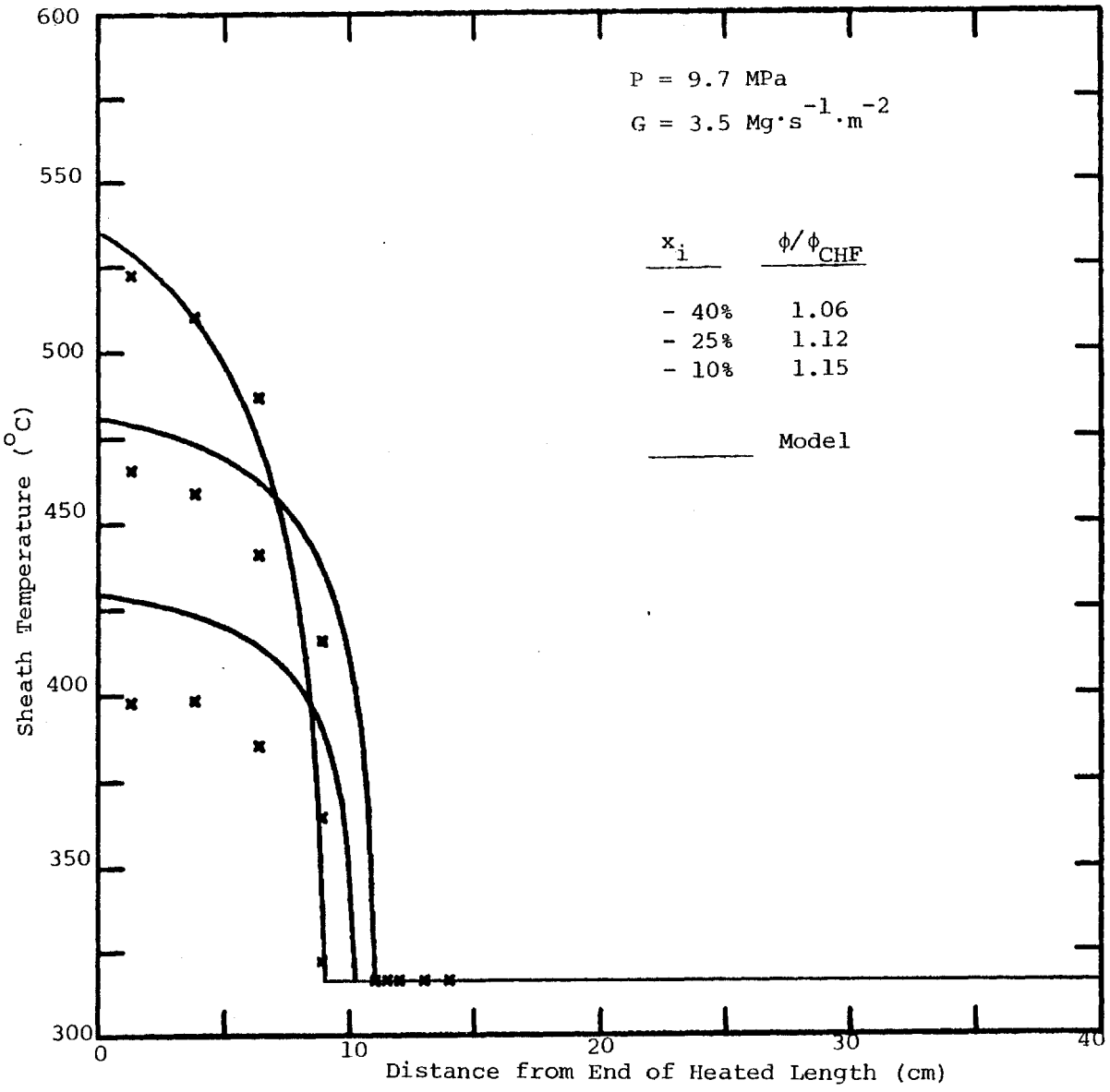

FIGURE 33: COMPARISON OF PREDICTED AND EXPERIMENTAL WALL TEMPERATURES AT G = 3.5 Mg·s^{-1}·m^{-2}

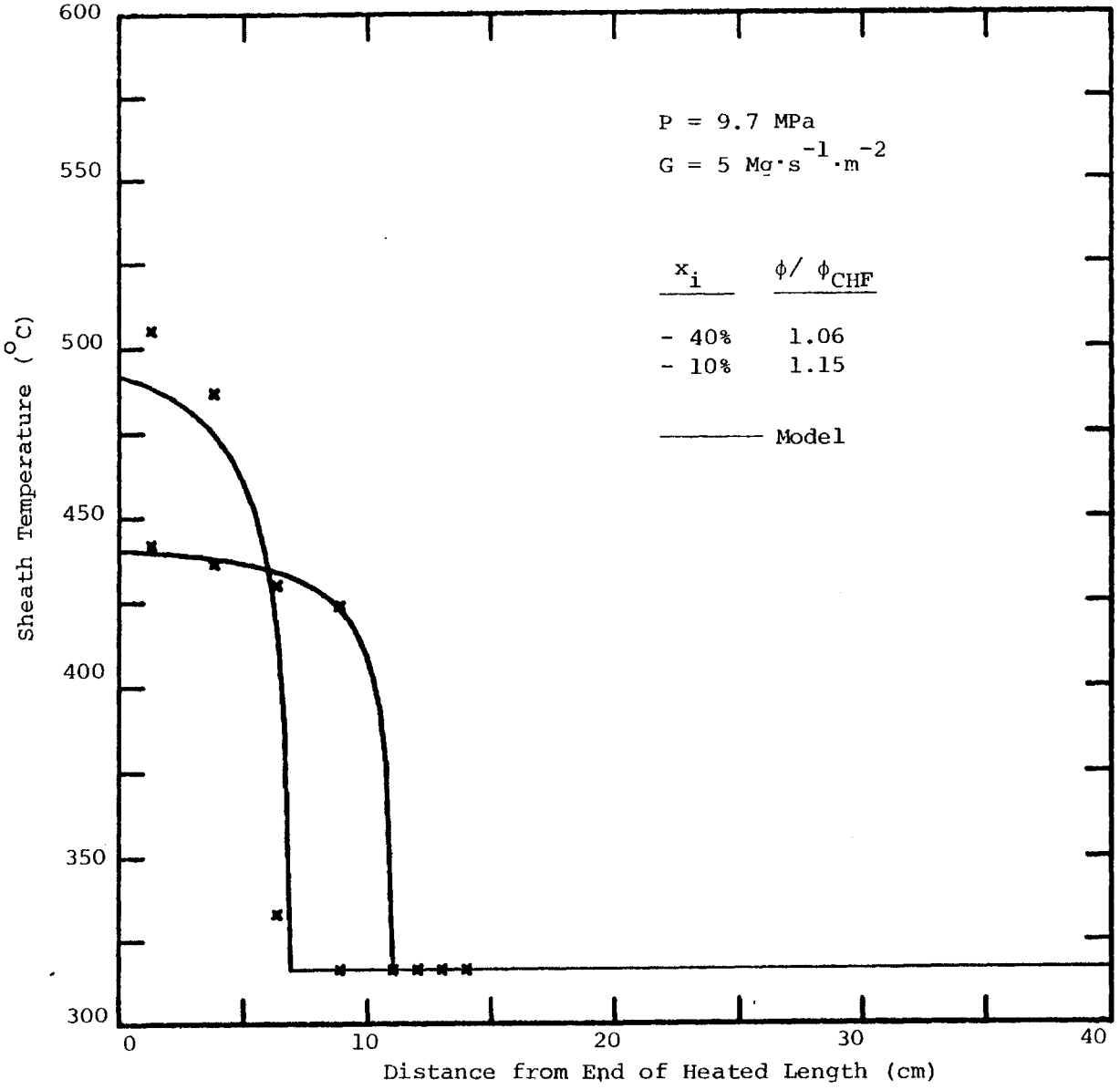

FIGURE 34: COMPARISON OF PREDICTED AND EXPERIMENTAL WALL TEMPERATURES AT G = 5 $Mg \cdot s^{-1} \cdot m^{-2}$

uniform as well. The experimental wall temperatures shown in the figures are the maximum circumferential dry wall temperatures which remain at the same angular location independent of the axial position. In general the agreement between the prediction and experiment is very good. The wall temperatures were predicted to within $20^{o}C$ in most of the cases shown in the figures. Furthermore, the characteristics of the temperature profile with increasing wall temperatures in the developing region (as a result of enhanced heat transfer caused by the spacer effects) were captured.

If the effects of the spacers are ignored, the resulting wall temperature profiles are shown in Figure 35. Since the spacers increase the turbulence level downstream, and hence the heat transfer, without the spacers, the wall temperatures, as expected, were overpredicted especially in the developing regions just downstream of the dryout location.

With the presence of the shroud film and net entrainment of liquid from the shroud film, the effective droplet flux is increased gradually with distance from the dryout location. As the number of droplets increases, the total surface area of the droplets available for heat transfer from the superheated steam increases. The net result is to lower the vapour temperatures and hence the wall temperatures. The effects of entrainment of liquid from the shroud film are shown clearly in Figure 36. When no liquid entrainment is allowed, the model predicted higher wall temperatures. Near the dryout location, almost all the heat is to superheat the vapour and there is little heat transfer to the

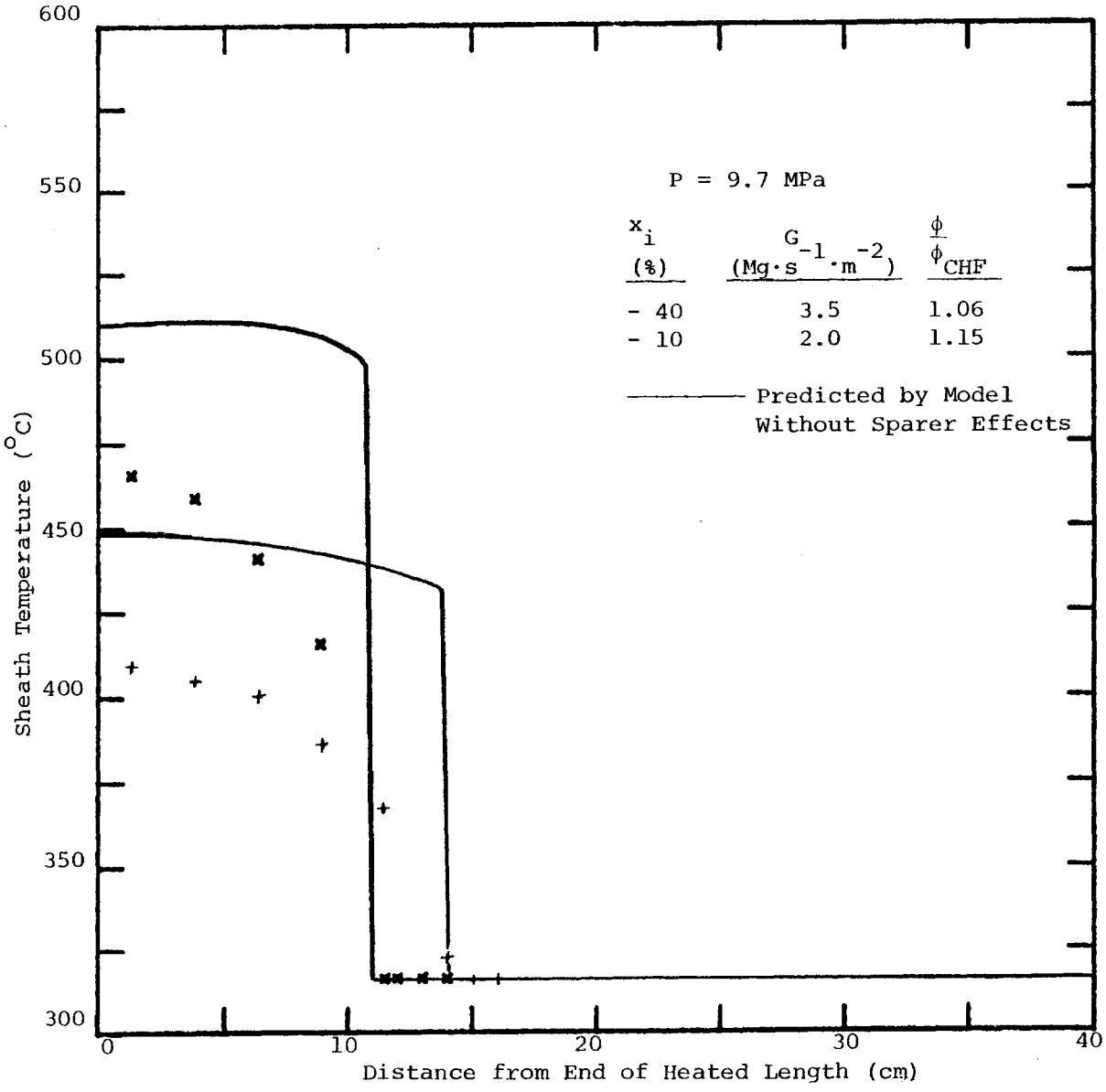

FIGURE 35: PREDICTION WITHOUT SPACER EFFECTS MODELLED

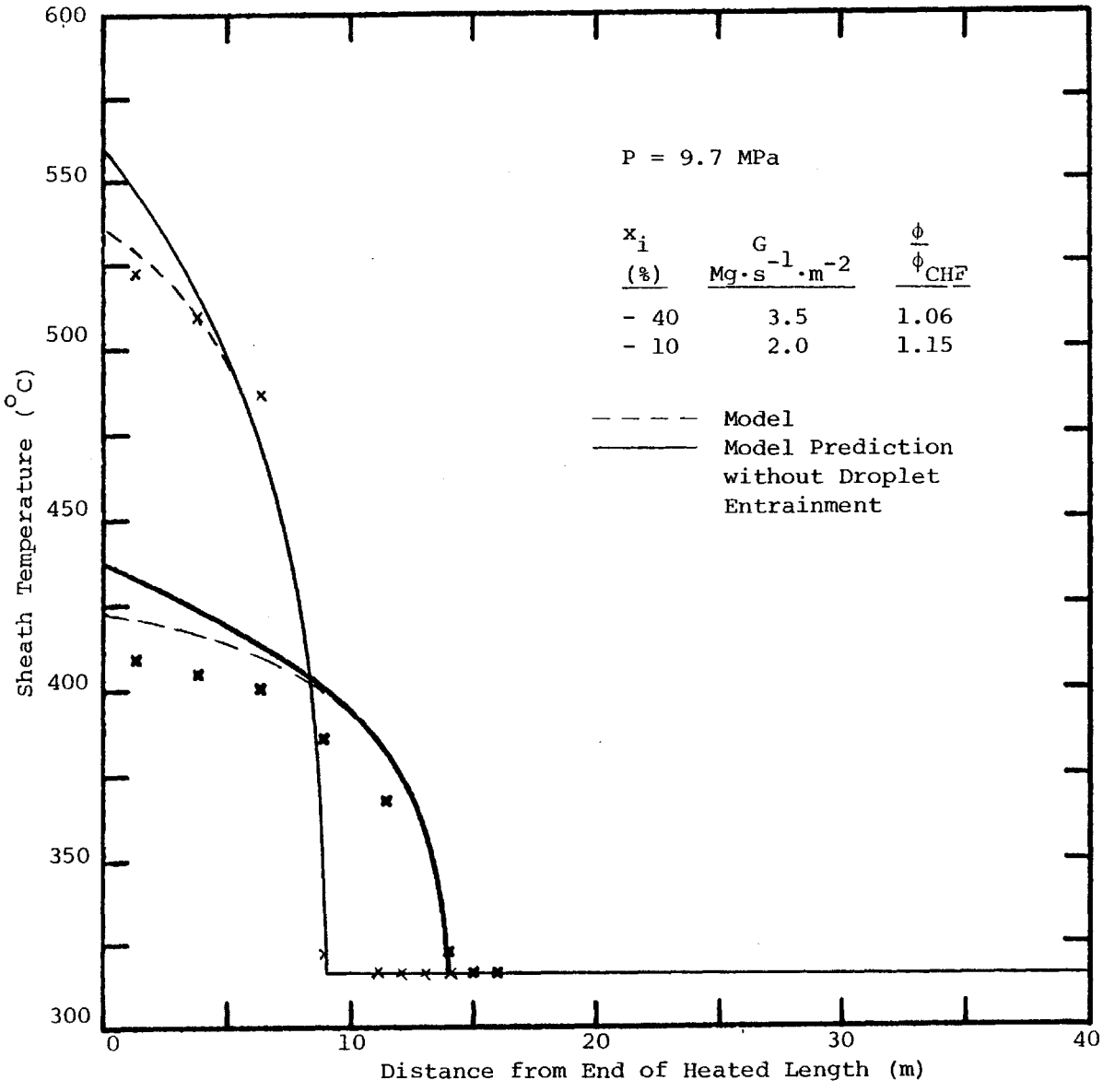

FIGURE 36: EFFECT OF DROPLET ENTRAINMENT ON PREDICTED WALL TEMPERATURES

droplets. Therefore, just downstream of the dryout location, the predicted wall temperatures with and without liquid entrainment from the shroud film were about the same.

It has been reported, in [35,36 and 39], and generally accepted that, in the liquid deficient regime, the steam and water are not in thermodynamic equilibrium. Thus assuming no droplet evaporation takes place, the wall temperatures will be higher, and assuming complete thermodynamic equilibrium (i.e. $T_v = T_{sat}$), the wall temperatures will be lower than the actual case in which some degree of superheating occurs. Such a trend is predicted correctly by the model in Figure 37.

Since the droplet flux at dryout is dependent on the initial film flow rate of the shroud film, it seems that the initial film flow rate is one of the important parameters affecting the predicted results. The shroud film flow rate at dryout is difficult to estimate accurately, therefore a sensitivity study was performed around the assumed shroud film flow rate at dryout. The predicted results for 20% higher in the shroud film flow rates at dryout is shown in Figure 38. It is obvious that the calculated wall temperatures did not differ significantly. In comparison it appears that as the shroud film flow rate at dryout is increase, the droplet flux, and hence the vapour-droplet heat transfer just downstream of dryout is reduced. Due to low vapour superheat at this location where the vapour-droplet heat transfer is small, further reduction in this heat transfer would not be reflected noticably in the wall temperatures. Because of the increase shroud film flow rate, the

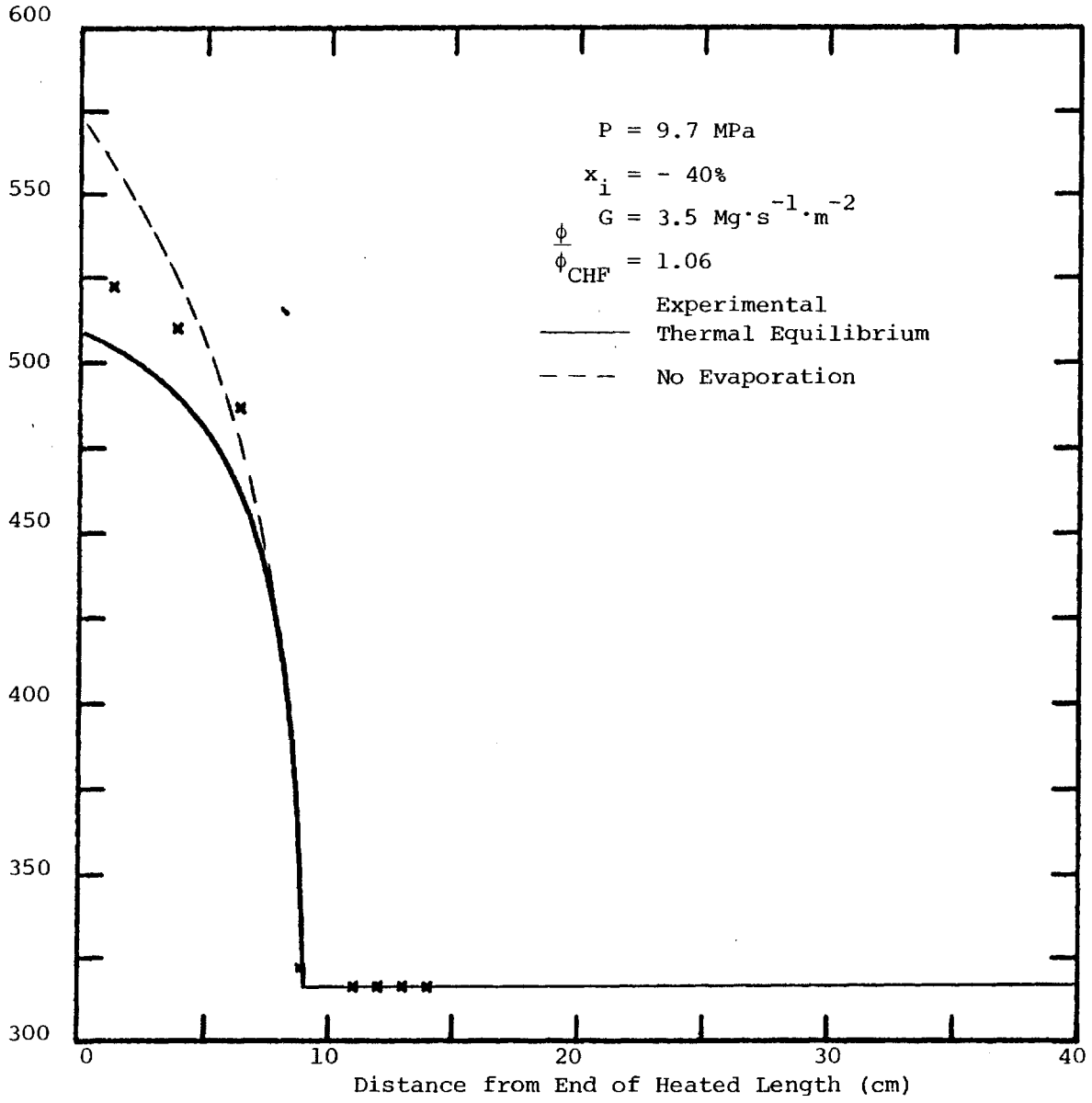

FIGURE 37: EFFECT OF THERMAL EQUILIBRIUM AND NO EVAPORATION ON PREDICTED WALL TEMPERATURES

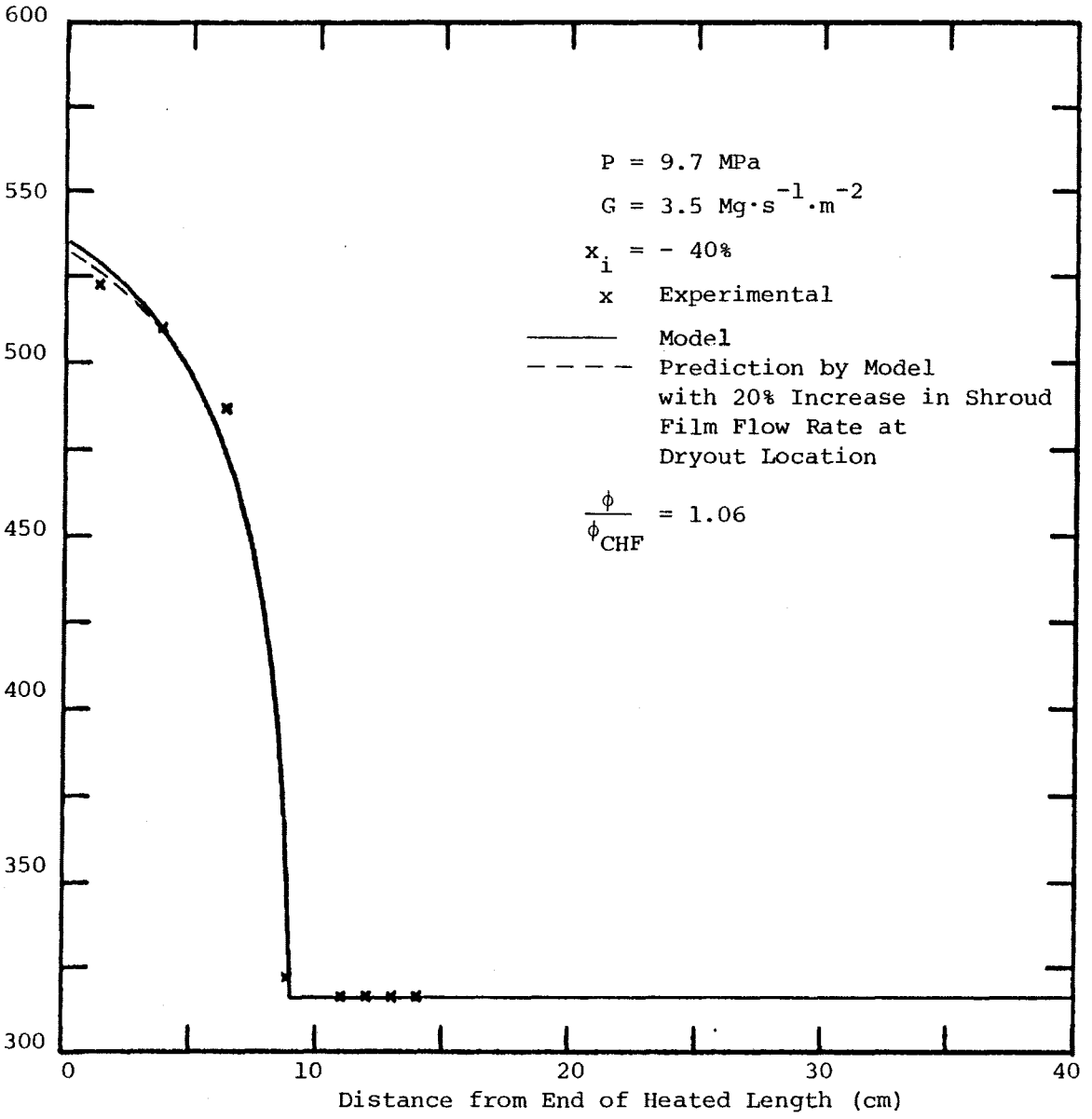

FIGURE 38: SENSITIVITY OF SHROUD FILM FLOW RATE AT DRYOUT LOCATION

droplet concentration, and hence the droplet deposition, is decreased. On the other hand, the film thickness, and hence the entrainment rate, is increased. As a result, the net mass transfer from the shroud film into the vapour core is increased. Eventually the vapour-droplet heat transfer some distance downstream from the dryout location is increased to values higher than that in the case before the shroud film flow rate at dryout is increased. Therefore in Figure 38, the wall temperatures for the increased shroud film flow rate were found to be lower. Fortunately, the predicted results are insensitive to the shroud film thickness at dryout.

7. CONCLUSIONS

The present studies of the characteristics of heater types and the application of a theoretical model to predict CHF has resulted in the following findings:

(a) The direct and indirect heaters are similar in CHF performance on a system parameter basis.

(b) At heat fluxes above CHF, the heaters have similar heat transfer performance, except at high mass fluxes where the indirect heater has better heat transfer. Slower thermal response of the indirect heater appears to result in better Post-CHF heat transfer at high mass flux compared to the direct heater.

(c) Differences in the internal thermal conduction of the heaters have little effect on the maximum wall temperature of the heaters.

(d) In the direct heater, complete circumferential spreading of the dryout patch required heat fluxes of more than 6% above CHF. Although there was limited Post-CHF data for the indirect heater, there were indications that lower heat fluxes than for the direct heater was required to spread the dryout patch around the indirect heater.

(e) The presence of spacers appeared to improve the Post-CHF heat transfer. The effect of the spacers was to increase the development length of the heat transfer coefficient and limit the axial spreading of the dryout patch.

(f) A theoretical model predicted CHF to within 13% for the most of the experimental data. CHF was under predicted at low inlet subcoolings and over predicted at high inlet subcoolings. The error trend is consistent with that in the prediction methods of other researchers. The prediction model may be suitable for predicting CHF in rod bundles.

(g) A theoretical model predicted the wall temperature in the dry region to within $20^{\circ}C$ for most of the experimental data. The Post-CHF prediction model captured the main characteristics of the temperature profile in the developing region. The predicted error trends were random. The theoretical approach may be suitable in modelling the heat transfer in rod bundles.

REFERENCES

1. Collier, J.G., "Convective Boiling and Condensation", Second Edition, McGraw-Hill, 1981.

2. Bergles, A.E., Collier, J.G., Delhaye, J.M., Hewitt, G.F. and Mayinger, F.M., "Two-Phase Flow and Heat Transfer in the Power and Process Industries", Hemisphere Publishing Corporation, 1981.

3. Groeneveld, D.C., "The Thermal Behaviour of a Heated Surface at and Beyond Dryout", AECL-4309, 1972.

4. Groeneveld, D.C. and Gardiner, S.R.M., "Post-CHF Heat Transfer Under Forced Convective Conditions", AECL-5883

5. Bennett, A.W., Hewitt, G.F. Kearsey, H.A., Keeys, R.K.F. and Lacey, P.M.C., "Flow Visualisation Studies of Boiling at High Pressure", AERE-R4874, 1965.

6. Saito, T., "Multi-Fluid Modeling of Two-Phase Flow and Heat Transfer: Application for CHF Prediction for BWR Conditions", Ph.D. Thesis, 1977, Department of Nuclear Engineering, University of Wisconsin-Madison.

7. Taitel, Y. and Dukler, A.E., "Flow Regime Transition for Vertical Upward Gas-Liquid Flow: A Preliminary Approach Through Physical Modelling", AIChE, 70th Annual Meeting, New York, Session on Fundamental Research in Fluid Mechanics, November 13-17, 1977, paper No. 17C.

8. Tong, L.S., "Boiling Crisis and Critical Heat Flux "USAEC Critical Review Series, TID-25887, 1972.

9. Kirby, J.G., Staniforth, R. and Kinneir, L.H., "A visual Study of Forced Convective Boiling. Part II: Flow Patterns and Burnout for a Round Test Section", AEEW-R506, 1967.

10. Hewitt, G.F. and Hall-Taylor, N.S., "Annular Two-Phase Flow", Pergamon Press, 1st edition, 1970.

11. Hewitt, G.F. Kearsey, H.A., Lacey, P.M.C. and Pulling, D., "Burn-out and Nucleation in Climbing Film Flow", UKAE report AERE-R4374, 1963.

12. Styrikovich, M.A., Tsiklauri, G.V., Baryskev, Ya.A. and Sakhno, V.P., "Wave Pattern and Liquid Film Burnout With Cocurrent Vapour Flow", 6th Int. Heat Transfer Conference, Vol. 1., pp. 379-404.

13. Mueller, R.E., "Film Boiling Heat Transfer Measurements in a Tubular Test Section", EURAEC-1871/GEAP-5423, 1967.

14. Kalinin, E.K., et al., "Heat Transfer in Tubes With Rod Regime in the Case of Flow Boiling of a Subcooled Liquid", Cocurrent Gas-Liquid Flow, Plenum, New York, 1969, pp. 497-525.

15. Macbeth, R.V., "The Burnout Phenomenon in Forced Convection Boiling", Advances in Chemical Engineering Vol. 7, pp. 207-289.

16. Theofanous, T.G., "The Boiling Crisis in Nuclear Reactor Safety and Performance", Int. J. Multiphase Flow, Vol. 6, pp. 67-95.

17. Lee, D.H., "An Experimental Investigation of Forced Convection Boiling in High Pressure Water", Pt. III AEEW-R 355 (1965).

18. Jeffries, N.P., "The Wall Thickness Effect on the Burnout Heat Flux", Thesis, 1963, Dept. of Mechanical Engineering, Stanford University.

19. Tolubinskiy, V.I., Ostrovskiy, Yu.N. and Pisarev, V.Ye., "Boiling Crisis Generated Upon a Steep Increase in Power in Heaters With Different Heat Capacities (Tube-Wall Thicknesses)", Heat Transfer, Soviet Research, Vol. 7, No. 3, May-June 1975.

20. Groeneveld, D.C., Moeck, E.O., "An Investigation of Heat Transfer in the Liquid Deficient Regime", AECL-3281.

21. Rohsenow, W.M., Griffith, P., Plummer, D.N. and Iloeje, O.C., "An Investigation of the Collapse and Surface Rewet in Film Boiling in Forced Vertical Flow", ASME 73-WA/HT-20.

22. Pederson, C.O., "An Experimental Study of the Dynamic Behaviour and Heat Transfer Characteristics of Water Droplets Impinging Upon a Heated Surface", Int. J. Heat Transfer Vol. 13, pp. 369-381

23. Groeneveld, D.C., "Variation in Heat Transfer Parameters Near the Dryout Location", Proceedings of the Fifth Canadian Congress of Applied Mechanics, Fredericton, May 26-30, 1975.

24. Würtz, J.W., "An Experimental and Theoretical Investigation of Annular Steam-Water Flow in Tubes and Annuli at 30 to 90 bar", RISO Report No. 372.

25. Hewitt, G.F., Hutchinson, P. and Whalley, P.B., "The Calculation of Critical Heat Flux in Forced Convection Boiling", AERE-R7520, 1973.

26. Whalley, P.B., "The Calculation of Dryout in a Rod Bundle", Int. J. Multiphase Flow, Vol. 3, pp. 501-515.

27. Ahmad, S.Y., "Axial Distribution of Bulk Temperature and Void Fraction in a Heated Channel With Inlet Subcooling", J. of Heat Transfer, Vol. 92, pp. 595-609, 1970.

28. Thom, J.R.S., "Prediction of Pressure Drop During Forced Convection Boiling of Water", Int. J. Heat Mass Transfer, Vol. 7, pp. 709-724.

29. El-Shanawany, M., El-Shirbini, A.A. and Murgatroyd, W., "A Model for Predicting the Dry-Out Position for Annular Flow in a Uniformly Heated Vertical Tube", Int. J. Heat Mass Transfer, Vol. 21, pp. 529-536.

30. Lockhart, R.W. and Martinelli, R.C., "Proposed Correlation of Data for Isothermal Two-Phase, Two Component Flow in a Pipe", Chem. Eng. Prog. 45, 39, 1949.

31. Hutchinson, P. and Whalley, P.B., "A Possible Characteristic of Entrainment in Annular Flow", Chem Eng. Sci., Vol. 28, pp. 974-975, 1973.

32. Singh, K., St. Pierre, C.C., Crago, W.A. and Moeck, E.O., "Liquid Film Flow-Rates in Two-Phase Flow of Steam and Water at 1000 psia.", AIChE J., 15, pp. 51-56, 1969.

33. Keeys, R.K.F., Ralph, J.C. and Roberts, D.N., "The Effect of Heat Flux on Liquid Entrainment in Steam-Water Flow in a Vertical Tube at 1000 psia.", AERE-R6294, 1970.

34. Hutchinson, P., Hewitt, G.F. and Dukler, A.E., "Deposition of Liquid or Solid Dispersons From Turbulent Gas Streams: A Stochastic Model", Chem. Eng. Sci., Vol. 26, pp 419-439, 1971.

35. Bennett, A.W., Hewitt, G.F., Kearsey, H.A. and Keeys, R.K.F., "Heat Transfer to Steam-Water Mixtures Flowing in Uniformly Heated Tubes in Which the Critical Heat Flux Has Been Exceeded", UKAEA Report AERE-R5373, 1967.

36. Keeys, R.K.F., Ralph, J.C. and Roberts, D.N., "Post Burnout Heat Transfer in High Pressure Steam Water Mixtures in a Tube With Cosine Heat Flux Distribution", UKAEA Report AERE-R6411, 1971.

37. Isshiki, N., "Theoretical and Experimental Study on Atomization of Liquid Drop in High Speed Gas Stream", Report No. 35, Transportation Technical Research Institute, Tokyo, Japan.

38. Ingebo, R.D., "Drag Coefficient for Droplets and Solid Spheres in Clouds Accelerating in Air-Streams", N.A.C.A. Tech. Note 3762, 1956.

39. Collier, J.G., Bennett, A.W. and Lacey, P.M.C., "Heat Transfer to Mixtures of High Pressure Steam and Water in an Annulus, Part 1. Single Phase Experiments: Superheated Steam", AERE-R3653, 1961.

40. Groeneveld, D.C. and Yousef, W.W., "Spacing Devices for Nuclear Fuel Bundles: A Survey of Their Effect on CHF, Post-CHF Heat Transfer and Pressure Drop", ANS/ASME Meeting on Nuclear Reactor Thermohydraulics, Saratoga, New York, 1980.

41. McAdams, W.H., "Heat Transmission", 3rd edition, McGraw-Hill Book Company, New York, 1954.

42. Whalley, P.B., Hewitt, G.F. and Terry, J.W., "Photographic Studies of Two-Phase Flow Using a Parallel Light Technique", AERE-R9389, 1979.

NOMENCLATURE

A	flow area of test section	m
B	roughness function in the velocity profile	--
C_{eq}	homogeneous droplet concentration	$kg.m^{-3}$
C_D	drag coefficient	--
$\frac{dP}{dZ}$	frictional pressure gradient	kPa
d	droplet diameter	m
D	tube diameter	m
D_e	equivalent diameter	m
F_d	developing factor	--
F_s	flow split factor	--
g	acceleration due to gravity	$m.s^{-2}$
g_c	gravitational constant	$kg.m.N^{-1}.s^{-1}$
G	total mass flux	$kg.s^{-1}.m^{-2}$
G_D	deposition mass flux	$kg.s^{-1}.m^{-2}$
G_E	entrainment mass flux	$kg.s^{-1}.m^{-2}$
G_{evap}	evaporation mass flux	$kg.s^{-1}.m^{-2}$
h_{fg}	latent heat of vaporation	$kJ.kg^{-1}$
H	heat transfer coefficient	$W.m^{-2}.C^{-1}$
J_k	superficial velocity of phase k	$m.s^{-1}$
k	thermal conductivity	$W.m^{-1}.C^{-1}$
k_D	deposition coefficient	$m.s^{-1}$
k_s	equivalent sand roughness	m
K_D	diffusion coefficient	$m^2.s^{-1}$

ℓ	distance downstream of dryout	m
M	total mass flow rate	$kg.s^{-1}$
M_E	entrained droplet mass flow rate	$kg.s^{-1}$
M_G	vapour mass flow rate	$kg.s^{-1}$
M_{LF}	liquid film mass flow rate	$kg.s^{-1}$
M^+	dimensionless mass flow defined in equation (26)	--
N_D	droplet flux	$droplets.m^{-2}.s^{-1}$
P	pressure	kPa
q"	heat flux	$W.m^{-2}$
r	radial coordinate	m
r_s	radius of zero shear stress	m
r_1	outside radius of the rod	m
r_2	inside radius of the shroud	m
R	gas constant	$kJ.kg^{-1}.K^{-1}$
Re	Reynolds number	--
S	slip ratio	--
S_δ	entrainment parameter defined in equation (37)	--
T	temperature	^oC
U	axial velocity	$m.s^{-1}$
U*	shear velocity defined in equation (20)	$m.s^{-1}$
U^+	dimensionless velocity defined in equation (19)	--
$\overline{U}$	average axial velocity	$m.s^{-1}$
V_G	radial velocity of evaporating steam	$m.s^{-1}$
W_e	Weber number	--
x	thermal equilibrium quality	--
x_a	actual quality	--
χ	Lockhart-Martinelli parameter	--

Y	distance from wall	m
Y_D	constant in equation (46)	m
Y^+	dimensionless wall distance defined in equation (21)	--
Z	distance from inlet of test section	m
α	void fraction	--
β	volumatric quality	--
Γ	net interfacial mass exchange rate per unit volume	$kg.s^{-1}.m^{-3}$
δ	film thickness	m
δ^+	dimensionless film thickness defined in equation (28)	--
κ	von Karmon constant	--
ρ	density	$kg.m^{-1}$
μ	dynamic viscosity	$kg.m^{-1}.s^{-1}$
ϕ_f^2	Thom's two-phase frictional multiplier	--
ψ	CHF ratio defined in page 48	--
σ	surface tension	$N.m^{-2}$
τ	shear stress	$N.m^{-2}$
θ_V	absolute vapour temperature	^oK
γ	index for isentropic expansion	--

SUBSCRIPTS

1	refers to inner zone
2	refers to outer zone
c	critical
d	droplet
DO	dryout

E	entrained liquid
g	gas phase
G	gas phase
i	interface
L	liquid phase
LF	liquid film
m	mixture
sat	saturation condition
S-D	from superheated steam to droplet
TP	two-phase
V	superheated vapour
w	wall
W-S	from wall to superheated steam

APPENDIX A

CHF AND POST-CHF EXPERIMENTAL DATA

A1. INTERPRETATION OF RUN NAME

(A) CHF RUNS

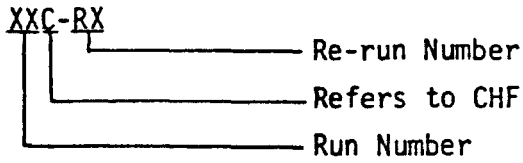

(B) POST-CHF RUNS

(a) Direct Heater Tests

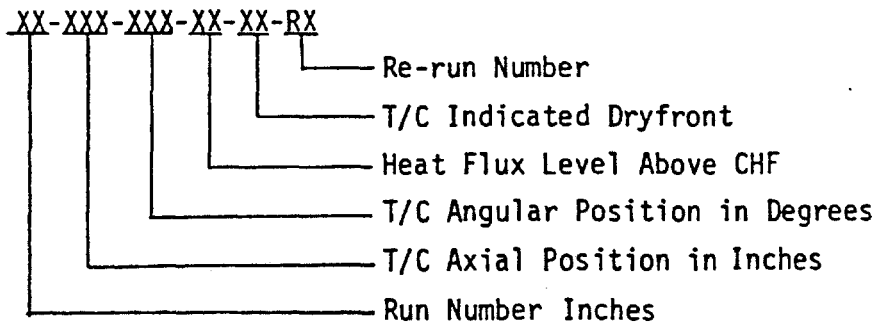

(b) Indirect Heater Tests

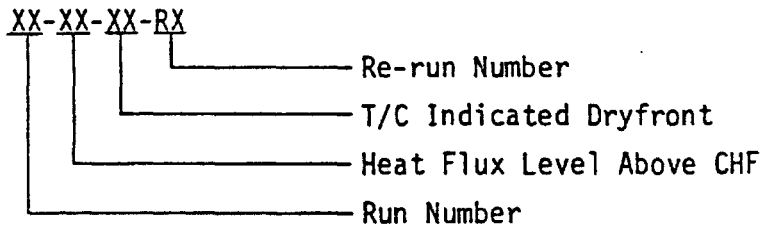

A2. CHF AND POST-CHF DATA OF THE DIRECT HEATER

Run Name	Exit Press. (MPa)	Mass Flux ($\frac{Mg}{s.m^2}$)	Qualities (%)				Heat Flux ($\frac{MW}{m^2}$)	Outside Wall Temperatures (°C)				
			Inlet	Exit	At T/C A	At T/C B		A1	A2	A3	B1	B3
1A-0.0-070-C	9.72	2.0186	-40.0	20.1	20.0	17.2	.812	317.2	317.0	315.8	316.5	319.6
1A-0.0-000-2	9.72	2.0165	-40.1	21.1	21.0	18.1	.827	334.2	386.8	319.8	315.9	320.4
1A-0.0-060-2	9.69	2.0052	-39.9	21.7	21.5	18.6	.828	396.3	318.5	318.1	316.5	319.7
1A-0.0-030-2-A2	9.73	2.0062	-40.2	21.4	21.2	18.3	.827	389.8	328.6	319.5	316.9	320.3
1A-0.0-110-2-A3	9.72	1.9907	-40.3	21.9	21.7	18.8	.828	415.1	319.8	329.7	316.6	319.2
1A-0.5-060-2	9.73	1.9969	-40.3	21.6	21.3	18.4	.827	382.3	317.1	317.0	315.4	319.2
1A-0.5-015-2-A1,A2	9.70	2.0041	-40.1	21.5	21.2	18.3	.827	339.4	330.5	318.1	316.0	319.8
1A-1.0-060-2-A1	9.70	1.9938	-40.2	21.7	21.2	18.3	.827	320.4	318.0	317.8	315.4	318.7
1A-0.0-000-4	9.71	1.9814	-39.9	23.8	23.6	20.7	.844	447.0	455.6	328.7	316.0	320.5
1A-0.0-060-4-A3	9.73	1.9814	-40.1	23.5	23.3	20.3	.842	455.0	431.4	330.9	317.1	320.0
1A-0.0-105-4-A2	9.73	1.9855	-40.0	23.5	23.4	20.4	.843	455.6	338.4	430.4	316.7	318.8
1A-1.0-000-4	9.70	1.9897	-39.8	23.6	23.1	20.2	.845	424.1	433.2	325.0	314.9	319.5
1A-1.0-060-4-A2	9.71	2.0010	-39.9	23.2	22.7	19.7	.844	441.8	332.1	324.2	315.9	318.9
1A-1.0-085-4-A3	9.71	1.9938	-39.9	23.3	22.8	19.8	.843	435.2	323.7	329.7	315.5	318.3
1A-1.5-000-4	9.72	2.0155	-40.1	22.6	22.0	19.0	.845	341.4	333.1	319.5	313.8	318.6
1A-1.5-060-4	9.73	2.0041	-40.1	22.8	22.1	19.2	.842	375.6	317.8	318.3	314.7	318.3
1A-1.5-010-4-A2	9.70	1.9979	-40.0	23.2	22.6	19.6	.846	356.3	328.3	319.2	314.3	318.4
1A-2.0-060-4-A1	9.71	2.0041	-39.9	23.0	22.2	19.2	.843	321.7	319.4	319.6	313.5	317.8
1A-0.0-000-6	9.71	2.0083	-40.1	23.9	23.8	20.8	.860	463.9	465.6	334.8	316.0	320.5
1A-0.0-060-6	9.74	2.0083	-40.2	23.8	23.6	20.6	.859	467.5	452.0	363.2	317.0	320.1
1A-1.0-000-6	9.70	1.9938	-40.1	24.5	24.0	20.9	.861	461.7	456.5	331.0	319.1	321.2
1A-1.0-060-6	9.72	2.0083	-40.2	23.9	23.4	20.4	.859	465.7	413.7	337.7	316.1	320.7
1A-2.0-000-6	9.73	1.9793	-40.2	24.8	24.0	20.9	.860	432.9	406.8	327.8	402.9	415.9
1A-2.0-060-6	9.71	1.9897	-40.1	24.5	23.7	20.7	.860	430.9	404.4	324.8	419.2	432.4
1A-2.0-300-6	9.70	1.9938	-40.1	24.4	23.6	20.6	.860	330.9	433.3	325.2	419.8	453.5
1A-3.0-000-6	9.72	2.0010	-40.1	24.1	22.9	19.9	.859	323.2	317.1	318.2	329.1	406.1
1A-3.0-300-6	9.70	1.9866	-40.0	24.6	23.4	20.4	.859	320.1	322.1	320.4	340.3	420.0

A2. CONTINUED

Run Name	Exit Press. (MPa)	Mass Flux ($\frac{Mg}{s.m^2}$)	Qualities (%) Inlet	Exit	At T/C A	At T/C B	Heat Flux ($\frac{MW}{m^2}$)	Outside Wall Temperatures (°C) A1	A2	A3	B1	B3
1C-00.0-000-C	9.69	1.9876	-9.9	28.4	28.3	26.5	.522	312.7	314.3	316.2	313.5	315.9
IC 00.5-060-0-A1	9.69	1.9897	-9.9	29.4	29.2	27.4	.535	331.2	314.8	315.6	313.1	315.6
1C-00.0-000-2	9.71	1.9990	-9.7	29.6	29.5	27.6	.537	353.4	343.9	317.4	313.3	315.8
1C-00.0-030-2	9.73	2.0052	-9.9	29.2	29.1	27.3	.536	363.0	322.1	316.9	313.4	316.1
1C-00.0-060-2	9.70	1.9979	-9.8	29.4	29.3	27.4	.535	362.0	315.9	317.1	313.3	315.9
1C-00.0-090-2	9.71	2.0041	-9.8	29.2	29.1	27.3	.535	361.5	317.2	330.9	313.4	315.3
1C-00.0-120-2	9.73	2.0114	-9.9	29.1	29.0	27.2	.536	346.8	317.7	355.6	313.7	315.5
1C-00.0-100-2-A1	9.69	1.9948	-9.8	29.4	29.3	27.5	.535	357.3	317.1	337.1	313.2	314.9
1C-00.5-000-2-A1	9.72	2.0103	-10.1	28.7	28.5	26.7	.533	315.0	314.9	316.4	313.2	316.1
1C-00.5-030-2-A1	9.68	2.0041	-9.9	29.2	29.0	27.1	.536	328.4	315.1	316.2	313.2	316.0
1C-00.5-090-2-A1	9.67	1.9876	-9.8	29.5	29.3	27.4	.535	346.2	316.0	315.5	313.4	314.9
1C-00.0-000-4	9.70	2.0196	-9.9	29.5	29.4	27.5	.543	364.2	358.8	318.2	313.5	316.2
1C-00.0-030-4	9.72	2.0072	-9.8	30.0	29.9	28.0	.545	372.4	342.0	317.9	313.7	316.4
1C-00.0-060-4	9.68	1.9897	-9.9	30.2	30.0	28.2	.545	372.1	323.0	320.3	313.2	316.2
1C-00.0-090-4	9.69	1.9990	-9.9	29.9	29.7	27.9	.543	371.8	317.5	354.8	313.2	315.3
1C-00.0-015-4-A2	9.70	2.0196	-9.8	29.7	29.6	27.8	.545	370.5	323.4	317.3	313.2	316.0
1C-00.0-070-4-A3	9.70	1.9917	-9.8	30.3	30.2	28.3	.546	374.4	319.5	330.7	313.2	316.1
1C-00.0-180-4-A1	9.71	2.0103	-10.0	29.7	29.5	27.7	.544	327.9	317.2	369.4	313.9	316.0
1C-01.0-000-4-A1	9.70	2.0010	-10.0	29.8	29.5	27.6	.544	327.8	319.6	316.6	314.4	316.3
1C-01.0-030-4-A1	9.67	2.0062	-10.0	29.7	29.4	27.5	.544	320.5	314.7	315.7	313.2	315.6
1C-01.0-060-4-A1	9.72	2.0072	-10.1	29.6	29.3	27.4	.544	334.2	314.7	315.4	313.5	315.9
1C-01.0-090-4-A1	9.72	2.0165	-10.1	29.5	29.2	27.3	.544	328.0	315.1	315.9	313.1	317.8
1C-00.0-000-6	9.68	2.0176	-9.7	30.5	30.4	28.6	.554	376.8	381.3	318.4	313.5	316.1
1C-00.0-030-6	9.69	2.0052	-9.7	30.7	30.6	28.7	.553	377.1	371.2	318.8	313.8	316.4
1C-00.0-060-6-A3	9.72	2.0196	-9.7	30.4	30.3	28.4	.553	376.3	336.5	331.2	314.0	316.6
1C-00.0-090-6	9.70	2.0083	-9.8	30.5	30.4	28.5	.553	376.7	319.1	365.1	313.2	315.8
1C-01.0-000-6	9.69	1.9990	-9.9	30.7	30.4	28.5	.555	364.7	351.6	316.0	314.9	316.9
1C-01.0-030-6-A2	9.72	2.0228	-10.0	30.2	29.8	28.0	.554	368.3	322.3	315.9	313.5	316.3
1C-01.0-060-6	9.68	2.0041	-9.9	30.5	30.2	28.3	.554	365.9	315.7	317.6	313.2	316.6
1C-01.0-090-6-B3	9.69	2.0010	-10.0	30.6	30.3	28.4	.554	366.5	316.3	351.0	313.3	328.6
1C-01.0-075-6-A3	9.69	2.0165	-9.9	30.3	30.0	28.1	.554	366.7	315.8	327.1	312.9	321.3

A2. CONTINUED

Run Name	Exit Press (MPa)	Mass Flux ($\frac{Mg}{s.m^2}$)	Qualities (%) Inlet	Exit	At T/C A	At T/C B	Heat Flux ($\frac{MW}{m^2}$)	Outside Wall Temperatures (°C) A1	A2	A3	B1	B3
1C-01.0-110-6-B3	9.71	2.0186	-9.8	30.4	30.1	28.2	.555	364.1	316.3	363.0	313.6	327.5
1C-02.0-000-6	9.69	2.0165	-9.8	30.2	29.7	27.8	.551	313.2	313.8	315.1	347.0	345.5
1C-02.0-030-6	9.71	2.0062	-9.8	30.5	30.0	28.1	.552	312.9	313.8	315.3	326.4	340.1
1C-02.0-090-6	9.70	2.0186	-9.8	30.5	30.0	28.1	.556	314.6	315.2	315.3	317.8	368.6
1C-02.0-120-6	9.70	2.0103	-9.8	30.4	29.9	28.0	.552	312.9	314.6	314.0	314.6	355.9
1C-02.0-040-6-B1	9.70	2.0145	-9.8	30.5	30.0	28.1	.554	313.0	313.8	315.0	327.5	352.1
1C-02.0-070-6-B1	9.70	2.0165	-9.8	30.4	29.9	28.0	.554	313.2	313.8	314.1	317.6	361.5
1C-02.0-180-6-B3	9.70	2.0186	-9.8	30.6	30.1	28.2	.557	313.3	314.1	314.7	348.1	340.9
1C-02.0-225-6-B1	9.70	2.0124	-9.9	30.3	29.8	27.9	.552	312.8	314.6	313.7	317.6	323.6
1C-2.25-000-6-B3	9.70	2.0145	-9.8	30.4	29.9	28.0	.554	312.7	313.8	315.6	357.3	338.9
1C-2.25-030-6	9.67	2.0134	-9.8	30.5	29.9	28.1	.554	312.7	313.5	315.4	325.7	341.9
1C-2.25-060-6-B3	9.69	2.0321	-9.8	30.1	29.5	27.6	.554	312.8	313.5	314.0	319.2	359.0
1C-2.25-090-6	9.71	2.0052	-9.9	30.7	30.1	28.2	.556	313.0	314.0	314.1	319.8	374.6
1C-2.25-120-6	9.71	2.0196	-9.9	30.4	29.8	27.9	.555	313.2	315.0	315.1	317.0	372.6
1C-2.25-150-6	9.69	2.0207	-9.9	30.4	29.8	27.9	.556	313.0	315.1	313.9	319.2	364.7
1C-2.25-165-6-B1	9.73	2.0238	-10.1	30.3	29.7	27.8	.556	313.1	315.1	313.9	324.1	344.7
1C-2.25-205-6-B3	9.67	2.0207	-9.8	30.4	29.8	28.0	.556	312.8	313.4	313.8	350.6	328.9
1C-2.25-300-6-B3	9.69	2.0021	-9.9	30.7	30.1	28.2	.555	313.4	313.5	314.1	368.9	335.4
1C-2.75-000-B1-6	9.70	2.0083	-9.9	30.8	30.1	28.2	.557	312.6	313.8	315.6	331.6	317.1
1C-2.75-070-6-B3	9.69	2.0072	-9.9	30.7	30.0	28.1	.557	312.6	313.9	314.5	316.4	327.4
1C-2.75-120-6	9.69	2.0114	-9.9	30.5	29.8	27.9	.555	313.1	315.1	313.8	313.8	327.0
1C-00.0-000-8	9.72	2.0217	-9.9	31.2	31.1	29.2	.566	384.9	387.7	320.7	314.8	316.7
1C-00.0-030-8	9.70	2.0103	-9.8	31.5	31.4	29.4	.566	383.4	384.2	321.3	314.1	316.6
1C-00.0-060-8	9.67	2.0103	-9.8	31.4	31.3	29.4	.565	382.2	371.6	351.0	313.8	316.4
1C-00.0-090-8	9.70	2.0052	-9.9	31.5	31.4	29.4	.566	382.7	328.1	379.8	314.4	317.8
1C-01.0-000-8	9.73	2.0103	-9.9	31.5	31.2	29.2	.566	382.6	383.2	319.1	316.9	318.1
1C-01.0-030-8	9.70	2.0062	-9.7	31.7	31.4	29.4	.567	381.9	375.5	319.0	314.3	317.2
1C-01.0-060-8	9.71	2.0165	-9.8	31.4	31.1	29.2	.566	380.2	353.5	332.3	314.9	317.8
1C-01.0-090-8-B3	9.70	1.9948	-9.7	32.0	31.7	29.7	.567	381.6	321.6	375.6	316.7	331.1
1C-02.0-000-8-B3	9.71	2.0062	-10.0	31.4	30.9	29.0	.566	355.2	321.6	315.4	374.8	376.4
1C-02.0-030-8-A1	9.69	2.0083	-9.9	31.5	30.9	29.0	.566	331.7	315.0	315.5	349.1	361.4
1C-02.0-060-8-A1,B1	9.72	2.0134	-9.9	31.5	31.0	29.0	.568	319.2	315.1	317.2	375.1	376.1
1C-02.0-090-8-A1,A3	9.70	2.0165	-9.8	31.5	31.0	29.0	.567	332.2	315.8	345.0	377.9	384.6
1C-02.0-105-8-B3	9.71	2.0010	-9.9	31.4	30.9	28.9	.563	319.6	314.7	320.0	379.8	381.1

A2. CONTINUED

Run Name	Exit Press. (MPa)	Mass Flux ($\frac{Mg}{s.m^2}$)	Qualities (%) Inlet	Exit	At T/C A	At T/C B	Heat Flux ($\frac{MW}{m^2}$)	Outside Wall Temperatures (°C) A1	A2	A3	B1	B3
1C-02.0-180-8-B1	9.71	2.0041	-9.9	31.3	30.8	28.9	.563	314.1	314.8	320.7	371.7	361.2
1C-03.0-000-8	9.70	2.0010	-9.7	31.5	30.8	28.8	.563	314.0	314.2	315.1	386.4	351.4
1C-03.0-030-8-B3	9.72	1.9959	-9.9	31.7	30.9	29.0	.565	313.2	314.3	316.2	390.6	347.8
1C-03.0-060-8	9.70	1.9917	-9.8	31.9	31.1	29.2	.566	313.1	313.8	314.6	386.8	373.1
1C-03.0-090-8	9.69	1.9959	-9.8	31.7	30.9	29.0	.564	312.8	314.3	314.6	363.6	384.0
1C-03.0-120-8-B1	9.68	2.0052	-9.8	31.6	30.9	28.9	.567	312.9	314.2	314.9	326.1	393.2
1C-03.0-150-8-B1	9.68	1.9897	-9.8	31.9	31.2	29.2	.566	313.3	315.3	313.9	325.0	395.6
1C-03.0-180-8	9.70	2.0083	-9.9	31.6	30.9	28.9	.568	313.1	314.2	314.3	347.3	393.1
1C-03.5-000-8	9.70	2.0052	-9.9	31.4	30.6	28.7	.565	313.2	314.4	315.2	367.5	319.2
1C-03.5-030-8	9.69	2.0072	-9.9	31.4	30.5	28.6	.565	313.0	315.3	315.7	355.8	318.3
1C-03.5-060-8-B3	9.70	1.9990	-9.9	31.6	30.7	28.8	.566	313.2	315.4	315.0	342.4	325.4
1C-03.5-090-8	9.69	2.0083	-9.9	31.4	30.6	28.6	.566	312.9	314.3	314.3	348.7	359.3
1C-03.5-105-8-B1	9.71	2.0072	-10.0	31.5	30.6	28.7	.566	313.4	314.1	314.2	330.3	374.9
1C-00.0-000-10	9.70	1.9897	-10.0	32.5	32.4	30.4	.576	390.4	391.2	323.1	316.2	317.6
1C-00.0-030-10	9.68	1.9866	-9.9	32.6	32.5	30.5	.576	389.0	389.4	328.8	314.1	316.4
1C-00.0-060-10	9.69	2.0072	-9.9	32.2	32.1	30.1	.575	387.7	384.0	377.1	314.0	316.4
1C-00.0-090-10	9.72	2.0134	-10.0	32.0	31.9	30.0	.575	390.4	365.2	394.4	314.1	318.4
1C-00.0-085-10-A2	9.67	2.0145	-9.7	32.1	32.0	30.0	.575	389.4	372.3	392.4	313.9	316.8
1C-1.0-000-10	9.68	1.9917	-9.6	32.7	32.4	30.4	.575	391.4	389.7	321.4	316.6	318.7
1C-1.0-030-10-A2	9.70	1.9917	-9.7	32.7	32.3	30.3	.575	390.5	385.2	321.9	315.3	317.4
1C-01.0-060-10	9.71	1.9979	-9.8	32.5	32.1	30.2	.575	386.2	371.3	357.7	314.9	317.9
1C-01.0-090-10-B3	9.69	2.0000	-9.7	32.5	32.2	30.2	.576	388.3	344.8	390.9	318.2	333.4
1C-1.0-045-10-A3	9.69	1.9897	-9.7	32.7	32.4	30.4	.576	388.8	379.3	333.1	315.1	317.5
1C-2.0-000-10	9.68	2.0000	-9.9	32.5	31.9	30.0	.578	381.9	368.9	319.0	370.6	373.7
1C-2.0-030-10-A2	9.69	1.9938	-10.0	32.6	32.0	30.0	.578	379.7	330.6	318.7	341.7	354.8
1C-2.0-060-10-A3	9.67	1.9959	-10.0	32.4	31.8	29.8	.577	377.8	318.7	337.3	376.9	376.0
1C-2.0-090-10	9.69	1.9990	-10.0	32.5	31.9	29.9	.578	379.2	318.1	380.2	393.0	393.5
1C-3.0-000-10	9.68	2.0134	-9.6	32.6	31.9	29.9	.580	361.0	316.2	315.3	406.8	394.1
1C-3.0-030-10	9.71	2.0072	-9.8	32.7	31.9	29.9	.579	336.8	315.0	316.1	412.1	397.3
1C-3.0-060-10	9.67	1.9938	-9.6	32.8	32.0	30.0	.576	315.2	314.7	316.9	408.7	399.1
1C-3.0-090-10	9.73	2.0103	-9.8	32.3	31.5	29.5	.576	315.8	315.5	346.3	401.3	405.0
1C-3.0-120-10	9.71	2.0072	-9.8	32.4	31.6	29.6	.576	315.5	315.0	359.3	393.0	409.7
1C-3.0-080-10-A3	9.73	2.0207	-9.9	32.0	31.3	29.3	.577	315.4	315.1	324.1	403.1	400.5
1C-3.5-000-10	9.71	2.0186	-9.9	32.0	31.2	29.2	.577	317.9	314.0	314.8	394.6	330.3

A2. CONTINUED

Run Name	Exit Press. (MPa)	Mass Flux ($\frac{Mg}{s.m^2}$)	Qualitites (%) Inlet	Exit	At T/C A	At T/C B	Heat Flux ($\frac{MW}{m^2}$)	Outside Wall Temperatures (°C) A1	A2	A3	B1	B3
1C-3.5-030-10	9.71	2.0207	-10.0	32.0	31.1	29.1	.578	313.4	314.1	315.7	397.2	337.0
1C-3.5-060-10	9.68	2.0093	-9.9	32.3	31.4	29.5	.578	312.7	314.1	314.7	392.7	369.4
1C-3.5-090-10	9.70	1.9917	-10.0	32.5	31.6	29.6	.577	313.3	314.4	315.9	376.8	389.4
1C-3.5-120-10	9.69	2.0155	-10.0	32.0	31.1	29.1	.577	313.3	314.3	315.5	342.6	395.6
1C-0.0-000-12	9.72	2.0021	-10.1	32.9	32.8	30.8	.586	400.8	399.1	401.8	316.0	317.4
1C-0.0-030-12	9.67	1.9866	-9.8	33.5	33.4	31.3	.586	396.9	398.5	408.6	314.5	316.5
1C-0.0-060-12	9.68	2.0041	-9.8	33.1	33.0	31.0	.586	392.2	394.5	402.4	314.3	315.9
1C-0.0-090-12	9.71	2.0093	-10.2	32.7	32.6	30.6	.586	394.9	387.7	403.1	314.4	320.3
1C-1.0-000-12	9.73	2.0331	-9.8	32.7	32.3	30.3	.587	396.7	393.1	334.1	319.0	319.7
1C-1.0-030-12	9.70	2.0114	-9.7	33.1	32.7	30.7	.585	395.3	392.0	346.9	315.4	317.8
1C-1.0-060-12	9.69	1.9928	-9.8	33.5	33.2	31.2	.587	393.5	389.5	391.0	315.4	318.4
1C-1.0-090-12-B1,B2	9.70	1.9876	-10.0	33.4	33.1	31.0	.587	395.2	389.4	407.3	320.1	342.7
1C-1.0-040-12-A3	9.72	2.0052	-9.9	33.2	32.9	30.9	.588	392.4	388.5	348.9	315.1	317.9
1C-1.0-080-12-B1	9.70	2.0114	-10.1	32.8	32.5	30.5	.587	391.8	379.1	398.2	321.5	329.4
1C-2.0-000-12	9.71	2.0021	-10.0	33.1	32.5	30.5	.587	384.7	373.7	320.5	388.4	383.7
1C-2.0-030-12	9.70	2.0196	-10.0	32.7	32.2	30.2	.587	383.6	351.6	319.9	375.8	379.5
1C-2.0-060-12-A3	9.70	2.0062	-9.9	32.9	32.4	30.4	.585	379.4	327.3	336.7	393.5	386.8
1C-2.0-090-12	9.71	2.0165	-10.0	32.8	32.2	30.2	.586	379.9	320.0	381.5	402.6	397.3
1C-2.0-120-12	9.71	2.0217	-9.8	32.7	32.2	30.2	.585	375.8	318.8	386.1	393.9	398.9
1C-2.0-150-12	9.69	2.0010	-9.9	33.2	32.6	30.6	.587	355.3	319.2	384.2	387.8	386.2
1C-2.0-180-12	9.68	1.9969	-10.0	33.2	32.7	30.6	.587	324.7	330.6	380.0	386.4	396.2
1C-3.0-000-12	9.69	2.0155	-9.7	33.1	32.3	30.3	.587	374.2	326.2	317.9	413.6	394.1
1C-3.0-030-12	9.69	2.0000	-9.8	33.3	32.5	30.5	.586	357.2	316.2	316.6	417.7	396.0
1C-3.0-060-12	9.70	2.0072	-9.9	33.1	32.3	30.3	.587	321.8	316.0	323.3	418.3	401.6
1C-3.0-090-12	9.72	1.9876	-10.0	33.5	32.7	30.6	.588	326.0	316.7	370.9	413.4	409.8
1C-3.0-150-12	9.72	1.9990	-10.2	32.9	32.1	30.1	.586	315.5	316.5	351.3	391.0	420.5
1C-3.0-180-12	9.68	2.0000	-10.1	33.0	32.2	30.2	.586	315.5	319.4	321.7	385.2	420.3
1C-3.0-070-12-A3	9.71	2.0114	-9.8	33.0	32.3	30.2	.587	319.0	315.9	338.5	417.4	403.6
1C-3.0-120-12-A1	9.70	2.0031	-10.1	32.9	32.1	30.1	.586	321.7	316.0	373.0	401.2	415.6
1C-4.0-030-12	9.70	2.0010	-9.8	33.3	32.3	30.3	.587	314.7	315.5	315.2	399.7	322.4
1C-4.0-060-12	9.69	1.9928	-9.8	33.3	32.3	30.3	.585	313.8	314.9	315.5	399.5	351.8
1C-4.0-120-12	9.73	2.0083	-10.1	33.0	32.0	29.9	.587	314.1	314.9	321.1	384.1	395.9
1C-4.0-150-12	9.71	1.9928	-10.0	33.2	32.2	30.2	.586	314.4	314.5	315.2	344.5	402.3
1C-4.0-210-12	9.70	2.0134	-9.9	33.1	32.1	30.1	.589	314.3	320.4	314.6	323.9	402.7

A2. CONTINUED

Run Name	Exit Press. (MPa)	Mass Flux ($\frac{Mg}{s.m^2}$)	Qualities (%) Inlet	Exit	At T/C A	At T/C B	Heat Flux ($\frac{MW}{m^2}$)	Outside Wall Temperatures (°C) A1	A2	A3	B1	B3
1C-4.0-010-12-A1	9.69	1.9948	-9.7	33.5	32.5	30.4	.587	322.3	314.5	315.2	397.6	321.2
1C-4.0-090-12-A3-B3	9.71	2.0093	-9.9	33.0	32.0	29.9	.586	314.2	315.0	334.6	392.9	386.8
1C-4.0-180-12-B1	9.69	1.9979	-10.0	33.3	32.3	30.2	.588	314.3	314.1	314.5	323.9	402.9
1C-5.0-030-12-B1	9.69	1.9990	-9.7	33.5	32.3	30.3	.589	313.2	315.5	316.0	327.2	316.7
1C-5.0-060-12	9.73	2.0155	-10.0	32.9	31.7	29.7	.588	314.2	315.9	316.2	348.0	317.6
1C-5.0-090-12	9.69	2.0052	-10.0	33.1	31.9	29.9	.588	313.6	314.8	314.8	357.6	323.4
1C-5.0-120-12-B1	9.72	1.9959	-10.1	33.2	31.9	29.9	.588	314.0	314.8	314.8	323.0	332.0
1C-5.3-090-12-B1	9.71	1.9928	-10.1	33.3	32.0	30.0	.589	314.3	314.9	314.8	336.3	321.7
1C-0.0-000-15	9.70	2.0021	-9.9	34.3	34.1	32.1	.601	401.8	399.6	409.1	323.3	324.4
1C-0.0-030-15	9.70	2.0217	-9.9	33.9	33.7	31.7	.601	401.1	400.8	410.5	315.6	317.7
1C-0.0-060-15	9.67	2.0196	-9.8	34.0	33.8	31.8	.601	399.0	401.8	415.6	314.7	317.3
1C-0.0-090-15	9.70	2.0207	-9.9	34.0	33.8	31.8	.602	400.1	406.2	413.6	314.8	324.9
1C-0.0-120-15-B3	9.71	2.0124	-10.0	34.1	34.0	31.9	.603	402.5	409.9	408.8	315.1	323.2
1C-2.0-000-15	9.69	1.9948	-9.8	34.7	34.1	32.0	.602	406.0	401.2	409.8	318.2	319.5
1C-2.0-030-15	9.69	1.9979	-9.9	34.4	33.8	31.7	.601	402.1	399.0	408.8	315.8	318.2
1C-2.0-060-15	9.73	1.9938	-10.1	34.4	33.8	31.7	.601	398.4	398.6	413.3	316.2	319.0
1C-2.0-090-15	9.71	1.9948	-10.1	34.3	33.8	31.7	.602	398.9	402.6	414.5	325.8	341.0
1C-2.0-075-15-B1	9.69	2.0072	-9.7	34.5	33.9	31.8	.603	397.3	400.5	415.7	323.2	325.1
1C-2.0-095-15-B1	9.71	2.0062	-9.8	34.4	33.8	31.7	.602	398.0	400.8	412.6	324.6	343.7
1C-2.0-120-15-B3	9.71	2.0114	-10.2	33.8	33.2	31.2	.601	400.2	403.8	409.5	315.3	338.0
1C-2.0-180-15-B1	9.70	1.9979	-10.0	34.5	33.9	31.8	.604	397.7	410.9	400.5	324.5	318.7
1C-2.0-180-15-B1	9.73	2.0155	-9.9	34.3	33.7	31.6	.603	396.7	407.0	401.0	321.6	318.7
1C-2.0-210-15-B3	9.71	2.0103	-10.1	34.0	33.4	31.4	.602	396.2	409.5	399.5	346.5	327.0
1C-2.0-240-15-B1	9.72	2.0083	-9.8	34.4	33.8	31.7	.602	397.0	408.1	400.9	325.7	321.6
1C-3.0-000-15	9.74	2.0072	-10.1	34.2	33.4	31.3	.603	386.8	354.1	321.7	422.4	403.8
1C-3.0-090-15	9.74	2.0072	-10.1	34.2	33.4	31.3	.603	359.2	320.3	381.0	421.1	417.0
1C-3.0-120-15	9.71	2.0052	-10.0	34.2	33.3	31.3	.602	354.3	320.0	385.8	410.6	424.1
1C-3.0-150-15	9.69	2.0083	-9.9	34.1	33.3	31.3	.602	322.7	317.6	377.4	403.4	427.8
1C-3.0-180-15	9.71	2.0207	-10.0	33.9	33.1	31.0	.602	316.9	322.4	362.0	399.1	430.4
1C-3.0-210-15	9.71	2.0145	-10.0	34.1	33.3	31.2	.603	317.9	321.6	360.5	396.6	426.8
1C-3.0-240-15	9.72	2.0093	-9.9	34.3	33.5	31.5	.603	326.7	388.3	363.0	392.4	412.9
1C-3.0-030-15-A2	9.72	2.0052	-10.0	34.4	33.6	31.5	.604	380.5	321.0	319.2	426.5	406.2
1C-3.0-060-15-A3	9.70	2.0041	-9.9	34.4	33.6	31.5	.603	362.1	317.4	335.3	426.0	410.0
1C-4.0-000-15	9.71	2.0031	-9.8	34.5	33.5	31.4	.603	368.3	315.6	317.4	411.6	343.1

A2. CONTINUED

Run Name	Exit Press. (MPa)	Mass Flux ($\frac{Mg}{s.m^2}$)	Qualities (%)				Heat Flux ($\frac{MW}{m^2}$)	Outside Wall Temperatures (°C)				
			Inlet	Exit	At T/C A	At T/C B		A1	A2	A3	B1	B3
1C-4.0-060-15	9.70	1.9979	-9.8	34.5	33.5	31.4	.601	314.9	315.2	316.8	410.6	382.0
1C-4.0-090-15	9.73	2.0103	-9.9	34.2	33.1	31.1	.601	314.8	315.8	352.9	406.6	403.1
1C-4.0-120-15	9.71	2.0103	-9.7	34.3	33.2	31.2	.601	314.8	315.9	362.6	395.7	409.3
1C-4.0-150-15	9.71	1.9990	-9.9	34.5	33.4	31.3	.602	314.8	315.8	324.7	378.7	412.2
1C-4.0-180-15	9.72	2.0176	-9.9	34.0	32.9	30.9	.601	315.0	316.2	316.4	349.2	413.8
1C-4.0-210-15	9.68	2.0145	-9.9	33.9	32.9	30.8	.600	314.7	336.2	315.4	332.0	407.9
1C-4.0-030-15-A1	9.73	1.9917	-9.9	34.6	33.6	31.5	.601	328.1	315.6	316.5	412.3	348.2
1C-4.0-080-15-A3	9.69	2.0031	-9.7	34.4	33.3	31.3	.600	314.5	315.2	331.8	408.4	397.7
1C-5.0-030-13	9.69	2.0031	-10.0	34.2	32.9	30.8	.601	313.7	315.7	316.3	390.5	319.6
1C-5.0-090-15	9.69	2.0145	-10.0	33.9	32.6	30.6	.601	314.2	314.9	317.0	389.1	368.7
1C-5.0-120-15	9.71	2.0124	-10.1	33.8	32.6	30.5	.600	314.4	314.8	318.7	368.8	387.0
1C-5.0-180-15	9.69	2.0093	-9.9	34.0	32.8	30.7	.601	315.7	315.2	314.7	320.0	392.0
1C-5.0-210-15	9.72	2.0031	-10.0	34.1	32.9	30.8	.601	314.6	316.8	315.4	321.1	388.1
1C-5.0-000-15-A1	9.69	2.0103	-9.9	34.1	32.8	30.8	.602	323.2	314.7	315.1	387.0	319.2
1C-5.0-060-15	9.72	2.0145	-10.1	33.8	32.6	30.5	.601	314.3	315.8	315.8	390.0	324.9
1C-5.0-150-15-B1	9.71	2.0103	-10.1	33.9	32.7	30.6	.601	315.5	315.5	314.7	326.4	388.1
1C-5.5-000-15	9.70	2.0000	-10.0	34.2	32.8	30.8	.601	314.5	315.1	315.5	347.2	318.5
1C-5.5-030-15	9.71	2.0031	-10.1	34.1	32.7	30.6	.601	313.8	315.8	316.5	343.1	318.1
1C-5.5-060-15	9.71	2.0114	-10.1	34.0	32.6	30.5	.602	314.4	315.9	316.3	367.1	319.1
1C-5.5-090-15	9.71	2.0155	-10.1	33.8	32.4	30.4	.601	314.6	315.1	315.1	376.4	339.8
1C-5.5-240-15	9.71	2.0062	-10.1	33.9	32.6	30.5	.600	314.6	315.4	315.2	315.9	363.4
1C-5.5-080-15-B3	9.70	2.0062	-10.1	34.0	32.6	30.6	.601	314.6	315.6	315.2	378.9	327.9
1C-5.5-130-15-B1	9.69	2.0124	-10.0	33.9	32.5	30.5	.600	314.9	315.3	315.2	336.3	338.9
1C-6.0-000-15	9.73	2.0176	-10.0	34.0	32.5	30.4	.602	314.5	315.9	316.2	318.3	317.4
1C-6.0-055-15-B1	9.73	2.0145	-10.0	33.9	32.4	30.4	.601	314.8	316.2	316.6	323.3	316.4
1C-6.0-090-15	9.68	2.0031	-9.9	34.2	32.7	30.7	.601	315.1	314.9	314.9	349.6	320.0
1C-6.0-120-15	9.68	2.0031	-9.9	34.2	32.7	30.7	.601	315.2	315.0	314.6	319.5	319.4

A2. CONTINUED

Run Name	(MPa	Mass Flux ($\frac{Mg}{s.m^2}$)	Qualities (%) Inlet	Exit	At T/C A	At T/C B	Heat Flux ($\frac{MW}{m^2}$)	Outside Wall Temperatures(°C) A1	A2	A3	B1	B3
2A-0.0-000-C-R1	9.71	3.5026	-39.9	13.9	13.7	11.2	1.245	423.6	323.8	322.2	317.1	322.6
2A-0.0-060-C	9.72	3.5171	-40.2	13.5	13.4	10.9	1.248	370.1	321.1	321.1	318.2	322.3
2A-0.0-095-C-A1	9.69	3.5233	-39.9	13.6	13.4	10.9	1.246	339.3	320.8	324.5	318.2	321.7
2A-0.0-105-C-A3	9.71	3.5160	-40.1	13.5	13.4	10.9	1.246	322.0	320.8	325.7	318.4	321.5
2A-.25-090-C-A1	9.70	3.5160	-40.0	13.7	13.5	11.0	1.249	324.9	320.5	320.9	319.0	322.3
2A-.25-115-C-A3	9.71	3.5057	-40.1	13.8	13.6	11.1	1.249	319.4	320.0	323.4	319.0	321.4
2A-0.5-030-C-A1	9.70	3.5160	-40.1	13.7	13.4	10.9	1.250	330.0	320.2	320.8	318.5	322.8
2A-0.0-060-2	9.73	3.5109	-40.1	15.1	14.9	12.4	1.279	467.2	325.4	329.8	318.8	322.5
2A-0.0-000-2-A2	9.72	3.5233	-40.1	14.9	14.8	12.2	1.279	464.9	342.2	328.8	318.8	323.0
2A-0.0-060-2-A3	9.71	3.5150	-40.0	15.1	15.0	12.4	1.281	461.4	328.7	339.9	318.7	322.2
2A-1.0-060-2	9.71	3.4922	-40.1	15.3	14.9	12.3	1.278	464.7	325.5	328.4	318.4	322.6
2A-1.0-080-2-A3	9.71	3.4860	-40.1	15.4	15.0	12.4	1.278	417.3	324.8	342.4	318.2	322.5
2A-1.0-120-2-A1	9.70	3.4716	-40.0	15.7	15.3	12.7	1.278	341.8	326.2	466.1	319.2	321.1
2A-2.0-045-2-A1	9.71	3.4819	-40.0	15.6	14.8	12.2	1.279	331.6	320.8	323.6	316.6	320.5
2A-2.0-120-2-A3	9.70	3.4757	-40.0	15.7	14.9	12.3	1.278	321.0	323.7	328.1	316.6	319.9
2A-2.25-030-2-A1	9.72	3.4685	-40.0	15.9	15.1	12.5	1.280	338.5	320.1	323.7	316.6	320.3
2A-0.0-000-4	9.72	3.5016	-39.9	16.5	16.4	13.7	1.305	499.4	451.6	329.4	317.6	321.9
2A-0.0-060-4-A3	9.70	3.4829	-40.1	16.6	16.4	13.8	1.305	490.5	329.1	355.6	318.0	322.3
2A-0.0-035-4-A2	9.71	3.4829	-40.0	16.7	16.6	13.9	1.306	495.3	358.5	329.8	316.9	321.2
2A-1.0-000-4	9.70	3.5191	-39.8	16.2	15.8	13.1	1.303	483.8	333.2	328.7	316.0	320.2
2A-1.0-060-4	9.71	3.5047	-39.9	16.4	16.0	13.4	1.304	475.0	324.4	333.4	316.0	319.5
2A-1.0-070-4-A1,A2	9.69	3.5068	-39.9	16.3	15.8	13.2	1.302	462.6	324.8	351.3	316.5	319.3
2A-2.0-000-4	9.70	3.4840	-39.9	16.6	16.1	13.4	1.306	436.0	320.6	324.6	313.6	316.2
2A-2.0-060-4-A1	9.68	3.5233	-39.8	16.1	15.4	12.8	1.304	333.5	321.8	322.1	313.6	318.0
2A-2.0-090-4-A3	9.68	3.4776	-39.8	16.9	16.2	13.5	1.304	327.7	322.6	345.7	313.6	315.9
2A-2.7-000-4-A1	9.71	3.4984	-40.0	16.5	15.5	12.9	1.305	323.6	318.0	321.2	319.4	321.6
2A-0.0-000-6	9.70	3.4757	-40.0	17.9	17.7	15.0	1.329	506.1	465.3	331.4	319.1	323.4
2A-0.0-060-6-A3	9.73	3.4840	-40.2	17.7	17.6	14.9	1.331	497.7	334.4	394.3	318.8	322.8
2A-0.0-070-6-A2	9.67	3.5005	-39.9	17.7	17.5	14.8	1.330	513.8	358.9	364.9	318.6	322.9
2A-1.0-000-6	9.71	3.4798	-40.0	17.9	17.6	14.7	1.331	520.9	483.5	332.8	319.4	324.7
2A-1.0-060-6	9.67	3.4902	-39.8	17.7	17.3	14.6	1.329	510.7	333.3	343.6	319.3	323.6
2A-1.0-045-6-A2	9.71	3.4984	-40.0	17.6	17.1	14.4	1.330	515.0	342.2	337.8	320.2	324.3
2A-1.0-060-6-A3	9.68	3.4881	-39.9	17.8	17.4	14.7	1.330	511.7	333.5	351.9	318.7	323.6

A2. CONTINUED

Run Name	Exit Press. (MPa)	Mass Flux ($\frac{Mg}{s.m^2}$)	Qualities (%) Inlet	Exit	At T/C A	At T/C B	Heat Flux ($\frac{MW}{m^2}$)	Outside Wall Temperatures (°C) A1	A2	A3	B1	B3
2A-2.0-000-6	9.71	3.4860	-40.0	17.7	17.0	14.3	1.329	487.5	345.6	331.7	317.5	322.5
2A-2.0-060-6	9.70	3.5129	-40.0	17.4	16.7	14.0	1.331	487.5	327.7	337.3	318.2	322.2
2A-2.0-070-6-A3	9.70	3.4922	-40.0	17.7	16.9	14.2	1.330	473.4	327.7	348.2	318.9	321.8
2A-2.0-130-6-A1	9.68	3.5067	-39.9	17.5	16.7	14.0	1.329	339.0	330.8	485.1	318.9	320.2
2A-2.8-030-6-A1	9.70	3.5047	-39.9	17.5	16.8	14.1	1.330	343.7	320.2	322.4	316.5	320.0
2A-3.0-060-6	9.68	3.5047	-39.9	17.5	16.5	13.8	1.330	322.4	319.0	321.3	317.0	318.6
2A-3.0-120-6	9.68	3.5047	-39.9	17.6	16.5	13.8	1.331	321.2	321.6	361.8	316.5	318.2
2A-3.0-045-6-A1	9.70	3.5109	-40.0	17.3	16.2	13.6	1.327	319.6	319.4	321.0	316.7	319.0
2A-3.0-110-6-A3	9.70	3.5088	-39.9	17.4	16.4	13.7	1.329	317.7	319.6	328.1	317.0	318.8

A2. CONTINUED

Run Name	Exit Press. (MPa)	Mass Flux ($\frac{Mg}{s.m^2}$)	Qualities (%) Inlet	Exit	At T/C A	At T/C B	Heat Flux ($\frac{MW}{m^2}$)	Outside Wall Temperatures(°C) A1	A2	A3	B1	B3
28-0.0-000-C	9.70	3.5140	-25.3	18.2	18.1	16.1	1.016	329.1	319.7	321.0	315.9	317.3
28-0.0-000-2	9.71	3.4871	-25.2	19.5	19.3	17.3	1.035	405.3	320.7	322.3	316.3	314.4
28-0.0-060-2	9.75	3.4840	-25.3	19.6	19.5	17.4	1.037	392.3	323.3	323.5	315.8	317.7
28-0.0-095-2-A1	9.77	3.4829	-25.3	19.5	19.4	17.3	1.035	335.4	323.5	369.6	315.5	318.0
28-0.0-080-2-A3	9.72	3.4871	-25.1	19.7	19.6	17.5	1.038	373.5	322.5	332.2	315.1	317.6
28-0.5-000-2	9.72	3.4736	-25.1	19.8	19.6	17.5	1.037	386.6	319.2	323.4	315.6	317.7
28-0.5-060-2	9.72	3.4829	-25.0	19.7	19.5	17.4	1.035	366.9	322.6	322.8	315.5	320.2
28-0.5-070-2-A1	9.74	3.4850	-25.2	19.6	19.4	17.3	1.036	329.3	322.1	322.7	316.6	319.2
28-0.5-095-2-A3	9.72	3.4809	-25.1	19.7	19.4	17.3	1.034	319.8	322.5	324.4	315.7	319.3
28-0.8-000-2-A1	9.74	3.4819	-25.3	19.7	19.4	17.3	1.038	319.2	318.7	321.0	316.0	320.3
28-0.0-000-4	9.73	3.4829	-25.2	20.6	20.5	18.3	1.059	422.5	323.4	324.9	314.9	312.6
28-0.0-060-4	9.75	3.4716	-25.3	20.5	20.4	18.3	1.055	420.4	321.5	325.6	315.1	314.0
28-0.0-060-4-A3	9.76	3.4850	-25.3	20.3	20.2	18.1	1.054	415.8	321.8	328.0	315.3	320.0
28-0.0-115-4-A1	9.76	3.4984	-25.3	20.3	20.2	18.0	1.057	339.8	324.6	423.2	315.5	320.3
28-1.0-085-4-A3	9.75	3.4695	-25.2	20.8	20.4	18.3	1.058	337.0	322.4	332.2	316.1	318.7
28-1.0-090-4-A1	9.73	3.4829	-25.2	20.7	20.3	18.1	1.059	329.4	322.7	343.5	315.6	318.7
28-1.8-050-4-A1	9.71	3.4716	-25.0	20.9	20.4	18.2	1.058	320.4	320.3	320.4	315.5	319.0
28-0.0-000-6-A2	9.70	3.4747	-25.1	21.5	21.4	19.2	1.076	443.5	335.0	324.7	316.1	316.8
28-0.0-060-6-A3	9.71	3.4850	-25.2	21.4	21.3	19.1	1.077	428.3	323.3	340.7	315.4	319.7
28-2.0-180-6	9.74	3.5098	-25.1	21.2	20.6	18.4	1.076	321.1	320.7	317.7	316.5	315.8
28-1.0-000-6	9.72	3.4881	-25.1	21.5	21.1	19.0	1.079	427.8	322.1	324.7	316.5	320.0
28-1.0-060-6	9.72	3.4829	-25.2	21.4	21.1	18.9	1.078	411.6	322.3	327.7	315.3	319.7
28-1.0-075-6-A3	9.74	3.4881	-25.3	21.3	21.0	18.8	1.077	398.7	321.8	333.5	315.4	319.5
28-1.0-105-6-A1	9.73	3.4922	-25.2	21.4	21.0	18.8	1.078	331.3	322.1	408.4	316.3	324.6
28-2.0-000-8	9.72	3.4871	-25.1	21.5	20.9	18.7	1.078	321.0	319.1	321.8	320.1	318.8
28-0.0-000-8	9.73	3.5222	-25.3	21.6	21.5	19.3	1.095	441.0	342.9	323.0	316.4	320.5
28-0.0-060-8	9.72	3.4840	-25.2	22.3	22.1	19.9	1.097	434.7	324.9	376.8	315.4	319.8
28-0.0-015-8-A2	9.75	3.4881	-25.3	22.2	22.1	19.9	1.097	443.0	334.8	324.5	315.6	320.4
28-0.0-040-8-A3	9.72	3.4840	-25.2	22.4	22.2	20.0	1.098	439.4	325.8	332.8	315.6	319.6
28-1.0-000-8	9.71	3.4778	-25.1	22.4	22.1	19.8	1.096	438.0	325.8	324.3	319.7	321.0
28-1.0-060-8-A3	9.73	3.4778	-25.1	22.4	22.1	19.8	1.096	423.1	323.5	347.5	316.6	321.0
28-1.0-095-8-B3	9.75	3.5016	-25.1	22.2	21.8	19.6	1.097	366.5	323.2	422.9	317.3	326.0
28-1.0-105-8-A1	9.76	3.5026	-25.2	22.1	21.7	19.5	1.096	332.4	323.5	432.3	317.5	336.2

A2. CONTINUED

Run Name	Exit Press. (MPa)	Mass Flux ($\frac{Mg}{s.m^2}$)	Qualities (%) Inlet	Exit	At T/C A	At T/C B	Heat Flux ($\frac{MW}{m^2}$)	Outside Wall Temperatures (°C) A1	A2	A3	B1	B3
28-1.0-120-8-B3	9.73	3.4850	-25.0	22.4	22.1	19.8	1.096	327.4	324.1	436.2	317.3	330.7
28-1.6-060-8-B3,B1	9.71	3.4922	-25.0	22.5	22.0	19.7	1.099	366.6	321.9	323.7	340.5	334.8
28-2.0-000-8	9.70	3.5005	-24.9	22.3	21.7	19.5	1.097	397.6	319.4	322.6	377.1	327.8
28-2.0-060-8	9.72	3.5057	-25.0	22.2	21.5	19.3	1.096	354.5	322.9	323.8	351.5	337.0
28-2.0-180-8	9.71	3.4881	-25.0	22.5	21.9	19.7	1.098	322.4	322.6	368.2	392.5	352.0
28-2.0-020-8-B1	9.74	3.4902	-25.1	22.4	21.8	19.6	1.098	407.2	321.1	323.1	345.9	330.3
28-2.0-055-8-B1,B3	9.71	3.4922	-25.0	22.4	21.8	19.6	1.097	359.4	321.4	322.5	349.2	336.1
28-2.0-075-8-A1	9.71	3.4850	-25.0	22.6	21.9	19.7	1.099	331.8	321.2	327.4	389.8	387.8
28-2.0-085-8-A3	9.75	3.4964	-25.1	22.2	21.6	19.4	1.097	323.2	320.8	332.2	382.3	401.8
28-2.0-105-8-B1	9.72	3.4840	-25.0	22.5	21.9	19.7	1.098	320.7	320.4	379.5	341.9	415.5
28-2.0-130-8-B1	9.73	3.4912	-25.1	22.4	21.8	19.6	1.098	321.2	323.2	405.4	338.0	382.9
28-2.0-240-8-B1	9.72	3.4943	-25.0	22.4	21.8	19.6	1.099	321.3	397.3	321.3	343.9	337.5
28-2.1-030-8-B1	9.73	3.4881	-25.1	22.4	21.8	19.6	1.098	401.1	321.3	323.3	361.6	333.8
28-2.8-310-8-B3	9.75	3.5026	-25.2	22.2	21.4	19.2	1.099	319.2	317.6	319.7	392.5	339.2
28-3.0-000-8	9.74	3.5005	-25.1	22.3	21.4	19.2	1.098	317.8	319.8	319.7	376.5	324.3
28-3.0-180-8	9.74	3.4922	-25.1	22.4	21.6	19.3	1.098	321.1	321.8	319.0	325.4	399.6
28-3.0-070-8-B3	9.72	3.4922	-25.0	22.5	21.6	19.4	1.099	317.7	320.0	320.4	403.1	339.3
28-3.0-100-8-B1	9.74	3.5067	-25.1	22.2	21.4	19.2	1.099	319.2	318.9	318.2	336.8	404.6
28-3.2-000-8-B1	9.73	3.5098	-25.2	22.0	21.1	18.9	1.098	318.1	319.6	319.7	338.1	322.1
28-0.0-000-10	9.71	3.4912	-25.2	23.0	22.9	20.6	1.117	452.7	398.4	347.5	316.5	321.1
28-0.0-060-10-A2	9.76	3.4798	-25.4	23.2	23.0	20.8	1.118	445.4	338.1	409.4	316.2	320.2
28-1.0-000-10	9.72	3.5171	-25.1	22.9	22.5	20.3	1.118	449.3	333.1	326.1	323.3	322.9
28-1.0-060-10	9.75	3.4829	-25.3	23.2	22.9	20.6	1.118	442.2	327.7	371.0	317.0	321.1
28-2.0-000-10	9.73	3.4984	-25.1	23.1	22.5	20.3	1.117	428.1	324.2	325.3	372.6	376.8
28-2.0-060-10	9.73	3.4953	-25.0	23.2	22.6	20.3	1.117	403.1	322.6	330.1	370.8	370.8
28-2.0-300-10	9.74	3.5005	-25.0	23.3	22.7	20.4	1.119	353.4	382.5	321.8	385.4	429.0
28-3.0-000-10	9.75	3.4902	-25.0	23.5	22.6	20.3	1.120	333.1	320.6	320.9	453.5	336.9
28-3.0-300-10	9.72	3.5026	-24.9	23.3	22.4	20.2	1.118	321.8	319.6	322.3	387.3	380.7
28-0.0-000-12	9.72	3.5191	-25.0	23.8	23.7	21.4	1.138	466.7	448.1	440.4	319.8	321.4
28-0.0-060-12	9.71	3.5057	-25.0	24.0	23.9	21.6	1.137	455.0	443.2	457.7	316.4	319.8
28-1.0-000-12	9.72	3.4964	-25.0	24.1	23.8	21.5	1.137	459.7	358.9	344.2	334.7	324.5
28-1.0-060-12	9.74	3.5036	-25.0	24.0	23.6	21.3	1.136	450.2	331.8	385.7	317.9	322.0
28-1.0-090-12-B3	9.71	3.4891	-24.9	24.4	24.0	21.7	1.139	432.2	334.2	452.3	323.8	338.8
28-1.0-010-12-A2,B1	9.73	3.5036	-25.0	24.0	23.7	21.4	1.138	458.5	337.8	331.8	324.6	323.7

A2. CONTINUED

Run Name	Exit Press. (MPa)	Mass Flux ($\frac{Mg}{s.m^2}$)	Qualities (%)				Heat Flux ($\frac{MW}{m^2}$)	Outside Wall Temperatures (°C)				
			Inlet	Exit	At $_A$ T/C	At $_B$ T/C		A1	A2	A3	B1	B3
2B-1.0-045-12-A3	9.74	3.5150	-25.1	23.9	23.5	21.2	1.138	452.2	327.5	343.0	319.7	323.2
2B-2.0-000-12	9.72	3.4984	-25.0	24.2	23.6	21.3	1.140	441.9	325.4	325.2	399.4	400.0
2B-2.0-060-12	9.74	3.4922	-25.0	24.2	23.6	21.3	1.138	429.3	324.4	350.3	385.6	379.6
2B-2.0-300-12	9.74	3.4809	-25.1	24.3	23.7	21.4	1.138	368.7	419.6	323.4	398.4	437.5
2B-2.0-050-12-A3	9.74	3.5129	-25.1	23.9	23.2	20.9	1.139	432.6	323.2	334.0	367.6	373.2
2B-2.0-100-12-A1	9.74	3.5078	-25.2	23.9	23.2	20.9	1.139	342.8	324.8	435.5	444.9	443.2
2B-3.0-000-12	9.73	3.5036	-25.2	23.9	23.0	20.7	1.139	416.5	321.9	322.8	474.4	377.8
2B-3.0-060-12	9.75	3.4953	-25.3	23.9	23.0	20.7	1.138	371.6	322.8	325.7	478.5	386.7
2B-3.0-300-12	9.74	3.4995	-25.2	23.9	23.0	20.7	1.138	325.3	358.0	322.9	411.7	447.0
2B-3.0-075-12-A3	9.73	3.4860	-25.2	24.2	23.3	21.0	1.139	342.1	323.1	337.5	478.5	432.6
2B-3.0-080-12-A1	9.73	3.4840	-25.1	24.2	23.3	20.9	1.137	335.2	322.7	337.5	477.8	436.3
2B-4.0-000-12	9.73	3.4891	-25.1	24.2	23.1	20.7	1.140	319.0	319.4	321.0	436.3	327.0
2B-4.0-060-12	9.71	3.4912	-25.1	24.2	23.1	20.7	1.140	317.6	319.5	321.1	439.3	333.3
2B-4.0-300-12	9.72	3.4850	-25.1	24.2	23.1	20.8	1.139	321.6	316.7	320.5	346.1	326.6
2B-4.0-130-12-B1	9.70	3.5109	-25.1	23.9	22.7	20.4	1.139	320.6	319.1	316.6	332.9	425.2
2B-4.7-015-12-B1	9.74	3.4922	-25.1	24.2	22.8	20.5	1.139	318.1	319.6	321.1	324.9	323.6
2B-5.0-000-12-B1	9.72	3.4840	-25.2	24.2	22.8	20.5	1.139	318.7	319.1	320.9	326.4	322.7
2B-5.0-030-12-B1	9.76	3.4933	-25.2	24.1	22.7	20.4	1.139	320.0	320.2	320.4	329.2	330.8
2B-5.0-035-12-B1	9.73	3.4974	-25.2	24.0	22.6	20.3	1.139	318.4	319.6	321.0	343.1	323.3
2B-5.0-075-12-B3	9.70	3.4960	-25.1	24.2	22.8	20.5	1.139	318.3	319.8	321.0	387.1	334.4
2B-5.0-110-12-B1	9.75	3.4984	-25.3	24.0	22.5	20.2	1.139	320.2	319.8	319.1	332.2	362.3

A2. CONTINUED

Run Name	Exit Press. (MPa)	Mass Flux ($\frac{Mg}{s.m^2}$)	Qualities (%) Inlet	Exit	At T/C A	At T/C B	Heat Flux ($\frac{MW}{m^2}$)	Outside Wall Temperatures (°C) A1	A2	A3	B1	B3
2C-00.0-000-C	9.67	3.4736	-9.9	20.9	20.8	19.4	.720	326.8	314.7	315.4	313.1	315.3
2C-00.0-000-2	9.70	3.5150	-9.7	21.5	21.5	20.0	.738	359.7	314.9	316.3	312.6	310.1
2C-00.0-030-2	9.71	3.5078	-9.8	21.4	21.3	19.9	.736	333.2	315.1	315.3	312.7	311.2
2C-00.0-060-2	9.71	3.5098	-9.9	21.1	21.1	19.6	.732	314.3	316.2	314.8	314.0	309.7
2C-00.0-090-2	9.67	3.5047	-9.7	21.2	21.2	19.7	.731	313.0	316.1	323.9	312.6	310.1
2C-00.0-120-2	9.70	3.5026	-9.8	21.2	21.1	19.7	.730	312.7	316.4	347.5	313.4	310.2
2C-01.0-060-2	9.71	3.5057	-9.8	21.4	21.1	19.7	.735	313.6	316.1	314.3	312.5	311.7
2C-01.0-090-2	9.71	3.4933	-9.8	21.4	21.2	19.7	.733	313.9	316.4	314.5	313.9	310.2
2C-01.0-120-2	9.72	3.4984	-9.8	21.4	21.1	19.7	.734	315.5	315.9	313.1	313.2	311.8
2C-00.0-000-4	9.67	3.5026	-9.6	22.3	22.2	20.7	.752	370.3	314.6	316.4	312.4	314.5
2C-00.0-030-4	9.70	3.4819	-9.8	22.3	22.2	20.7	.751	361.2	315.8	319.7	313.6	309.4
2C-00.0-060-4	9.69	3.4871	-9.7	22.5	22.4	20.9	.754	349.4	317.4	324.7	313.3	311.8
2C-00.0-090-4	9.69	3.4809	-9.7	22.3	22.3	20.8	.750	316.1	318.0	360.7	314.1	309.1
2C-00.5-000-4-A1	9.70	3.4829	-10.0	22.0	21.8	20.3	.750	353.4	315.3	317.8	313.0	317.3
2C-00.5-080-4-A3	9.70	3.4798	-10.0	22.1	22.0	20.5	.752	313.7	317.4	338.9	312.5	308.8
2C-01.0-090-4	9.71	3.4860	-9.8	22.4	22.1	20.6	.753	312.9	316.9	318.4	313.3	308.5
2C-00.0-000-6	9.71	3.4819	-10.0	22.8	22.7	21.1	.765	374.3	316.9	319.1	313.2	316.4
2C-00.0-030-6	9.69	3.4850	-9.9	22.7	22.6	21.1	.763	368.2	316.3	321.1	314.2	312.4
2C-00.0-060-6	9.71	3.5047	-10.0	22.5	22.4	20.9	.764	351.1	317.3	329.1	314.1	309.3
2C-00.0-090-6	9.71	3.4891	-10.0	22.6	22.6	21.0	.765	319.2	318.3	368.4	313.3	312.0
2C-01.0-030-6	9.69	3.4850	-9.9	22.8	22.6	21.0	.767	358.1	314.7	318.4	312.9	314.1
2C-01.0-060-6	9.71	3.4819	-10.0	22.7	22.4	20.9	.764	331.4	316.4	318.8	314.1	309.6
2C-01.0-090-6	9.66	3.4798	-9.8	22.8	22.6	21.0	.764	315.5	316.4	315.7	312.0	308.9
2C-01.0-090-6	9.73	3.5016	-10.1	22.4	22.1	20.6	.762	313.7	317.9	327.4	313.8	307.0
2C-01.5-000-6-A1	9.71	3.4912	-10.0	22.7	22.4	20.8	.767	319.5	315.3	317.2	312.5	317.1
2C-01.5-030-6	9.69	3.4767	-10.0	22.7	22.4	20.8	.763	313.4	316.0	316.4	313.7	316.5
2C-01.5-060-6	9.68	3.4809	-9.9	22.7	22.3	20.8	.763	312.9	315.5	315.6	312.6	316.1
2C-01.5-090-6	9.72	3.4912	-10.1	22.6	22.3	20.7	.765	313.4	316.1	315.1	312.6	315.3
2C-00.0-000-8	9.67	3.4964	-9.8	23.1	23.0	21.5	.774	378.4	317.3	319.6	313.4	316.9
2C-00.0-030-8	9.71	3.4840	-10.0	23.3	23.2	21.7	.779	377.1	317.3	320.5	313.8	317.3
2C-00.0-060-8	9.70	3.4819	-10.0	23.3	23.2	21.6	.778	365.0	317.3	338.1	314.1	312.2

A2. CONTINUED

Run Name	Exit Press. (MPa)	Mass Flux ($\frac{Mg}{s.m^2}$)	Qualities (%) Inlet	Exit	At T/C A	At T/C B	Heat Flux ($\frac{MW}{m^2}$)	Outside Wall Temperatures (°C) A1	A2	A3	B1	B3
2C-00.0-090-8	9.71	3.4964	-10.0	23.1	23.0	21.5	.778	328.7	318.5	376.4	313.0	309.7
2C-01.0-000-6	9.72	3.4974	-10.0	23.0	22.8	21.2	.775	369.1	315.8	317.7	312.9	317.1
2C-01.0-030-8	9.68	3.5078	-9.8	23.1	22.8	21.3	.775	355.9	315.8	317.7	313.4	317.0
2C-01.0-060-8	9.73	3.4953	-9.9	23.1	22.9	21.3	.775	322.2	317.4	318.5	313.6	316.9
2C-01.0-090-8	9.70	3.4974	-9.8	23.2	22.9	21.4	.775	315.0	317.6	359.6	312.8	315.6
2C-01.0-065-8-A3	9.72	3.4974	-9.9	23.3	23.1	21.5	.778	316.9	317.4	332.0	312.9	316.6
2C-02.0-000-8-A1	9.71	3.5057	-9.8	23.3	22.8	21.3	.778	315.0	315.6	316.3	336.3	316.6
2C-02.7-000-8-B1	9.69	3.4891	-9.7	23.5	22.9	21.4	.777	312.9	315.7	316.8	314.1	316.1
2C-0.0-000-10	9.66	3.4685	-9.7	24.3	24.2	22.6	.793	388.1	340.3	318.6	313.0	317.4
2C-1.0-000-10	9.70	3.4695	-9.9	24.2	23.9	22.3	.794	385.2	319.0	320.2	319.3	318.4
2C-1.0-060-10	9.71	3.4943	-9.8	24.0	23.7	22.1	.793	355.6	316.6	319.1	317.2	319.9
2C-2.0-000-10	9.70	3.4819	-9.9	24.1	23.7	22.1	.794	356.8	316.0	318.0	379.9	372.7
2C-2.0-060-10	9.71	3.4705	-9.8	24.3	23.8	22.2	.793	317.1	316.7	316.9	382.6	377.6
2C-2.0-180-10	9.70	3.5150	-9.8	23.8	23.3	21.8	.792	316.3	316.0	316.7	355.3	337.3
2C-3.0-120-10	9.72	3.5047	-9.9	24.0	23.4	21.8	.795	315.3	316.4	316.5	318.5	364.6
2C-3.0-180-10	9.71	3.4860	-9.8	24.2	23.6	22.0	.794	315.3	315.3	315.8	318.9	321.8
2C-0.0-000-12	9.74	3.5036	-10.0	24.3	24.2	22.6	.805	389.9	341.2	320.1	314.4	318.3
2C-1.0-000-12	9.70	3.5222	-9.9	24.2	24.0	22.4	.806	387.1	318.5	319.4	320.5	319.0
2C-1.0-060-12	9.73	3.5026	-10.0	24.4	24.1	22.5	.806	364.6	318.2	322.5	315.2	318.6
2C-2.0-000-12	9.68	3.4974	-9.8	24.5	24.0	22.4	.805	364.9	315.7	317.7	372.2	371.8
2C-2.0-060-12	9.71	3.5202	-10.0	24.2	23.7	22.1	.806	319.9	317.5	318.6	364.4	362.5
2C-2.0-180-12	9.74	3.5171	-10.1	24.2	23.7	22.1	.807	317.2	316.9	319.8	377.7	358.8
2C-3.0-000-12	9.70	3.5181	-10.0	24.2	23.6	22.0	.806	315.3	315.1	316.6	387.2	322.1
2C-3.0-180-12	9.70	3.5150	-9.9	24.3	23.7	22.1	.807	315.6	315.9	316.1	322.0	389.2
2C-0.0-000-15	9.72	3.4974	-10.0	25.4	25.3	23.7	.830	398.5	387.0	337.8	317.9	319.1
2C-1.0-000-15	9.69	3.4850	-9.9	25.6	25.4	23.7	.830	398.9	324.9	322.3	326.3	322.2
2C-1.0-060-15	9.73	3.5160	-10.1	25.2	24.9	23.3	.829	366.1	331.7	333.0	317.0	320.2
2C-2.0-000-15	9.71	3.5026	-9.9	25.4	25.0	23.3	.830	385.9	317.6	319.4	370.7	374.5
2C-2.0-060-15	9.68	3.5016	-9.9	25.5	25.1	23.4	.831	360.9	318.2	321.5	364.3	360.6
2C-2.0-180-15	9.72	3.4860	-9.9	25.6	25.2	23.5	.830	318.1	320.7	358.4	381.8	354.0
2C-3.0-000-15	9.71	3.4747	-9.8	25.8	25.2	23.5	.829	365.2	316.4	317.6	413.3	366.8
2C-3.0-060-15	9.70	3.4840	-9.8	25.7	25.1	23.4	.830	320.4	316.3	318.5	415.7	399.8
2C-3.0-180-15	9.72	3.5067	-9.9	25.4	24.8	23.1	.830	317.1	317.9	321.8	383.9	419.8

A2. CONTINUED

Run Name	Exit Press. (MPa)	Mass Flux ($\frac{Mg}{s.m^2}$)	Qualities (%) Inlet	Exit	At T/C A	At T/C B	Heat Flux ($\frac{MW}{m^2}$)	Outside Wall Temperatures (°C) A1	A2	A3	B1	B3
38-0.0-000-C	9.74	5.0021	-25.0	16.4	16.3	14.4	1.366	316.6	319.0	319.4	316.0	321.1
38-0.0-060-2	9.73	4.9762	-24.9	17.6	17.5	15.5	1.394	409.5	325.2	449.1	316.6	320.9
38-0.0-000-2-A3	9.73	5.0228	-25.0	17.2	17.1	15.1	1.395	432.0	323.1	333.1	315.9	321.4
38-1.0-060-2	9.74	4.9959	-25.0	17.3	17.0	15.0	1.394	317.5	319.8	318.7	315.7	319.8
38-0.0-000-4	9.73	4.9866	-25.2	18.1	18.0	16.0	1.421	468.2	333.6	463.5	317.2	323.1
38-0.0-060-4-A2	9.75	4.9979	-25.2	18.0	17.8	15.8	1.420	451.5	334.8	479.5	318.1	322.6
38-0.0-150-4-A1	9.75	4.9855	-25.1	18.2	18.1	16.0	1.419	348.3	430.4	472.0	318.2	321.1
38-1.0-000-4	9.75	5.0114	-25.0	18.2	17.8	15.8	1.422	325.8	326.2	437.9	316.9	319.2
38-1.0-060-4	9.71	5.0207	-24.9	18.0	17.7	15.7	1.420	382.3	322.7	366.1	315.7	319.8
38-1.0-050-4-A3	9.70	5.0217	-24.9	18.0	17.7	15.6	1.421	378.2	321.7	331.5	315.9	320.3
38-1.0-090-4-A1	9.73	5.0165	-24.9	18.1	17.8	15.8	1.422	338.8	323.2	431.2	315.4	318.8
38-1.25-60-4-A3	9.75	4.9897	-25.1	18.2	17.8	15.8	1.422	362.4	321.7	345.9	316.5	320.3
38-1.25-75-4-A1	9.72	4.9917	-25.0	18.3	17.9	15.8	1.423	350.2	323.4	400.5	318.4	319.8
38-1.5-000-4-A1	9.75	5.0000	-25.2	18.0	17.6	15.6	1.422	327.7	318.5	319.8	314.8	319.8
38-2.0-060-4	9.73	4.9855	-25.1	18.2	17.6	15.6	1.421	316.8	318.7	318.2	314.1	316.5
38-0.0-000-6	9.71	5.0021	-25.1	18.8	18.7	16.6	1.448	472.0	337.1	490.8	318.1	323.0
38-0.0-060-6	9.72	4.9948	-25.1	18.9	18.8	16.7	1.447	462.9	418.9	506.2	319.2	323.1
38-1.0-000-6	9.71	5.0134	-25.0	18.8	18.5	16.4	1.448	469.1	329.9	456.7	316.8	322.1
38-1.0-060-6	9.72	5.0145	-25.1	18.8	18.4	16.4	1.448	426.9	334.9	470.6	320.4	321.8
38-1.0-070-6-A2	9.70	5.0186	-24.9	18.9	18.6	16.5	1.449	409.6	346.5	487.7	325.2	321.4
38-1.0-100-6-A1	9.72	4.9990	-25.0	19.0	18.7	16.6	1.447	341.0	418.9	484.1	331.9	320.5
38-2.0-055-6-A1	9.70	4.9979	-24.9	19.1	18.5	16.4	1.446	331.0	323.9	333.7	355.8	323.8
38-2.0-100-6-A2	9.74	5.0290	-25.0	18.7	18.1	16.1	1.447	319.9	326.2	335.5	419.0	329.5

A2. CONTINUED

Run Name	Exit Press. (MPa)	Heat Flux ($\frac{Mg}{s.m^2}$)	Qualities (%) Inlet	Exit	At T/C A	At T/C B	Heat Flux ($\frac{MW}{m^2}$)	Outside Wall Temperatures (°C) A1	A2	A3	B1	B3
3C-0.3-000-C	9.69	5.0114	-10.1	19.6	19.6	18.2	.992	319.4	318.0	317.1	314.9	319.0
3C-0.3-000-2	9.69	5.0010	-10.1	20.3	20.2	18.8	1.011	369.6	317.1	319.3	315.0	319.0
3C-0.3-060-2-A3	9.72	5.0165	-10.1	20.3	20.2	18.8	1.013	316.1	317.7	325.9	315.0	319.1
3C-0.3-045-2-A1	9.69	4.9917	-9.9	20.6	20.5	19.1	1.013	326.3	318.0	333.2	315.0	319.1
3C-0.5-000-2	9.69	5.0155	-9.9	20.5	20.3	18.9	1.014	357.1	317.0	317.4	315.3	319.3
3C-0.5-040-2-A1	9.71	4.9907	-9.9	20.6	20.5	19.0	1.015	325.6	317.1	317.4	315.1	319.3
3C-0.5-090-2-A3	9.70	4.9969	-9.9	20.6	20.4	19.0	1.013	316.5	317.5	334.9	314.4	318.6
3C-0.8-000-2-A1	9.70	4.9855	-9.9	20.7	20.5	19.1	1.014	324.8	317.7	317.4	315.5	318.9
3C-0.3-000-4	9.73	5.0165	-10.1	20.8	20.7	19.3	1.028	386.6	320.4	385.3	314.8	319.1
3C-0.3-050-4-A2	9.72	5.0238	-10.1	20.7	20.6	19.2	1.029	328.3	328.8	374.1	314.8	319.2
3C-0.3-060-4	9.70	5.0196	-10.0	20.8	20.7	19.3	1.029	323.4	335.3	386.8	314.5	319.0
3C-0.5-000-4	9.71	4.9845	-10.0	21.1	21.0	19.5	1.032	383.4	318.8	343.4	314.6	318.7
3C-0.5-060-4-A1	9.74	5.0207	-10.2	20.9	20.7	19.3	1.033	322.5	322.5	361.2	315.2	319.1
3C-0.5-075-4-A1	9.69	4.9855	-10.0	21.1	21.0	19.5	1.033	318.5	322.1	372.7	314.7	318.7
3C-1.0-000-4	9.74	4.9969	-10.2	20.9	20.7	19.2	1.032	344.9	316.8	317.7	315.1	318.9
3C-1.0-060-4	9.75	4.9959	-10.3	20.8	20.6	19.1	1.031	317.3	318.6	318.5	315.6	318.6
3C-1.0-030-4-A1	9.73	5.0062	-10.2	20.8	20.6	19.1	1.033	322.3	316.9	316.9	315.9	318.7
3C-1.0-070-4-B1	9.74	4.9907	-10.1	21.1	20.9	19.4	1.033	316.8	317.2	317.5	324.7	318.7
3C-1.0-100-4-A3	9.68	5.0062	-9.9	21.1	20.8	19.4	1.032	317.2	318.0	330.4	322.9	317.8
3C-1.0-100-4-B1	9.73	5.0052	-10.0	21.0	20.8	19.3	1.033	317.2	317.9	321.8	327.4	317.9
3C-1.8-060-4-B1	9.73	5.0010	-9.9	21.1	20.8	19.3	1.031	316.5	317.3	316.3	325.9	318.4
3C-2.0-060-4	9.71	5.0072	-10.1	20.9	20.4	19.0	1.029	317.5	318.5	318.3	338.3	317.6
3C-2.0-015-4-B1	9.67	4.9948	-9.9	21.0	20.6	19.2	1.030	316.2	317.3	316.9	321.2	319.0
3C-2.0-135-4-B1	9.70	5.0021	-10.1	20.9	20.5	19.0	1.029	318.4	316.4	315.9	318.7	320.8
3C-2.5-060-4	9.72	4.9990	-10.1	20.9	20.4	18.9	1.030	317.2	318.2	317.6	355.6	318.7
3C-2.5-015-4-B1	9.71	5.0072	-10.1	20.8	20.3	18.9	1.029	315.9	317.9	317.6	322.7	319.0
3C-2.5-085-4-B1	9.72	5.0196	-10.1	20.8	20.3	18.9	1.032	318.4	318.5	317.1	321.1	319.0
3C-3.0-060-4-B1	9.74	5.0228	-10.2	20.8	20.2	18.8	1.031	317.9	318.4	318.9	320.7	319.2
3C-0.3-000-6	9.70	4.9938	-9.9	21.7	21.6	20.1	1.050	397.4	323.1	414.8	314.0	319.8
3C-0.3-060-6	9.69	4.9897	-9.9	21.7	21.6	20.1	1.049	368.6	388.4	411.2	314.3	318.9
3C-0.3-025-6-A2	9.68	4.9866	-9.9	21.7	21.7	20.2	1.050	391.8	332.1	415.6	314.0	319.2

A2. CONTINUED

Run Name	Exit Press. (MPa)	Mass Flux ($\frac{Mg}{s.m^2}$)	Qualities (%) Inlet	Exit	At T/C A	At T/C B	Heat Flux ($\frac{MW}{m^2}$)	Outside Wall Temperatures (°C) A1	A2	A3	B1	B3
3C-0.0-085-6-A1	9.70	4.9917	-10.1	21.6	21.5	20.0	1.049	328.3	403.8	407.9	313.9	318.2
3C-1.0-000-6	9.72	4.9948	-10.1	21.6	21.3	19.8	1.049	385.4	318.3	373.7	314.5	323.0
3C-1.0-060-6-A1	9.70	5.0000	-10.0	21.5	21.3	19.8	1.048	320.8	321.0	353.1	316.7	319.0
3C-1.0-070-6-B1	9.70	4.9897	-10.1	21.6	21.4	19.9	1.052	320.3	323.5	381.4	322.5	319.2
3C-1.0-080-6-A2	9.73	4.9969	-10.2	21.4	21.2	19.7	1.048	317.6	320.8	340.0	332.4	318.1
3C-1.0-105-6-B1	9.70	4.9990	-9.9	21.7	21.5	20.0	1.050	319.2	371.7	391.1	321.2	337.5
3C-1.5-000-6	9.71	4.9876	-10.0	21.7	21.4	19.9	1.051	317.9	317.7	323.2	324.7	319.5
3C-1.5-060-6	9.68	4.9886	-9.8	21.9	21.5	20.1	1.052	319.1	318.1	347.0	323.5	319.9
3C-1.5-075-6-A1	9.72	4.9917	-10.0	21.7	21.4	19.9	1.052	327.2	317.0	321.1	315.9	319.8
3C-1.5-090-6-A3	9.73	4.9948	-10.0	21.7	21.3	19.9	1.051	317.1	321.3	335.2	340.4	320.7
3C-2.0-000-6	9.72	5.0083	-10.0	21.6	21.2	19.7	1.050	316.1	317.5	317.3	342.7	357.4
3C-2.0-060-6	9.74	5.0238	-10.0	21.4	21.0	19.5	1.049	316.3	317.0	316.6	367.9	337.3
3C-2.0-180-6	9.70	5.0031	-9.9	21.7	21.3	19.8	1.051	317.5	316.2	316.5	356.9	362.2
3C-2.0-090-6-B3	9.69	5.0165	-9.9	21.5	21.1	19.7	1.048	318.1	316.6	316.0	387.4	324.9
3C-3.0-060-6	9.69	5.0176	-9.9	21.5	20.9	19.4	1.048	317.6	318.4	318.3	382.3	321.0
3C-3.0-180-6	9.70	5.0010	-9.9	21.6	21.1	19.6	1.049	319.1	318.1	317.4	320.3	380.9
3C-3.0-010-6-B1	9.73	5.0217	-10.1	21.3	20.8	19.3	1.049	316.8	318.4	318.2	325.0	320.6
3C-3.0-090-6 B1	9.71	4.9948	-10.2	21.4	20.8	19.4	1.047	318.4	318.4	317.3	323.0	319.8
3C-3.25-060-6	9.71	5.0165	-10.1	21.4	20.7	19.3	1.049	318.0	318.3	318.8	343.4	319.6
3C-3.25-080-6-A1	9.70	5.0228	-10.0	21.5	20.8	19.4	1.051	318.5	318.4	318.8	325.2	319.4
3C-0.0-000-8	9.73	4.9990	-10.1	22.2	22.1	20.6	1.070	405.6	328.9	424.1	316.1	320.1
3C-0.0-060-8	9.72	5.0207	-10.0	22.1	22.0	20.5	1.070	387.9	400.7	421.0	314.4	319.5
3C-0.0-015-8-A2	9.71	4.9835	-9.9	22.4	22.3	20.8	1.069	402.4	334.7	424.1	314.8	319.7
3C-0.0-100-8-A1	9.68	4.9959	-9.7	22.4	22.3	20.8	1.068	333.8	417.9	412.7	314.2	330.6
3C-1.0-000-8	9.70	5.0072	-9.9	22.3	22.1	20.6	1.071	403.2	323.0	409.5	324.7	325.5
3C-1.0-060-8	9.70	4.9979	-9.9	22.3	22.1	20.6	1.069	360.2	370.7	410.0	317.9	320.6
3C-1.0-030-8-A2	9.73	5.0155	-10.1	22.1	21.9	20.3	1.070	390.0	324.8	404.6	317.0	320.8
3C-1.0-070-8-B1	9.69	5.0010	-10.1	22.1	21.9	20.4	1.069	324.9	331.5	402.5	325.6	320.7
3C-1.0-075-8-A1	9.76	5.0186	-10.2	22.1	21.8	20.3	1.072	329.1	357.3	407.8	328.0	322.9
3C-1.0-085-8-B3	9.70	5.0176	-10.1	22.0	21.7	20.2	1.070	322.3	354.4	403.7	338.8	329.8
3C-1.0-130-8-B3	9.67	4.9979	-10.0	22.2	22.0	20.5	1.070	321.6	399.5	400.2	317.0	331.3
3C-1.0-105-8-B1	9.71	4.9907	-10.1	22.2	22.0	20.4	1.069	321.4	381.6	404.1	330.9	347.3
3C-1.5-000-8	9.71	4.9855	-10.0	22.4	22.0	20.5	1.072	388.2	319.5	376.3	320.8	324.6
3C-1.5-060-8-B1	9.71	4.9969	-10.0	22.2	21.9	20.4	1.070	323.6	319.7	373.3	324.4	323.4

A2. CONTINUED

Run Name	Exit Press. (MPa)	Mass Flux ($\frac{Mg}{s.m^2}$)	Qualitites (%) Inlet	Exit	At T/C A	At T/C B	Heat Flux ($\frac{MW}{m^2}$)	Outside Wall Temperatures (°C) A1	A2	A3	B1	B3
3C-1.5-050-8-A1	9.71	5.0186	-10.0	22.1	21.8	20.3	1.072	346.6	319.5	359.2	318.5	321.7
3C-1.5-090-8-A2,B3	9.71	4.9835	-10.0	22.4	22.1	20.5	1.071	319.6	332.3	387.7	346.5	331.4
3C-1.5-180-8-B1	9.69	4.9845	-10.0	22.4	22.1	20.5	1.072	321.3	376.9	330.0	323.7	324.3
3C-1.5-240-8-B1	9.77	5.0217	-10.2	22.0	21.7	20.2	1.070	372.5	388.2	320.8	323.7	333.2
3C-2.0-000-8	9.72	4.9990	-10.0	22.1	21.7	20.2	1.067	324.1	316.7	319.1	377.9	390.6
3C-2.0-060-8	9.71	4.9959	-10.0	22.1	21.7	20.2	1.067	317.6	318.2	318.3	387.8	375.8
3C-2.0-030-8-A1	9.70	4.9907	-10.0	22.3	21.9	20.3	1.069	329.0	316.3	316.9	372.4	378.9
3C-3.0-030-8	9.70	5.0196	-9.9	22.3	21.7	20.2	1.073	316.4	318.1	318.0	405.7	387.6
3C-3.0-060-8	9.75	4.9969	-10.1	22.3	21.7	20.2	1.073	317.5	318.9	318.0	409.0	355.0
3C-3.0-120-8	9.73	5.0021	-10.0	22.3	21.7	20.2	1.073	319.2	317.6	317.3	403.0	351.4
3C-3.0-180-8	9.69	5.0041	-9.9	22.4	21.8	20.3	1.073	319.0	317.2	317.8	348.4	413.1
3C-3.5-080-8-B1	9.72	4.9824	-10.2	22.1	21.4	19.9	1.068	318.2	318.2	317.9	326.7	320.3
3C-3.5-110-8-B3	9.72	4.9835	-10.0	22.5	21.8	20.3	1.072	318.4	317.5	318.0	324.7	323.6
3C-3.5-220-8-B3	9.71	4.9772	-10.1	22.3	21.6	20.1	1.073	318.6	316.9	318.5	319.5	334.3
3C-4.0-060-8-B1	9.73	4.9938	-10.1	22.3	21.5	20.0	1.072	318.1	318.1	319.4	323.9	321.0
3C-0.0-000-10-A2	9.69	4.9886	-9.8	23.0	22.9	21.4	1.089	409.2	339.5	427.1	316.9	320.6
3C-0.0-060-10	9.72	4.9948	-9.9	23.0	22.9	21.4	1.088	398.4	399.2	427.2	314.6	319.6
3C-1.0-000-10	9.72	4.9804	-9.9	23.2	22.9	21.4	1.090	412.6	327.5	421.2	326.1	326.9
3C-1.0-060-10	9.72	4.9886	-9.9	23.0	22.8	21.2	1.090	391.9	390.5	420.6	318.9	322.1
3C-1.0-180-10	9.72	5.0155	-10.0	22.8	22.6	21.0	1.091	384.7	418.9	387.2	331.7	321.9
3C-1.0-105-10-A1	9.71	5.0000	-10.0	22.9	22.7	21.1	1.091	329.1	411.8	417.0	327.9	354.6
3C-1.0-150-10-A1	9.71	4.9897	-10.0	23.0	22.7	21.2	1.092	336.5	418.9	405.6	318.3	321.9
3C-2.0-000-10	9.71	5.0062	-10.0	22.8	22.4	20.9	1.092	380.9	319.0	373.8	361.5	380.8
3C-2.0-060-10	9.66	4.9866	-9.9	23.0	22.6	21.1	1.091	338.2	319.6	361.6	361.9	360.0
3C-2.0-180-10	9.73	4.9938	-10.2	22.8	22.4	20.9	1.092	320.1	346.5	340.4	377.5	348.7
3C-2.0-075-10-A1	9.71	5.0248	-10.1	22.6	22.2	20.6	1.090	320.6	320.0	361.5	386.0	375.7
3C-2.0-090-10-A2	9.69	4.9876	-10.0	23.0	22.6	21.0	1.092	320.9	328.5	385.4	396.7	389.1
3C-2.5-000-10	9.71	4.9886	-10.0	23.0	22.5	21.0	1.092	330.7	317.1	329.0	421.4	420.1
3C-2.5-060-10-A3	9.73	5.0031	-10.0	22.9	22.4	20.8	1.091	318.4	317.6	320.5	429.8	423.4
3C-2.5-110-10-A2	9.75	4.9938	-10.1	22.9	22.4	20.8	1.091	317.1	323.0	322.2	426.0	424.9
3C-3.0-000-10	9.72	4.9876	-10.0	23.0	22.4	20.8	1.091	316.6	318.5	318.2	412.6	408.5
3C-3.0-180-10	9.73	5.0010	-10.1	22.9	22.3	20.7	1.092	317.7	317.2	317.9	394.9	427.3
3C-0.0-000-12	9.70	4.9917	-10.1	23.4	23.3	21.7	1.108	414.4	381.0	433.8	317.3	320.4
3C-0.0-060-12	9.74	4.9948	-10.2	23.3	23.2	21.6	1.109	405.1	409.3	435.1	315.2	320.2

A2. CONTINUED

Run Name	Exit Press. (MPa)	Mass Flux ($\frac{Mg}{s.m^2}$)	Qualities (%) Inlet	Exit	At T/C A	At T/C B	Heat Flux ($\frac{MW}{m^2}$)	Outside Wall Temperatures (°C) A1	A2	A3	B1	B3
3C-1.0-000-12	9.70	5.0269	-10.1	23.1	22.9	21.3	1.108	419.9	333.0	416.6	349.4	349.9
3C-1.0-060-12	9.69	5.0041	-10.0	23.4	23.1	21.5	1.109	403.1	399.7	428.0	318.0	321.6
3C-1.0-105-12-A1	9.73	4.9897	-10.2	23.3	23.0	21.4	1.107	337.8	416.7	421.6	323.3	354.9
3C-1.0-160-12-A1	9.70	5.0041	-10.1	23.3	23.0	21.5	1.107	346.3	422.4	407.6	319.2	321.7
3C-2.0-000-12	9.66	4.9979	-10.0	23.5	23.0	21.5	1.111	400.0	321.5	399.5	384.7	397.6
3C-2.0-060-12	9.71	5.0052	-10.2	23.3	22.9	21.3	1.111	365.9	325.8	404.6	381.5	378.7
3C-2.0-075-12-A2	9.71	4.9814	-10.1	23.6	23.1	21.6	1.111	335.9	328.8	406.5	409.2	400.5
3C-2.0-085-12-A1	9.70	4.9948	-9.9	23.6	23.2	21.6	1.112	330.2	343.2	409.2	413.0	405.5
3C-2.5-075-12-A1	9.72	4.9866	-10.1	23.5	23.0	21.4	1.110	321.3	319.1	342.8	436.0	430.3
3C-2.5-100-12-A2	9.74	5.0021	-10.1	23.3	22.8	21.2	1.108	319.1	324.7	346.0	433.7	432.4
3C-3.0-000-12	9.69	4.9793	-9.9	23.7	23.0	21.5	1.109	320.0	318.9	322.4	427.4	424.2
3C-3.0-060-12-A1	9.71	5.0176	-10.0	23.4	22.8	21.2	1.111	318.7	317.9	318.8	433.4	427.5
3C-0.0-000-15	9.77	5.0052	-10.2	24.1	24.0	22.4	1.136	418.6	408.3	437.8	325.0	326.8
3C-0.0-060-15	9.72	5.0217	-10.0	24.3	24.2	22.6	1.139	409.3	418.4	443.1	315.6	320.3
3C-1.0-000-15-B3,B1	9.73	4.9917	-9.9	24.6	24.3	22.7	1.140	425.9	354.2	434.6	330.7	328.5
3C-1.0-060-15	9.71	4.9814	-9.9	24.7	24.4	22.8	1.141	412.5	412.3	437.2	320.0	322.1
3C-3.0-000-15	9.74	5.0165	-10.2	24.1	23.5	21.8	1.140	341.3	318.6	338.7	437.1	432.5
3C-3.0-060-15	9.72	4.9990	-10.0	24.5	23.8	22.2	1.139	396.0	371.0	424.7	380.9	376.4
3C-3.0-045-15-A3	9.72	5.0207	-9.9	24.4	23.8	22.2	1.141	407.5	333.5	422.7	347.8	361.9
3C-3.0-085-15-A1	9.73	5.0186	-10.0	24.3	23.7	22.1	1.140	346.2	397.4	420.1	414.0	403.1
3C-3.0-180-15	9.72	5.0072	-10.1	24.3	23.6	22.0	1.141	319.5	322.5	329.6	425.8	450.1
3C-4.0-205-15-B1	9.74	5.0196	-10.2	24.2	23.4	21.7	1.141	319.7	316.8	319.3	340.9	428.9
3C-5.0-100-15-B3	9.70	5.0186	-10.0	24.3	23.3	21.7	1.140	318.3	317.6	318.2	331.7	336.3
3C-5.0-105-15-B1	9.74	5.0217	-10.1	24.1	23.2	21.6	1.139	318.6	317.6	318.2	323.4	337.3
3C-5.25-090-15-B1	9.72	5.0155	-9.9	24.4	23.3	21.7	1.139	318.2	318.4	319.3	326.6	322.6
3C-5.25-110-15-B3	9.71	5.0021	-9.9	24.5	23.5	21.9	1.141	318.9	317.6	318.0	318.7	334.0
3C-5.5-060-15-B1	9.73	5.0155	-10.1	24.2	23.2	21.6	1.141	317.4	318.9	319.7	318.7	319.7

A3. CHF AND POST-CHF DATA OF THE INDIRECT HEATER

Run Name	Exit Press. (MPa)	Mass Flux ($\frac{Mg}{s.m^2}$)	Qualities (%) Inlet	Exit	Plane A	Plane B	Plane C	Plane D	Heat Flux ($\frac{MW}{m^2}$)	Outside Wall Temperatures (°C) A1	A3	B1	B2	C1	C2	D1	D2
1AC-R1	9.70	1.981	-40.0	19.1	18.94	18.63	18.32	15.56	.804	323.0	374.2	314.1	314.2	316.2	318.0	317.7	316.8
1A-01-A1,B1	9.68	1.977	-39.8	20.1	19.90	19.59	19.28	16.48	.812	376.3	396.8	326.8	319.0	315.0	316.8	317.4	316.4
1A-02-B2	9.72	2.003	-40.0	19.9	19.79	19.48	19.17	16.36	.822	386.0	400.0	337.5	324.1	314.7	316.3	317.0	316.2
1A-04-C1	9.71	2.000	-40.0	20.8	20.67	20.35	20.03	17.18	.834	415.1	418.9	406.0	365.0	319.0	317.5	316.6	314.6
1A-06-C2-D1	9.69	1.990	-40.1	22.4	22.21	21.89	21.56	18.64	.852	449.5	448.5	444.4	405.0	413.9	370.6	320.1	314.8
1CC-R2	9.70	2.021	-9.9	26.2	26.08	25.89	25.70	24.02	.512	317.4	335.1	317.3	313.4	317.8	318.5	316.7	316.8
1C-3.2-A1-R2	9.68	1.987	-9.6	27.9	27.80	27.61	27.41	25.66	.523	334.4	357.5	318.2	314.8	316.5	317.0	318.3	325.8
1C-3.5-B1,B2-R2	9.68	2.025	-9.5	27.8	27.67	27.47	27.28	25.54	.529	336.3	357.7	317.7	314.9	316.3	316.6	317.2	324.2
1C-04-B1-R2	9.68	2.005	-10.0	28.0	27.86	27.66	27.46	25.69	.534	336.6	357.2	327.2	312.7	317.5	317.0	313.4	338.1
1C-06-B2,D1-R2	9.70	2.007	-10.0	28.7	28.63	28.43	28.23	26.42	.544	327.6	356.6	317.5	314.3	316.0	316.4	320.9	312.7
1C-08-C2,D2-R2	9.68	1.989	-9.7	30.0	29.93	29.72	29.51	27.65	.553	346.0	368.4	324.4	351.5	316.6	317.8	355.6	357.6
1C-10-R2	9.69	1.992	-9.8	30.6	30.47	30.26	30.05	28.16	.562	363.4	375.3	329.0	362.3	317.8	324.2	363.6	365.2
1C-12-R2	9.71	2.012	-10.0	30.8	30.65	30.44	30.23	29.32	.572	375.7	382.3	333.0	369.3	319.0	339.1	366.4	368.7
1C-15-R2	9.68	2.024	-9.8	32.0	31.91	31.69	31.48	29.52	.590	391.4	393.3	393.5	404.6	325.4	383.7	389.6	390.8

A3. CONTINUED

Run Name	Exit Press. (MPa)	Mass Flux $\frac{Mg}{s.m^2}$	Qualities (%) Inlet	Exit	Plane A	Plane B	Plane C	Plane D	Heat Flux $(\frac{MW}{m^2})$	Outside Wall Temperatures (°C) A1	A3	B1	B2	C1	C2	D1	D2
2AC	9.76	3.497	-40.2	12.1	12.00	11.73	11.46	9.01	1.236	316.2	364.5	316.7	317.7	317.2	319.5	314.1	313.8
2A-01.5-A1,B1,B	9.76	3.482	-40.2	13.2	13.03	12.75	12.47	9.97	1.254	357.9	432.6	322.0	332.5	317.4	319.8	315.0	314.3
2A-02	9.78	3.469	-40.3	13.7	13.52	13.24	12.96	10.44	1.262	420.3	443.6	327.5	342.0	317.0	319.7	314.7	313.8
2A-03	9.62	3.467	-39.5	14.6	14.45	14.17	13.89	11.35	1.274	446.5	453.4	395.3	362.3	316.5	319.7	314.1	312.9
2A-04-C1,C2,D1	9.68	3.468	-39.9	14.9	14.79	14.51	14.22	11.65	1.289	468.7	473.7	460.3	405.3	327.4	335.8	323.4	319.4
2BC	9.67	3.508	-25.0	15.0	14.94	14.73	14.52	12.65	.959	313.9	332.5	315.6	315.8	316.2	318.6	317.0	316.0
2B-02	9.67	3.463	-25.1	16.3	16.23	16.01	15.80	13.86	.979	317.1	372.0	314.9	316.1	316.0	318.5	316.7	315.8
2B-04-A1,B2	9.73	3.492	-25.3	16.9	16.77	16.56	16.34	14.36	1.001	332.7	395.2	317.7	324.2	316.2	318.3	316.4	315.6
2B-06-B1	9.71	3.475	-24.9	18.1	17.95	17.73	17.50	15.49	1.017	383.3	407.9	332.5	338.8	315.4	317.4	313.5	314.4
2B-08	9.69	3.465	-24.8	19.1	18.96	18.73	18.50	16.44	1.035	420.4	424.3	400.6	357.7	315.7	317.4	314.1	312.6
2B-10-C1,D1	9.70	3.455	-24.9	19.9	19.76	19.53	19.30	17.20	1.053	445.1	440.7	430.1	367.1	322.5	318.8	341.5	315.8
2B-12-C2,D2	9.71	3.489	-25.1	20.4	20.27	20.03	19.80	17.67	1.077	452.2	447.2	448.8	417.2	380.2	324.5	392.1	330.9
2CC-R1	9.71	3.517	-9.9	19.6	19.54	19.39	19.23	17.85	.717	321.2	313.8	316.2	314.7	315.2	317.5	313.8	316.1
2C-02-R1	9.72	3.479	-10.1	20.4	20.36	20.21	20.05	18.62	.732	330.6	315.0	320.7	315.6	315.7	317.7	313.8	316.0
2C-04-A3,B1-R1	9.73	3.471	-10.0	21.2	21.10	20.94	20.78	19.32	.745	346.0	329.6	331.9	316.0	317.1	318.0	313.4	316.3
2C-06-R1	9.74	3.449	-10.0	22.0	21.96	21.80	21.63	20.13	.758	364.3	355.6	344.6	316.8	320.1	318.5	313.9	314.3
2C-07-C1,D1-R1	9.72	3.486	-9.8	22.4	22.28	22.11	21.94	20.43	.772	372.6	364.1	356.3	317.8	324.0	318.7	338.8	315.0
2C-08-R1	9.73	3.477	-10.0	22.6	22.52	22.35	22.18	20.65	.778	351.1	354.2	342.3	316.8	323.8	318.9	361.3	316.7
2C-10-R1	9.71	3.476	-10.0	23.0	22.95	22.77	22.60	21.06	.787	356.8	360.7	348.0	317.7	326.1	319.1	371.1	317.9
2C-12-B2-R1	9.72	3.457	-9.9	23.9	23.81	23.63	23.46	21.87	.802	363.0	368.5	352.8	325.4	339.7	319.2	388.6	327.7
2C-15-R1	9.73	3.487	-9.9	24.6	24.53	24.35	24.17	22.55	.824	393.4	387.8	369.8	366.4	352.8	319.5	405.0	377.5

A3. CONTINUED

Run Name	Exit Press. (MPa)	Mass Flux ($\frac{Mg}{s.m^2}$)	Qualities (%)						Heat Flux ($\frac{MW}{m^2}$)	Outside Wall Temperatures (°C)							
			Inlet	Exit	Plane A	Plane B	Plane C	Plane D		A1	A3	B1	B2	C1	C2	D1	D2
3BC	9.68	5.018	-24.8	15.2	15.08	14.88	14.67	12.80	1.355	315.7	320.0	315.3	318.9	316.4	318.7	314.1	311.8
3B-01-B2	9.72	4.994	-24.9	15.8	15.67	15.46	15.25	13.35	1.370	319.6	367.3	317.9	365.1	316.7	318.9	314.4	313.3
3B-02-C2	9.72	4.988	-24.9	16.1	16.02	15.80	15.59	13.67	1.380	321.8	393.7	320.3	406.2	317.5	327.2	314.4	311.1
3B-04	9.74	5.013	-25.2	16.6	16.48	16.27	16.05	14.09	1.410	343.5	428.9	322.6	443.0	319.2	385.4	315.1	315.3
3B-06-D2	9.75	5.005	-25.1	17.4	17.30	17.08	16.86	14.86	1.434	452.6	453.6	330.7	453.5	319.7	392.6	322.9	412.4
3CC-R2	9.70	5.025	-10.1	20.0	19.92	19.76	19.61	18.20	1.029	325.2	316.9	316.4	316.7	315.4	317.1	312.8	310.6
3C-02-B1,B2-R2	9.73	4.990	-10.2	20.6	20.51	20.35	20.19	18.75	1.044	338.2	321.7	337.5	324.4	319.9	317.8	317.3	331.3
3C-04-D1,D2-R2	9.73	5.003	-9.8	21.6	21.56	21.40	21.24	19.76	1.067	354.3	367.5	322.8	361.5	316.4	318.9	348.9	334.2
3C-06-C2-R2	9.74	5.022	-9.9	22.0	21.95	21.78	21.62	20.12	1.089	380.3	376.4	333.4	381.7	319.0	337.1	385.5	379.6
3C-08-R2	9.76	4.988	-10.0	22.8	22.70	22.53	22.36	20.82	1.109	398.5	391.6	357.2	401.2	323.0	365.0	409.5	404.3
3C-10-C1-R2	9.72	4.990	-9.9	23.6	23.53	23.36	23.18	21.61	1.134	403.4	396.5	384.5	412.8	324.9	388.5	417.8	410.4
3C-12-R2	9.75	5.006	-10.0	24.0	23.96	23.78	23.60	22.01	1.152	346.6	394.8	331.0	425.6	325.8	413.4	422.2	416.1
3C-15-R2	9.72	4.993	-10.1	24.8	24.68	24.50	24.32	22.68	1.180	408.0	408.4	411.8	441.7	344.0	426.3	421.1	420.5